Cooperation between root fungal endophytes and host-derived coumarins mediates iron nutrition in Arabidopsis

Doctoral thesis

for

the award of the doctoral degree

of the Faculty of Mathematics and Natural Sciences

of the University of Cologne

submitted by

Lara Van Dijck

Accepted in the year 2025

Publications (in preparation)

Van Dijck, L., Esposto, D., Hülsmann, C., Malisic, M., Piro, A., Giehl, R. F. H., Balcke, G. U., Tissier, A., & Parker, J. E. (2025). **Cooperation between a root fungal endophyte and host-derived coumarin scopoletin mediates Arabidopsis iron nutrition.** *BioRxiv*, 2025.06.04.657782. https://doi.org/10.1101/2025.06.04.657782 *Under revision in New Phytologist.* (Presented in Chapter 2)

Van Dijck, L., Hülsmann, C., Malisic, M., Piro, A., & Parker, J. E. **Fraxetin is essential for fungal root endophyte-meditated iron mobilisation for Arabidopsis growth at circum-neutral pH.** *In preparation.* (Presented in Chapter 3)

Abstract

Iron acquisition is a critical challenge for plants, particularly in iron-deficient soils. *Arabidopsis* plants employ “Strategy I” responses involving rhizosphere acidification, Fe^{3+} reduction and Fe^{2+} uptake to cope with iron limitation. Recent research has underscored the importance of root-exuded coumarins in modulating the root microbiome and facilitating iron uptake. However, specific interactions between fungal root endophytes and coumarins in plant iron nutrition remain unknown.

We identify a mechanism by which the fungal endophyte *Macrophomina phaseolina* (F80) cooperates with plant-derived coumarins to enhance *Arabidopsis* iron nutrition at acidic pH 5.7. The coumarin-deficient *f6'h1* mutants are unable to benefit from F80 colonisation. Our findings reveal that the interaction between the coumarin scopoletin and F80 rescues plant growth under iron-limiting conditions by resolving the iron mobility bottleneck. Notably, our genetic and metabolite-profiling data suggest that F80 transforms scopoletin into the iron-chelating catechol coumarin esculetin, thereby releasing available iron.

Under more alkaline (circum-neutral) pH conditions (pH 7.3), both F80 and a second endophyte, *Truncatella angustata* (F73), improve iron status indicators in fraxetin-producing genotypes, and exogenous fraxetin supplementation—but not scopoletin—reinstates fungal-mediated rescue in *f6'h1* plants. This parallels bacterial-coumarin interactions and underscores the centrality of fraxetin in iron acquisition at neutral to alkaline pH. Fungal culture assays reveal that F80 stabilises fraxetin’s iron-mobilising capacity and confers mobilisation activity to scopoletin, whereas F73 exhibits a delayed, coumarin-independent response, suggesting alternative mechanisms. Furthermore, plant rescue of iron-limitation requires iron reduction and uptake by the host at both pH conditions, placing fungal-coumarin activity upstream of the plant’s reductive iron uptake module.

Transcriptomic profiling of F80 exposed to scopoletin identified upregulated predicted monooxygenase and oxidoreductase genes, including a candidate enoyl reductase potentially analogous to the Botrytis cinerea scopoletin alteration factor (Bcsaf1). However, no single gene was definitively linked to scopoletin conversion, indicating that fungal detoxification of coumarins may involve complex enzymatic pathways or non-enzymatic oxidative processes.

By extending the known role of coumarins from bacterial to fungal members of the root microbiota, this study places coumarins at the centre of commensal-mediated enhancement of plant iron nutrition across microbial kingdoms. We also challenge the prevailing view that scopoletin primarily functions in shaping the microbiome, and reveal its important role in iron nutrition.

Preamble

A part of this dissertation is research that has been submitted or is currently under preparation, as detailed in the ‘Publications’ section. The submitted manuscript, with only minor changes, is presented in full in Chapter 2. All other sections presented in this thesis were not previously published. The majority of the experiments and analyses presented in this thesis were carried out by myself. Contributions by others are explicitly acknowledged in the ‘Author contributions’ sections.

Table of contents

Publications (in preparation) **3**

Abstract **4**

Preamble **5**

Table of contents **6**

Abbreviations **8**

1 Chapter 1: Main introduction **12**

1.1 Iron limitation in soils and impact on agriculture *12*

1.2 Solubilisation mechanisms of iron from insoluble soil minerals *14*

1.3 Iron uptake mechanisms in plants *14*

1.4 Coumarin biosynthesis and biological activities *15*

1.5 Aims of the Thesis *21*

2 Chapter 2 ..... **23**

Cooperation between a root fungal endophyte and host-derived coumarin scopoletin mediates Arabidopsis iron nutrition ***23***

Summary 23

Introduction 24

Material and methods 26

Results 30

Discussion 42

3 Chapter 3 ..... **46**

Fraxetin is essential for fungal root endophyte-meditated iron mobilisation for Arabidopsis growth at circum-neutral pH ***46***

Abstract 46

Introduction 46

Material and methods 48

Results 51

Discussion 66

4 Chapter 4 ..... **70**

Transcriptional changes in M. phaseolina (F80) in presence of scopoletin ***70***

Introduction 70

Material and methods 70

Results and discussion....72

5 Main discussion 78

5.1 Scopoletin–fungal cooperation mobilises Fe^{3+} resulting in plant rescue under iron limiting acidic conditions (Chapter 2)....79

5.2 Fraxetin as a keystone coumarin for Arabidopsis iron nutrition at circum-neutral pH (Chapter 3)....79

5.3 Fungal scopoletin degradation: a complex stress response (Chapter 4) 80

5.4 Broader implications and future directions....80

5.5 Conclusion....82

6 Supporting information 83

7 References....110

8 Eidesstattliche Erklärung .... Error! Bookmark not defined.

9 Acknowledgements.... Error! Bookmark not defined.

Abbreviations

%	percent
°C	degree Celsius
µg	microgram
µl	microliter(s)
µm	micrometre
µM	micromolar
ABCG37	ATP-BINDING CASSETTE transporter
AHA2	Autoinhibited plasma membrane H(+)-ATPase 2
AMF	Arbuscular mycorrhizal fungi
Arabidopsis	*Arabidopsis thaliana*
ARE	artificial root exudates
avFe	bio-available iron
BcSaf1	*Botrytis cinerea* scopoletin alteration factor 1
BGC	biosynthetic gene cluster
Cas9	CRISPR-associated protein 9
cDNA	complementary DNA
cm	centimetre(s)
COG	Clusters of Orthologues Genes
Col-0	*Arabidopsis thaliana* accession “Columbia 0”
COSY	COUMARIN SYNTHASE
CRISPR	Clustered Regularly Interspaced Short Palindromic Repeats
Cu	Copper
CYP82C4	CYTOCHROME P450 MONOOXYGENASE 82C4
DEG	differentially expressed genes
DMA	deoxymugineic acid
DMSO	dimethylsulfoxide
DNA	deoxyribonucleic acid
dpi	days past inoculation
DUF	domain of unknown function
EDTA	ethylenediaminetetraacetic acid
ENR	enoyl reductase domain
ESI-MS	negative electrospray ionisation and mass spectrometry
Fe^{2+}	ferrous iron
Fe^{3+}	ferric iron
F73	*Truncatella angustata*

F80	*Macrophomina phaseolina*
F6'H1	FERULOYL-COA 6-HYDROXYLASE 1
FAD	Flavin Adenine Dinucleotide
FAD OR	FAD-linked oxidoreductase
$FeCl_3$	iron chloride
Fe-EDDHA	Ethylenediamine-N,N'-bis(2-hydroxyphenylacetic acid) ferric-sodium complex
FeEDTA	ethylenediaminetetraacetic acid ferric-sodium salt
FIT	FER-LIKE IRON DEFICIENCY-INDUCED TRANSCRIPTION FACTOR
$FeSO_4$	ferrous sulphate
FRO2	FERRIC REDUCTION OXIDASE 2
FW	fresh weight
g	gram
h	hour
HK	heat-killed
HR-ICP-MS	high resolution inductively coupled plasma mass spectrometry
HRP	horse radish peroxidase
ICP-MS	inductively coupled plasma mass spectrometry
IgG	immunoglobulin G
IRT1	IRON-REGULATED TRANSPORTER 1
ISR	Induced Systemic Resistance
ITS	internal transcribed spacer
l	litre(s)
kDa	kilo Dalton
LC-MS	liquid chromatography mass spectrometry
m/z	mass-to-charge ratio
MES	2-(N-morpholino)ethanesulfonic acid
mg	milligram(s)
$MgCl_2$	magnesium chloride
min	minute(s)
ml	millilitre(s)
mM	millimolar
Mn	Manganese
MOPS	3-(N-morpholino)propanesulfonic acid
MS	mass spectrometry
MS medium	Murashige and Skoog medium
MS/MS	tandem mass spectrometry
MYB72	MYB domain protein 72 (R2R3-type transcription factor)

NaEDTA	ethylenediaminetetraacetic acid disodium salt
ng	nanogram(s)
nM	nanomolar
nm	nanometre
OD600	optical density at 600 nm
OMT	O-methyltransferase
ORFs	open reading frames
P	phosphorus
p450	cytochrome P450 monooxygenase
PAGE	polyacrylamide gel electrophoresis
PC	principal component
PCA	Principal component analysis
PCR	polymerase chain reaction
PDR9	PLEIOTROPIC DRUG RESISTANCE 9
PGPRs	plant growth-promoting rhizobacteria
pH	potential of hydrogen
PS	phytosiderophores
qPCR	quantitative PCR
RNA	ribonucleic acid
rpm	round(s) per minute
RT-PCR	reverse-transcriptase PCR
s	second(s)
S8H	SCOPOLETIN 8-HYDROXYLASE
seq	sequencing
SD	standard deviation
SD-W	Standard Defined medium lacking tryptophan
SDS	sodium dodecyl sulphate
SE	standard error
SFW	shoot fresh weight
TBS	TRIS-buffered saline
TOM1	Transporter Of Mugineic acid family phytosiderophores 1
TRIS	tris(hydroxymethyl)aminomethane
UHPLC	ultrahigh-performance liquid chromatography
unavFe	bio-unavailable iron
UV	ultraviolet light
V	Volt
WT	wild-type

YS1	Yellow Stripe 1
YSL	Yellow Stripe 1-Like
Zn	Zinc
xg	relative centrifugal force

1 Chapter 1: Main introduction

Iron is a vital micronutrient essential for many biological processes including chlorophyll synthesis, electron transport, and enzyme catalysis. Although iron is one of the most abundant elements in the earth's crust, its availability to plants is often severely restricted due to low solubility at neutral to alkaline pH. This problem is especially acute in calcareous soils, where high pH and low organic matter promote the formation of insoluble iron oxides, hydroxides, and other complexes (Lindsay & Schwab, 1982; Cornell & Schwertmann, 2003). As a result, iron-deficient plants typically exhibit interveinal chlorosis—particularly in young, developing leaves—leading to impaired photosynthesis, stunted growth, and ultimately reduced yield (Abadia & Terry, 1986).

Approximately 30% of the world's arable land suffers from limited iron bioavailability, imposing significant economic and nutritional challenges. Lower crop yields not only reduce farmer profitability but also diminish the iron content of edible plant parts, contributing to widespread dietary deficiencies (Morrissey & Guerinot, 2009). To mitigate these issues, it is essential to understand both the soil processes that mobilise iron and the specialised mechanisms plants have evolved to acquire it.

1.1 Iron limitation in soils and impact on agriculture

Despite its high total concentration in soils, iron's chemical form often renders it unavailable for plant uptake. In alkaline or calcareous soils, ferrous iron (Fe^{2+}) is rapidly oxidised to ferric iron (Fe^{3+}) which precipitates as insoluble oxides and hydroxides (Lindsay & Schwab, 1982). This inherent limitation forces plants to adopt specific strategies to mobilise iron from these sparingly soluble compounds. The resulting iron deficiency manifests as chlorosis, reduced photosynthetic efficiency, stunted growth, and reduced productivity. The consequences of iron limitation extend far beyond visible symptoms (Hindt & Guerinot, 2022). In crops like soybean and rice, iron deficiency has been directly linked to significant yield reductions and lower nutritional quality (Kobayashi *et al.*, 2014; Merry *et al.*, 2022). For example, studies have shown that iron deficiency can lead to yield losses ranging from 16% to 32% in sensitive crops, thereby imposing substantial economic burdens on farmers (Zulfiqar *et al.*, 2024). The inefficiency in iron uptake not only affects the photosynthetic capacity due to decreased chlorophyll content but also disrupts critical processes such as nitrogen fixation in leguminous crops, further compounding yield losses and reducing seed quality (Merry *et al.*, 2022; Ito *et al.*, 2024; Guillierme *et al.*, 2025).

Soil properties can direct iron availability. Factors such as soil pH, organic matter content, moisture, and carbonate levels can greatly influence the chemical forms of iron and its solubility. High soil pH, which is common in calcareous soils, promotes the conversion of

soluble Fe^{2+} to insoluble Fe^{3+}. In addition, organic matter can form complexes with iron that either enhance or inhibit its uptake, depending on the specific nature of the compounds present. These soil–chemical interactions require tailored management practices to mitigate iron deficiency in agricultural systems (Zuo & Zhang, 2011; Li *et al.*, 2023; Fodor, 2024)

Agronomic strategies have been developed to counteract iron deficiency. The application of iron chelates, such as Fe-EDDHA, can temporarily increase the pool of available iron in the soil, especially in alkaline conditions where traditional iron fertilisers (e.g., $FeSO_4$) are less effective. However, such applications are often expensive and can have transient effects on the crop iron status (Zuluaga *et al.*, 2023). Alternatively, genetic approaches—including the breeding of iron-efficient cultivars and biofortification strategies—offer promising, sustainable solutions. This approach tries to enhance a plant's intrinsic ability to mobilise and absorb iron under limiting conditions (Rehman *et al.*, 2021). The impact of iron deficiency is not confined solely to crop yield; it also has significant implications for human nutrition. Crops with low bioavailable iron contribute to dietary iron deficiencies, which are a major cause of anaemia worldwide (McLean *et al.*, 2009). Hence, improving iron uptake and accumulation in edible plant parts is a dual-purpose objective that can simultaneously boost agricultural productivity and enhance nutritional security.

In summary, although iron is an abundant element in soils, its limited bioavailability—primarily due to unfavourable soil chemical conditions—poses a major challenge in agriculture. The resulting iron deficiency affects plant growth, yield, and nutritional quality, creating a ripple effect from the field to the dinner table. Addressing these challenges through improved soil management practices, the use of specialised iron fertilisers, and the development of iron-efficient crop varieties remains a critical area of research and innovation in modern agriculture (Zuo & Zhang, 2011).

In addition to conventional agronomic and genetic strategies, exploiting the natural capabilities of soil microorganisms offers a promising avenue to alleviate iron deficiency. Beneficial soil microbes, including plant growth-promoting rhizobacteria (PGPRs) and (mycorrhizal) fungi, produce a variety of siderophores and organic acids that solubilise iron from insoluble mineral phases (Baakza *et al.*, 2004; Kramer *et al.*, 2019; Zhao *et al.*, 2020; Fasusi *et al.*, 2023). These microbial metabolites not only increase the pool of plant-available iron but may also induce changes in plant gene expression that further enhance iron uptake (Boukhalfa & Crumbliss, 2002; Aznar *et al.*, 2014). By integrating microbe-assisted strategies with conventional soil management practices, it is possible to reduce the dependence on synthetic fertilisers while simultaneously improving crop yield and nutritional quality (Bargaz *et al.*, 2018). This approach represents an environmentally sustainable solution with significant potential to address global challenges in iron nutrition for both crops and human diets.

1.2 Solubilisation mechanisms of iron from insoluble soil minerals

The release of bioavailable iron from insoluble soil minerals is governed by three principal mechanisms: (i) proton-promoted, (ii) ligand-controlled, and (iii) reductive mechanisms (Zinder *et al.*, 1986; Schwertmann, 1991; Suter *et al.*, 1991). In acidic conditions, protonation of the mineral surface facilitates the release of Fe^{3+} by replacing iron bound to oxygen with protons. This reaction can be summarised by the exchange of three protons for one Fe^{3+} ion, thereby increasing the solubility of iron (Cornell & Schwertmann, 2003). Certain organic ligands—including siderophores produced by microorganisms and phytosiderophores (PS) secreted by graminaceous plants—bind to Fe^{3+} at the mineral surface (Römheld & Marschner, 1986; Crowley *et al.*, 1991). This binding destabilises the iron mineral bonds and promotes the formation of soluble Fe^{3+}–ligand complexes (Kraemer, 2004). These complexes are then available for uptake by plant roots. Reductive processes involve the transfer of electrons to Fe^{3+} at the mineral surface, reducing it to the more soluble Fe^{2+}. This reduction is mediated by reductants such as phenolic compounds and organic acids exuded by plant roots and soil microbes, thereby breaking the Fe–O bonds and releasing iron into the soil solution (Mino *et al.*, 1983; Römheld & Marschner, 1986). Collectively, these processes underpin the two main strategies of iron mobilisation in plants. They establish the foundation for the subsequent uptake mechanisms that are critical for plant survival under iron-limited conditions.

1.3 Iron uptake mechanisms in plants

Iron is essential for plant growth and metabolism, yet its limited bioavailability in many soils has driven plants to evolve two distinct uptake strategies. Non-graminaceous plants adopt a reduction-based mechanism (Strategy I), while graminaceous plants rely on a chelation-based system (Strategy II) to acquire iron from the soil.

1.3.1 Strategy I: non-graminaceous plants

Non-graminaceous plants, such as *Arabidopsis thaliana* (*Arabidopsis*), rely on a reduction-based mechanism to acquire iron (Römheld, 1987). Under iron deficiency, these plants acidify the rhizosphere through increased proton extrusion mediated by plasma membrane H^+-ATPases, specifically by Autoinhibited PM H(+)-ATPase 2 (AHA2) in *Arabidopsis* (Santi & Schmidt, 2009). The resulting drop in pH enhances the solubility of Fe^{3+}. Concurrently, membrane-bound iron-chelate reductases—such as FERRIC REDUCTION OXIDASE 2 (FRO2) in *Arabidopsis* —reduce Fe^{3+} to Fe^{2+} (Robinson *et al.*, 1999). Finally, Fe^{2+} is taken up by high-affinity transporters like IRON-REGULATED TRANSPORTER 1 (IRT1) into the root epidermis (Eide *et al.*, 1996; Vert *et al.*, 2002; Varotto *et al.*, 2002). Although Strategy I is effective in acidic environments, its efficiency declines in alkaline soils due to the countervailing pH of the rhizosphere. As pH increases and soil acidification becomes more challenging, FRO2's *in vivo* reduction rate decreases (Santi & Schmidt, 2009; Tsai & Schmidt, 2017; Vélez-

Bermúdez & Schmidt, 2022a). To compensate, iron-starved non-graminaceous plants exude various organic compounds, including phenylpropanoid-derived coumarins. These molecules mobilise insoluble iron through both chelation and reduction, thereby supporting iron uptake even when traditional reduction mechanisms are less efficient (Schmidt *et al.*, 2014; Fourcroy *et al.*, 2014; Rajniak *et al.*, 2018).

1.3.2 Strategy II: graminaceous plants

Under iron-deficient conditions, grasses and other monocots activate a biosynthetic pathway that converts S-adenosyl methionine into a series of mugineic acid-type PS, such as deoxymugineic acid (DMA). These are then secreted into the rhizosphere via specialized efflux transporters like Transporter Of Mugineic acid family phytosiderophores 1 (TOM1) (Takagi *et al.*, 1984; Nozoye *et al.*, 2011). The secreted PS molecules rapidly bind Fe^{3+} to form soluble Fe^{3+}–PS complexes. This chelation not only increases the solubility of iron but also prevents it from re-precipitating with other soil constituents. The soluble Fe^{3+}–PS complexes are then specifically recognised by high-affinity transporters on the plasma membranes of root epidermal cells—members of the Yellow Stripe 1 (YS1) and Yellow Stripe 1-Like (YSL) transporter families play a key role here (Curie *et al.*, 2001; Murata *et al.*, 2006). These transporters facilitate the active uptake of the entire Fe^{3+}–PS complex into the root cells. Once internalised, the iron is either reduced to Fe^{2+} for incorporation into metabolic pathways or chelated further to be trafficked to various cellular compartments.

1.4 Coumarin biosynthesis and biological activities

1.4.1 Coumarin biosynthesis

Coumarins are a diverse group of naturally occurring 1,2-benzopyrone derivatives present in some monocotyledonous and most dicotyledonous plants (Harborne, 1982; Rajniak *et al.*, 2018; Stringlis *et al.*, 2019). These secondary metabolites have attracted considerable attention due to their multifunctional roles in plant physiology and defence, particularly under conditions of iron deficiency. In *Arabidopsis*, iron starvation induces the biosynthesis and release of coumarins such as scopoletin, fraxetin, sideretin, and esculetin (Kai *et al.*, 2006; Sisó-Terraza *et al.*, 2016; Robe *et al.*, 2021b; Paffrath *et al.*, 2023).

The biosynthetic pathway for these coumarins is generally linear and tightly regulated by a complex network of transcription factors and enzymes (Robe *et al.*, 2021b). A key regulator in this process is the root-specific R2R3-type MYB transcription factor, MYB72 (Palmer *et al.*, 2013; Zamioudis *et al.*, 2015; Stringlis *et al.*, 2018b). Expression of MYB72 is rapidly induced under alkaline conditions, where iron availability is restricted (Palmer *et al.*, 2013). MYB72 activates the transcription of genes involved in the coumarin biosynthetic pathway, hence it induces the synthesis of the enzyme 2-oxoglutarate-dependent dioxygenase FERULOYL-COA

6-HYDROXYLASE1 (F6'H1). F6'H1 catalyses the conversion of feruloyl-CoA to 6'-hydroxy-feruloyl-CoA, which is the critical precursor for the biosynthesis of scopoletin (Kai *et al.*, 2008). The conversion of 6′-hydroxy-feruloyl-CoA to scopoletin is a critical step in the coumarin biosynthetic pathway (Figure 1). This transformation involves a trans–cis isomerisation followed by lactonization and can occur spontaneously under the influence of light. However, the efficiency of this nonenzymatic reaction is quite low and may not produce sufficient scopoletin under stress conditions. Instead, the BAHD acyltransferase COUMARIN SYNTHASE (COSY) catalyses this conversion, significantly enhancing the reaction kinetics (Vanholme *et al.*, 2019). This enzymatic activity is particularly vital in plant organs shielded from light, such as roots, where spontaneous light-induced reactions are limited. Mutations in the COSY gene result in reduced coumarin levels and accumulation of o-hydroxyphenylpropanoids, leading to decreased iron content and growth defects under iron-limited conditions (Vanholme *et al.*, 2019). Once scopoletin is synthesised, it can be further modified by hydroxylation. Specifically, SCOPOLETIN 8-HYDROXYLASE (S8H) converts scopoletin into fraxetin (Tsai *et al.*, 2018) (Figure 1). In a subsequent step, fraxetin can be further hydroxylated by the CYTOCHROME P450 MONOOXYGENASE 82C4 (CYP82C4) to form sideretin (Rajniak *et al.*, 2018) (Figure 1). S8H and CYP82C4 expression is elevated in response to iron deficiency, with pH-dependent regulation; fraxetin is detected in higher amounts with increasing pH whereas sideretin is more important at acidic pH (Tsai *et al.*, 2018; Gautam *et al.*, 2021; Paffrath *et al.*, 2023). The genes responsible for the coumarins esculetin and umbelliferone biosynthesis remain uncharacterised. Nonetheless, recombinant COSY was shown to, apart from scopoletin, generate esculetin and umbelliferone from their respective o-hydroxycinnamoyl-CoA thioesters (Vanholme *et al.*, 2019). Coumarins are stored in the vacuole in glycosylated form, where they remain inactive until needed (Taguchi *et al.*, 2000; Stringlis *et al.*, 2019). Prior to secretion into the rhizosphere, the coumarins undergo deglycosylation, thereby releasing the active compounds that participate in iron acquisition (Zamioudis *et al.*, 2014; Robe *et al.*, 2021a). The export of coumarins is likely mediated by specific transporters, including the ATP-BINDING CASSETTE transporter PLEIOTROPIC DRUG RESISTANCE 9 (ABCG37/PDR9), which is upregulated under neutral to alkaline conditions (Rodríguez-Celma *et al.*, 2013a; Fourcroy *et al.*, 2014; Robe *et al.*, 2023) (Figure 1). Overall, the coordinated regulation of coumarin biosynthesis and secretion is a sophisticated response that enhances iron solubility and availability in the rhizosphere, thereby contributing to the overall iron homeostasis of the plant.

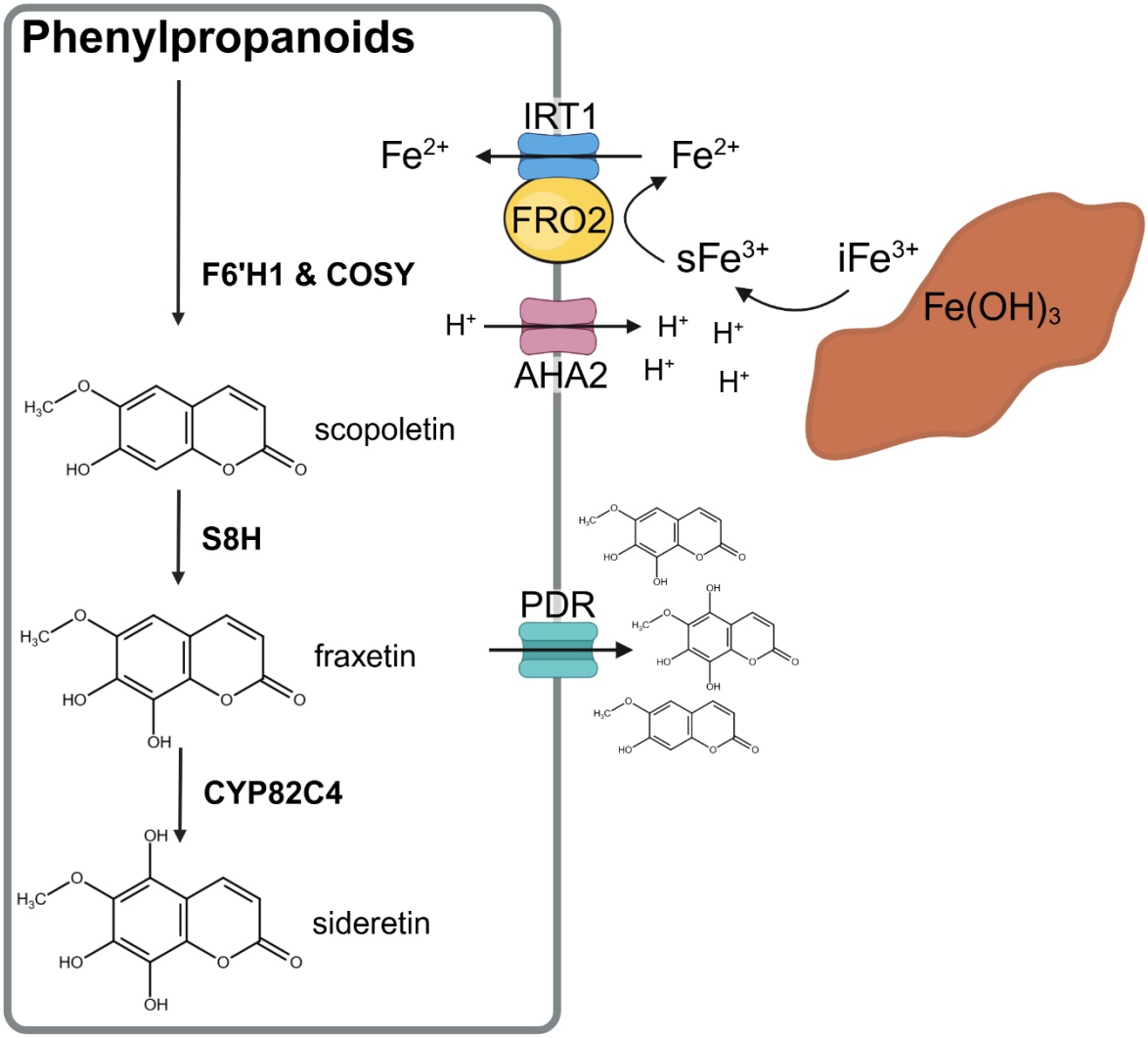

Figure 1. Reductive iron import, coumarin biosynthesis and exudation pathway in *Arabidopsis* roots. *Arabidopsis* plants use mechanisms referred to as "strategy I" to acquire iron from the soil. This involves a protein complex at the plasma membrane consisting of AHA2, FRO2, and IRT1. AHA2 releases protons that acidify the soil, mobilising Fe^{3+}, which is then reduced to Fe^{2+} by FRO2. Thereafter, Fe^{2+} is transported into the root cells via IRT1. The first steps in coumarin biosynthesis are catalysed by F6'H1 and COSY leading to the production of scopoletin, subsequent conversion to fraxetin and sideretin occurs through the activity of S8H and CYP82C4, respectively. Coumarins are secreted into the rhizosphere by PDR transporters. Once secreted to the rhizosphere, coumarins are involved in the mobilisation and reduction of iron from the soil environment. (Figure made with Biorender)

1.4.2 Role of coumarins in plant iron nutrition in concert with microbiota

Coumarins are multifunctional secondary metabolites that play pivotal roles in plant iron acquisition, acting both directly on soil iron chemistry and indirectly through modulation of the root microbiome. Their direct roles are primarily chemical: certain coumarins have the ability to mobilise and/or reduce Fe^{3+}. In particular, fraxetin, sideretin, and esculetin contain a catechol moiety essential for chelating and solubilising Fe^{3+} and/or reducing Fe^{3+} to Fe^{2+} (Hider *et al.*, 2001; Mladěnka *et al.*, 2010; Rajniak *et al.*, 2018). Although the iron reduction capacity of

coumarins decreases at elevated pH, fraxetin is noted for maintaining efficient iron mobilisation even under alkaline conditions (Sisó-Terraza *et al.*, 2016; Tsai *et al.*, 2018; Vélez-Bermúdez & Schmidt, 2022b; Paffrath *et al.*, 2023). In contrast, scopoletin lacks a catechol-group and is therefore not able to efficiently chelate iron. Due to the antimicrobial activity of scopoletin toward a wide variety of micro-organisms, it is primarily thought to function in defence (Stringlis *et al.*, 2018a; Voges *et al.*, 2019; Harbort *et al.*, 2020).

Beyond their intrinsic chemical properties, coumarins indirectly support plant iron nutrition by reshaping the microbial community in the rhizosphere. Multiple studies have shown the ability of coumarins to alter the species composition of the root microbiome (Voges *et al.*, 2019; Stringlis *et al.*, 2019; Harbort *et al.*, 2020). By inhibiting root colonisation of soil-borne pathogens and favouring the establishment of mutually beneficial interactions with rhizobacteria or fungi (Stringlis *et al.*, 2018a, 2019; Trapet *et al.*, 2021; Vismans *et al.*, 2022; Cao *et al.*, 2024; Spooren *et al.*, 2024). For instance, scopoletin and fraxetin have been shown to significantly change the composition and activity of the root microbiome in artificially limed soil (Stringlis *et al.*, 2018b) and in naturally iron-limiting calcareous soil (Harbort *et al.*, 2020). Coumarin-deficient *f6'h1* plants assemble an altered root microbiome composition and are more sensitive to iron stress compared to Col-0 wild-type (WT) plants (Harbort *et al.*, 2020). Among the genera most strongly associated with coumarin-producing Col-0 plants are those that promote plant metal uptake, improve plant growth, and possess antimicrobial properties (Stringlis *et al.*, 2018b; Stassen *et al.*, 2021). This modulation appears to be part of an integrated response involving plant immune signalling; Induced Systemic Resistance (ISR) eliciting rhizobacteria upregulate the root-specific transcription factor MYB72. Upregulation of MYB72 results in increased coumarin biosynthesis and exudation, which in turn, affects the species composition of the root microbiome (Zamioudis *et al.*, 2014, 2015; Stringlis *et al.*, 2018b).

Coumarins not only indirectly support the association of beneficial microbes by inhibiting pathogens but also interact with root commensal bacteria to enhance plant iron nutrition (Harbort *et al.*, 2020). For instance, a synthetic community of bacterial commensals isolated from *Arabidopsis* roots was shown to rescue iron-starved *Arabidopsis* in a coumarin-dependent manner at neutral to alkaline pH (Bai *et al.*, 2015; Harbort *et al.*, 2020). The underlying mechanism(s) of the bacterial community-mediated rescue of iron-starved *Arabidopsis* remain unknown. However, the growth-promoting effect of the commensals seems to involve ubiquitous microbial functions induced by fraxetin under iron-limited conditions (Harbort *et al.*, 2020).

Given that roots are colonised by a diverse microbial community, including both bacteria and fungi, it would be interesting to evaluate how root-associated fungi modulate their host under conditions of iron starvation.

1.4.3 Can fungal root endophytes influence plant iron nutrition?

Prior investigations into plant–microbe interactions have largely focused on bacterial contributions to iron acquisition (Harbort *et al.*, 2020). By contrast, the capacity of fungal root endophytes to modulate host iron nutrition has remained largely unexplored. Fungal endophytes are ubiquitous within plant roots and are recognised for enhancing plant tolerance to abiotic stresses such as drought, salinity and phosphate limitation. These beneficial fungal mechanisms include phytohormone production, nutrient solubilisation and siderophore secretion (Almario *et al.*, 2017; Pecoraro *et al.*, 2021; Verma *et al.*, 2022; De Rocchis *et al.*, 2022). For instance, the mutualistic fungus *Serendipita indica* promotes host growth under salt and drought stress by modulating phytohormone levels and antioxidant defences (Boorboori & Zhang, 2022; Saleem *et al.*, 2022). Many endophytes also produce siderophores—low-molecular-weight, high-affinity Fe^{3+} chelators—that can mobilise otherwise inaccessible iron in the rhizosphere (Winkelmann, 1992; Kraemer, 2004). Fungal-derived monohydroxamate and dihydroxamate siderophores have been shown to increase iron uptake in model systems, likely by forming soluble Fe^{3+}-siderophore complexes that plants can exploit (Hördt *et al.*, 2000). In *Trichoderma asperellum* Q1, siderophore production under iron limitation correlates with enhanced plant growth, underscoring the role of these molecules in nutrient acquisition (Zhao *et al.*, 2020). In the related *Trichoderma asperellum* strains and *Trichoderma harzianum* volatile compounds were found to induce MYB72 in *Arabidopsis* leading to enhanced iron uptake, with similar responses observed in *Solanum lycopersicum* (Martínez-Medina *et al.*, 2017). As a final example; Arbuscular mycorrhizal fungi (AMF)—the best-studied fungal symbionts—are renowned for markedly improving plant phosphorus (P) uptake, often supplying the majority of host P via extensive hyphal networks that dramatically extend soil exploration (Harley & Smith, 1983; Smith & Read, 2008). AMF additionally influence nitrogen acquisition by enhancing ammonium and nitrate uptake through modified rhizosphere chemistry and increased surface area (Govindarajulu *et al.*, 2005). AMF have also been shown to facilitate iron acquisition in various crops. Meta-analyses indicate that AMF can contribute to micronutrient (Cu, Mn, Zn and Fe) concentrations in crops (Lehmann & Rillig, 2015; Vyas *et al.*, 2024). Despite these insights, direct evidence that root endophytic fungi can partner with plant-derived metabolites—such as coumarins—to enhance iron nutrition remains absent.

To address this gap, we made use of a culture collection of phylogenetically diverse fungal endophytes originally isolated from the roots of healthy *Arabidopsis* plants growing in natural populations across Europe (Durán *et al.*, 2018; Thiergart *et al.*, 2020). From this collection,

Mesny et al., (2021) selected 41 members representative of the *Arabidopsis* root mycobiota and described the plant performance in MS agar-plate based seed inoculation assays with the fungal isolates in Phosphate limiting and replete conditions. In previous experiments in our lab all members were screened for tolerance to the antifungal coumarin scopoletin (Anthony Piro, unpublished). Based on the existing data we selected two strains for further investigation: *Macrophomina phaseolina* (F80) and *Truncatella angustata* (F73). Both fungi are less sensitive to the antimicrobial activity of scopoletin and showed neutral to beneficial effects on *Arabidopsis* seedlings after seed inoculation. *M. phaseolina* and *T. angustata* belong to fungal lineages known for versatile lifestyles, ranging from endophytism and saprotrophy to opportunistic pathogenicity—across a broad host spectrum. *M. phaseolina*, a soilborn ascomycete and member of the Botryosphaeriaceae, is notorious as the causal agent of charcoal rot in over 500 plant species (Su *et al.*, 2001; Islam *et al.*, 2012; Bandara *et al.*, 2018; Marquez *et al.*, 2021; Sinha *et al.*, 2022). Despite its pathogenic reputation, *M. phaseolina* is often isolated as an endophyte from apparently healthy roots, as asymptomatic colonisation can precede a necrotrophic phase (Schroeder *et al.*, 2019). *T. Angustata*, an ascomycetous coelomycete within the Sporocadaceae, similarly inhabits diverse ecological niches, colonising stems, leaves, fruits, and roots as either an endophyte, pathogen or saprotroph (Lee *et al.*, 2006; Wenneker *et al.*, 2017; Sokolova *et al.*, 2022).

In brief the research described in this thesis addresses the following, contributing to the field of beneficial fungal root endophytes: In Chapter 2 we demonstrate that F80 modifies scopoletin into the catechol coumarin esculetin, thereby resolving the iron solubility bottleneck in the rhizosphere and enabling plant uptake via FRO2/IRT1. This novel, coumarin-dependent mechanism of fungal-mediated iron acquisition provides the first clear example of cross-kingdom synergy between plant secondary metabolites and endophytic fungi in iron nutrition. F80 was thus shown to rescue iron-starved *Arabidopsis* under acidic pH in a scopoletin-dependent manner. In Chapter 3 we further build on this work by introducing F73 which reacts similarly to scopoletin in cultures, but is not able to alleviate iron-stress in *Arabidopsis* at acidic pH. However, the relevance of these interactions under agriculturally pertinent more alkaline conditions remained unknown. Given that Strategy I iron uptake mechanisms in dicots become less effective at high pH (Santi & Schmidt, 2009), and that coumarins such as fraxetin are strongly induced and stabilise iron solubility under these conditions (Rajniak *et al.*, 2018; Paffrath *et al.*, 2023), we hypothesised that F80 and F73 might similarly exploit root-secreted coumarins to alleviate host iron deficiency at a more alkaline pH. Our findings revealed that, under iron-limiting circum-neutral pH conditions, F80 and F73 enhanced plant iron status indicators in a coumarin-dependent manner. Interestingly, the beneficial effects were most pronounced in *cyp82c4* mutants, which produce scopoletin along with elevated levels of fraxetin, suggesting a specific role for fraxetin in fungal-mediated iron mobilisation at circum-

neutral pH. Future work should explore whether similar interactions occur across other fungal taxa and coumarin derivatives. This could potentially reveal a broadly conserved strategy for improving plant iron nutrition in challenging soil environments.

1.5 Aims of the Thesis

The overall aim of this doctoral thesis is to elucidate the molecular mechanisms by which fungal endophytes modulate plant iron nutrition through coumarin interaction. We focused on the soil-borne ascomycetes F80 and F73 part of the aforementioned *Arabidopsis* culture collection (Mesny *et al.*, 2021), exploring their capacity to enhance iron nutrition in different iron availability and pH conditions. The following chapters therefore examine (i) the requirement for plant coumarin biosynthesis and export in fungal-mediated iron rescue, (ii) the specific coumarins, and (iii) the mechanisms by which these fungi modulate coumarin-mediated Fe^{3+} mobilisation.

First, I dissected the mechanism of fungal-mediated *Arabidopsis* iron acquisition under acidic conditions (pH 5.7). Through a combination of *in planta* assays with wild-type, coumarin-biosynthesis (*f6'h1, s8h, cyp82c4*) and reductive iron import pathway (*fro2, irt1*) mutants, exogenous coumarin supplementation experiments, we demonstrated that F80 rescues iron-starved *Arabidopsis* only when scopoletin is present and the host's iron reduction and uptake system is functional. Metabolite profiling and iron mobilisation assays in F80 cultures incubated with coumarins revealed that F80 transforms scopoletin into catechol-coumarin esculetin, leading to increased iron mobilisation. This mechanism likely resolves the iron solubility bottleneck *in planta*, restoring both chlorophyll synthesis, biomass and iron accumulation in iron-limited conditions. (Chapter 2)

Recognising that alkaline soils further constrain iron uptake, we extended our investigations to higher-pH environments (pH 7.3), where Fe^{3+} solubility and reductive uptake decline sharply. In these assays, we compared F80 with a second endophyte F73, evaluated their interactions with scopoletin, fraxetin and esculetin *in planta* and by monitored fungal growth, scopoletin fluorescence and iron mobilisation and reduction in culture. Shoot fresh weight and chlorophyll content were quantified in coumarin biosynthesis and export (*prd9*) *Arabidopsis* mutants, revealing that both fungi require fraxetin to mobilise iron under circum-neutral pH conditions, though with differing efficacies. This work highlights the context-dependent nature of endophyte–coumarin synergy across pH gradients. (Chapter 3)

Finally, to pinpoint the fungal genes responsible for scopoletin conversion, I performed RNA-sequencing on F80 cultures exposed to scopoletin and conducted differential expression analyses. Despite extensive transcriptomic scrutiny, no single candidate gene emerged as the

definitive scopoletin-alteration enzyme, underscoring the complexity of fungal secondary-metabolite metabolism and suggesting redundant or novel enzymatic pathways. (Chapter 4)

Together, these studies illuminate a previously unrecognised, cross-kingdom mechanism in which plant secondary metabolites and beneficial root fungi co-operate to surmount iron limitation, offering new avenues for harnessing microbiome engineering to improve crop nutrition in challenging soils.

2 Chapter 2

Cooperation between a root fungal endophyte and host-derived coumarin scopoletin mediates *Arabidopsis* iron nutrition

Lara Van Dijck[1], Dario Esposto[2], Charlotte Hülsmann[1], Milena Malisic[1,3], Anthony Piro[1,3], Ricardo F. H. Giehl[4], Gerd U. Balcke[2], Alain Tissier[2], Jane E. Parker[1,3] *

[1] Department of Plant Microbe Interactions, Max Planck Institute for Plant Breeding Research, 50829 Cologne, Germany
[2] Department of Cell and Metabolic Biology, Leibniz Institute of Plant Biochemistry, 06120 Halle, Germany
[3] Cluster of Excellence on Plant Sciences (CEPLAS), Cologne, Germany
[4] Department of Physiology and Cell Biology, Leibniz Institute of Plant Genetics and Crop Plant Research, 06466 Gatersleben, Germany
* Corresponding author: Jane E. Parker; email: parker@mpipz.mpg.de

ORCID: 0009-0002-6141-981X (LVD); 0009-0008-5796-2602 (DE); 0000-0002-4861-1236 (MM); 0000-0002-8348-165X (AP); 0000-0003-1006-3163 (RFHG); 0000-0002-0475-0672 (GUB); 0000-0002-9406-4245 (AT); 0000-0002-4700-6480 (JEP)

Keywords: plant iron uptake, beneficial fungi, root exudates, esculetin, metabolite profiling

Summary

- Iron acquisition is a critical challenge for plants, especially in iron-deficient soils. Recent research underscores the importance of root-exuded coumarins in modulating the root microbiome community structure and facilitating iron uptake. However, interactions between root-associated fungi and coumarins in plant iron nutrition remain unknown. We investigated the mechanism by which a fungal endophyte, *Macrophomina phaseolina* (F80), enhances *Arabidopsis* iron nutrition.
- Fungal–coumarin interactions were assessed by profiling metabolites and measuring iron mobilisation in F80 cultures supplemented with specific coumarins, alongside quantifying growth performance and iron content in *Arabidopsis* coumarin-biosynthesis mutants inoculated with F80.uei
- Our findings reveal that an interaction between the coumarin scopoletin and F80 in the rhizosphere rescues plant growth under iron-limiting conditions by resolving the iron mobility bottleneck. F80 exhibits a capacity to modify scopoletin into iron-chelating catechol coumarin esculetin, thereby releasing available iron.
- We conclude that *Arabidopsis*-produced scopoletin functions as a precursor for fungal conversion into iron-chelating coumarins. By extending the role of coumarins from bacterial to fungal members of the root microbiota, this study places coumarins at the centre of commensal-mediated enhancement of plant iron nutrition across microbial kingdoms.

Introduction

Plants have evolved sophisticated mechanisms to shape their root microbiomes. Microbial community structure in the rhizosphere is influenced by various root-exuded compounds, including a diverse class of secondary metabolites known as coumarins (Stassen *et al.*, 2021). Coumarins are derived from the phenylpropanoid pathway and are produced by a wide range of dicotyledonous plants (Rajniak *et al.*, 2018). Their broad biological activities which include anti-microbial, anti-oxidant, and anti-inflammatory properties, have attracted attention in plant and medical sciences (Borges *et al.*, 2005). Coumarins can be found in above- and below-ground plant tissues (Stringlis *et al.*, 2019; Robe *et al.*, 2021b). Over 50 years ago, foliar coumarin accumulation was linked to pathogen defence (Sequeira & Kelman A., 1962; Reuveni & Cohen, 1978; Zaynab *et al.*, 2024), while more recent studies have highlighted their central role in plant iron acquisition at the root surface (Schmid *et al.*, 2014; Sisó-Terraza *et al.*, 2016; Rosenkranz *et al.*, 2021).

Iron is an essential micronutrient for almost all life forms including plants and their associated microbes (Aznar *et al.*, 2015). However, despite its high abundance in soil, iron is often bio-unavailable to soil-inhabiting organisms due to poor solubility as ferric oxide (Fe^{3+}) particularly in highly oxygenated, neutral or alkaline soils (Hindt & Guerinot, 2022). This limited bioavailability often leads to iron deficiency in plants and in natural and agricultural environments iron fertilisation is often necessary (Zuo & Zhang, 2011). To counter this challenge plants have evolved specialised iron acquisition strategies. Dicots and non-grass monocots employ “strategy I” which relies on the reduction of iron prior to its import (Römheld, 1987; Eide *et al.*, 1996). In the model strategy I plant *Arabidopsis thaliana* (*Arabidopsis*) this is conferred by the tripartite reductive import module consisting of H^+-ATPase AHA2, FERRIC REDUCTION OXIDASE 2 (FRO2) and IRON-REGULATED TRANSPORTER 1 (IRT1)(Tsai & Schmidt, 2017). AHA2-mediated proton extrusion into the rhizosphere is thought to contribute to ferric iron (Fe^{3+}) mobility through acidification of the rhizosphere (Santi & Schmidt, 2009). Acidification also lowers the redox potential to support Fe^{3+} reduction to ferrous iron (Fe^{2+}) by FRO2, and consequently Fe^{2+} is taken up via IRT1 (Vert *et al.*, 2002; Varotto *et al.*, 2002). Graminaceous plants, on the other hand, utilise “strategy II,” marked by the release of mugineic acid-type phytosiderophores that chelate Fe^{3+} and form complexes that can be efficiently absorbed by specific root transporters (Takagi *et al.*, 1984; Römheld & Marschner, 1986; Ishimaru *et al.*, 2006; Murata *et al.*, 2006; Nozoye *et al.*, 2011)

In addition to acidification, several strategy I plants also exude specific iron-chelating coumarins to assist in iron solubilisation. Iron chelation is facilitated by catechol coumarins such as esculetin, fraxetin, and sideretin, with two hydroxyl groups in ortho positions (Hider *et al.*, 2001; Mladěnka *et al.*, 2010). The effectiveness of these coumarin metabolites is pH-

dependent and expression of their biosynthesis genes responds to pH fluctuations (Sisó-Terraza *et al.*, 2016; Tsai & Schmidt, 2017, 2020; Gautam *et al.*, 2021; Paffrath *et al.*, 2023). Plants also exude the non-catechol containing coumarin scopoletin which is not effective in mobilising iron (Schmid *et al.*, 2014; Sisó-Terraza *et al.*, 2016; Rajniak *et al.*, 2018). The complexity of coumarin profiles and their biological activity is further increased by their ability to influence the composition and dynamics of the plant root microbiota. (Zamioudis *et al.*, 2014; Stringlis *et al.*, 2018b; Voges *et al.*, 2019; Harbort *et al.*, 2020). Several coumarins, especially scopoletin, were reported to possess selective antimicrobial activities (Stringlis *et al.*, 2019) and inhibit the growth of soil-borne fungi (Carpinella *et al.*, 2005; Kai *et al.*, 2006; Ba *et al.*, 2017; Stringlis *et al.*, 2018b). Moreover, Harbort *et al* (2020) demonstrated that root commensal bacteria can alleviate iron starvation in *Arabidopsis* through interactions with root-secreted fraxetin in alkaline pH conditions. *Arabidopsis* mutants lacking coumarins harboured altered bacterial communities and had heightened iron stress sensitivity (Harbort *et al.*, 2020).

The first step in the *Arabidopsis* coumarin biosynthesis pathway involves the 2-oxoglutarate-dependent dioxygenase FERULOYL-CoA 6'-HYDROXYLASE (F6'H1) (Kai *et al.*, 2008; Schmidt *et al.*, 2014; Schmid *et al.*, 2014). F6'H1 converts feruloyl-CoA to 6-hydroxyferuloyl-CoA, which is then converted to scopoletin spontaneously or by the BAHD acyltransferase-COUMARIN SYNTHASE (COSY) in organs shielded from light (Kai *et al.*, 2008; Vanholme *et al.*, 2019). COSY was also found to produce esculetin *in vitro* from its hydroxycinnamoyl-CoA thioester (Vanholme *et al.*, 2019). While the mode of esculetin biosynthesis in the plant remains unclear, Rajniak et al. (2018) suggested that F6'H1 is required, although *Arabidopsis* exudates contain relatively low levels of esculetin compared to scopoletin (Schmid *et al.*, 2014; Paffrath *et al.*, 2023). Fraxetin is synthesised from scopoletin by SCOPOLETIN-8-HYDROXYLASE (S8H) and can be further hydroxylated into sideretin by cytochrome P450 82C4 enzyme (CYP82C4) (Siwinska *et al.*, 2018; Rajniak *et al.*, 2018; Tsai *et al.*, 2018). These last steps in the coumarin biosynthesis pathway (S8H and CYP82C4) are highly induced in response to iron deficiency and lead to higher coumarin exudation rates (Rodríguez-Celma *et al.*, 2013a; Fourcroy *et al.*, 2014; Schmid *et al.*, 2014; Sisó-Terraza *et al.*, 2016; Tsai *et al.*, 2018; Paffrath *et al.*, 2023). Coumarins are secreted into the rhizosphere via ATP-binding cassette transporters like PLEIOTROPIC DRUG RESISTANCE 9 (PDR9) (Fourcroy *et al.*, 2014; Ziegler *et al.*, 2017), where they can directly contribute to iron uptake by chelating or reducing Fe^{3+} (Hider *et al.*, 2001; Mladěnka *et al.*, 2010; Schmidt *et al.*, 2014; Paffrath *et al.*, 2023).

While a critical role of coumarin interactions with root-associated bacterial microbiota for plant iron nutrition has been established (Harbort *et al.*, 2020), contributions of fungal root endophytes and their interplay with root-secreted coumarins for plant iron nutrition remain unreported. Here we used a fungal endophyte, *Macrophomina phaseolina* MPI-SDFR-AT-

0080 (F80), which is a member of the *Arabidopsis* mycobiota isolated from the roots of wild *Arabidopsis* populations and part of a microbial culture collection (Durán *et al.*, 2018). We demonstrate that *M. phaseolina* F80 alleviates host iron-starvation in a coumarin-dependent manner. We uncover a previously undescribed mechanism by which a root endophytic fungus promotes plant iron nutrition through cooperation with the plant-derived coumarin scopoletin. Ex planta assays suggest that F80 mediates the conversion of scopoletin to the iron-mobilising catechol coumarin esculetin which then relieves plant iron deficiency by providing soluble Fe^{3+} to FRO2 for reduction and import via IRT1. Our data highlight a role of coumarin-microbiota interactions for plant iron nutrition across microbial kingdoms and further suggest physiological importance of the highly abundant coumarin scopoletin for plant iron nutrition in nature.

Material and methods

Growth conditions

The following *A. thaliana* genotypes were used: Columbia-0 wildtype (Col-0), *f6'h1*-1 AT3G13610; SALK_132418C (*f6'h1*), *s8h-1* AT3G12900; SM_3_27151 (*s8h*), *cyp82c4-1* AT4G31940; SALK_001585 (*cyp82c4*), *frd1-1* AT1G01580; N3777 (*fro2*), and *irt1-1* AT4G19690; SALK_024525 (*irt1*). *Arabidopsis* seeds were surface sterilised for 15min with 70% ethanol + 0.1% Tween-20, subsequently for 2min in 95% ethanol, and after drying, seeds were kept in sterile distilled water for 2-3 days in the dark at 4°C for stratification. For germination, seeds were placed onto square Petri plates containing ½× Murashige & Skoog (MS) medium (vitamins, 0.5 g/L MES, pH 5.7, 0.5% sucrose, 1% BD DIFCO™ Agar). The plates were sealed with micropore tape and placed vertically into a growth chamber (10 h light, 21°C; 14 h dark, 19°C) for 7 d.

Fungal growth & hyphal harvesting

The fungus *Macrophomina phaseolina* (MPI-SDFR-AT-0080 v1.0) (F80) (Mesny *et al.*, 2021), was grown on Potato Dextrose Agar (PDA) at 22°C for approx. 1 week. Hyphae were harvested with a sterilised scalpel, transferred to grinding tubes with metal beads, diluted to 100 mg hyphae/ml with 10 mM $MgCl_2$, and ground for 5 min. To obtain heat-killed (HK) fungus, samples were incubated at 99°C for 1 h.

Gnotobiotic agar-plate system

The gnotobiotic agar-based system was adapted from (Harbort *et al.*, 2020) - STAR protocols. Adjusted half strength MS media without iron (750 µM $MgSO_4$, 625 µM KH_2PO_4, 10.3 mM NH_4NO_3, 9.4 mM KNO_3, 1.5 mM $CaCl_2$, 55 nM $CoCl_2$, 53 nM $CuCl_2$, 50 µM H_3BO_3, 2.5 µM KI, 50 µM $MnCl_2$, 520 nM Na_2MoO_4, 15 µM $ZnCl_2$, and 9.4 mM KCl, with 1% BD DIFCO™ Agar, Bacteriological) was prepared from stock solutions and supplied with 10 mM MES, 50 µM iron

(FeEDTA or $FeCl_3$), and fungal hyphae (1:2000 dilution, 50 µg/ml final concentration) after autoclaving. For coumarin supplementation experiments, coumarin were added from 100 mM DMSO stocks to a final concentration of 10 µM or an equal amount of DMSO as control. After solidifying, the top approx. 2.5 cm agar was removed from 12x12 square petri plates filled with 50 ml of medium, and seven germinated seedlings were transferred per plate (four replicate plates per experiment). Plates were sealed with micropore tape and vertically grown for 2 weeks in a growth chamber (10 h light, 21°C; 14 h dark, 19°C) with roots shielded from light. After 2 weeks, shoot samples were collected for chlorophyll measurements and whole shoots and roots were harvested to record shoot fresh weight (SFW) and assess fungal colonisation, respectively.

Shoot chlorophyll analysis

The protocol for chlorophyll extraction and quantification was based on Harbort et al., (2020) and Hiscox & Israelstam, (2011). 5-7 shoots from each plate were pooled, weighed and kept at -80°C until processing. To each sample, 1 ml DMSO per 30 mg of leaf tissue was added and they were incubated for 45 min at 65 °C with 300 rpm agitation. Chlorophyll absorbance was measured at 652 nm on a Nanodrop spectrophotometer (Thermo Fisher Scientific).

Shoot mineral element analysis

Mineral element analysis of whole shoots was performed as described previously (Paffrath *et al.*, 2023) Shoot samples were dried to constant weight at 65°C and weighed into polytetrafluoroethylene tubes. Dried plant material was digested using concentrated HNO_3 (67–69% v/v, Bernd Kraft) and subjected to pressurised digestion in a high-performance microwave reactor (UltraCLAVE IV, MLS GmbH). After digestion, the samples were diluted with deionised water (Milli-Q Reference A+, Merck Millipore) and analysed using high-resolution inductively coupled plasma mass spectrometry (HR-ICP-MS) (ELEMENT 2, Thermo Scientific, Germany). Element standards were prepared from certified reference single standards from CPI-International (USA).

Fungal colonisation assays

To assess fungal colonisation of *Arabidopsis* roots at 14 days post-inoculation (dpi), roots were collected into Lysing Matrix E 2 ml tubes (MP Biomedicals, USA). The tube content was crushed for 30 s at 6200 rpm. 980 µl sodium phosphate buffer (MP Biomedicals, USA) and 122.5 µl MT-buffer (MP Biomedicals, USA) were added, followed by two additional 30-secrounds of crushing at 6200 rpm. The samples were then centrifuged for 15 min at 13.000 rpm. 50 µl binding matrix (MP Biomedicals, USA) per sample was added to a 96-well plate. A filter plate (Acroprep Advance, 0.2 µm Supor filter, Pall) was placed on top of the 96-well plate, and 150 µl supernatant from each sample was transferred onto the filter plate. The plate was

centrifuged for 20 min at 1500 rpm, thereafter the flow-through was mixed with the binding matrix, by shaking for 3 min. 190 µl of each sample was transferred to a second filter plate and washed twice with 150 µl SEWS-M (MP Biomedicals, USA) by centrifuging for 5 min at 1500 rpm and the centrifuging step was repeated to dry the samples. DNA was eluted with 30 µl of ddH2O by centrifuging at 1500 rpm for 5 min, and stored at -20 °C until qPCR analysis. Fungal colonisation was then measured by qPCR as described (Mesny et al., 2021). Briefly, ITS1F/ITS2 primers for fungal ITS1 and UBQ10F/UBQ10R primers for *Arabidopsis* Ubiquitin10 were used. Reactions included iQ™ SYBR® Green Supermix, primers, and 1 µl DNA template. qPCR was run on a BioRad CFX Connect with 95°C denaturation (3 min), followed by 39 cycles of 95°C (15 s), 60°C (30 s), and 72°C (30 s). Colonisation index was calculated as $2^{-Cq(ITS1)/Cq(UBQ10)}$.

96-well fungal culture assay

Culture medium containing half strength MS medium without iron, ARE and vitamins (Table S1) was prepared, the pH was adjusted to pH 5.7 (buffered with 10 mM MES) with KOH and sterile-filtered (0.22 µm) using vacuum filtration. The medium was supplemented with scopoletin (0, 0.0625, 0.25, 1, or 2 mM) or pimaricin (0.1 mg/ml final concentration, used as an antifungal growth control) and 190µl was added per well in a 96-well plate. The wells were inoculated with 10 µl of fungal hyphal solution (stock solution of 100 mg mycelium per ml in 10mM $MgCl_2$; final concentration 5mg/ml) 10 µl of 10mM $MgCl_2$ as a blank control. The plates were sealed and incubated for 12 days at 22 °C with shaking (140 rpm), OD600 and scopoletin fluorescence (excitation 385 nm, emission 470 nm) measurements were taken daily around the same time using a TECAN spectrophotometer (Infinite® M Plex, Tecan Trading AG, Switzerland). To ensure consistency across experiments, detected fluorescence was normalised to OD600 and the initial fluorescence at day 0. To evaluate potential fungal growth inhibition by scopoletin, daily OD600 values were normalised to growth in the absence of scopoletin.

Metabolite profiling

For F80 liquid culture time-course assays, pure ethyl acetate (Honeywell Riedel-de HaënTM, LC-MS grade) was used to extract metabolites from fungal culture pellet and supernatant fractions. Extraction was performed by adding 500 µl of ethyl acetate to 1.5 ml fungal culture fractions, followed by 30 s vortexing and 10 min sonic bath. The sample was centrifuged for 10 min (13000 rpm, 4°C) and 450 µl of upper phase was collected in a new 1.5 ml test tube. The extraction was repeated two times. The combined solvent extract was dried in a TurboVap® Classic LV (Biotage) under nitrogen flow, and samples were stored at -80°C.

For exudate profiling in the plant medium, 5 ml pure ethyl acetate (Honeywell Riedel-de HaënTM, LC-MS grade) was added to 50 ml plant agar medium (harvested 1 week after transfer of 9-day-old seedlings), and samples were vortexed for 30 s and centrifuged for 10 min (4°C, 4000 rpm). The supernatant was collected and two more rounds of extraction were performed. Combined extracts were dried as described above and samples stored at -80°C.

For coumarin profiling of plant roots (harvested 1 week after transfer of 9-day-old seedlings on half strength MS medium), 200 mg (FW) ground root samples were extracted using a modified version of Blight & Dyer extraction. First, 900 µl dichloromethane/ethanol 2:1 and 100 µl HCl (pH 1.4) were consecutively added to each sample, followed by 30 s vortexing and 5 min centrifugation (4°C, 13600 rpm). The upper phase was discarded and the lower phase (approx. 700 µl) was collected into 2 ml test tubes. After adding 500 µl tetrahydrofuran to the remaining pellets, samples were vortexed for 30 s and centrifuged for 5 min (4°C, 13600 rpm). The supernatant was collected and combined with the lower phase fraction. The solvent mixture was dried as described above, and the samples stored at -80°C.

Before measurement, each sample was resuspended in 100 µl of pure methanol (Honeywell Riedel-de HaënTM, LC-MS grade) and transferred to a liquid chromatography vial with insert. Separation of metabolites by ultrahigh-performance liquid chromatography (UHPLC) was performed on a Nucleoshell RP18 (2.1 × 150 mm, particle size 2.1 µm, Macherey & Nagel, GmbH, Düren, Germany) using an ACQUITY UPLC System, equipped with a Binary Solvent Manager and Sample Manager (20 µl sample loop, partial loop injection mode, 2 µl injection volume, Waters GmbH Eschborn, Germany). Eluents A and B were aqueous 0.3 mmol/L NH4HCOO (adjusted to pH 3.5 with formic acid) and acetonitrile, respectively. Elution was performed isocratically for 2 min at 5% eluent B, from 2 to 7 min with a linear gradient to 30% B, from 7-9 min at 95% B, then 1 min at 95% B, from 10 to 11 min at 5% B, and then another minute at 5% B. The flow rate was set to 400 µl min−1 and the column temperature was maintained at 40 °C. Metabolites were detected by negative electrospray ionisation and mass spectrometry (ESI-QTOF-MS/MS). Serial dilutions of standards of scopoletin, esculetin, fraxetin and 3-(2,4-dihidroxy-5-methoxyphenyl) propanoic acid were injected every 24 samples for identification and quantification purposes. Mass spectrometric analysis was performed by MS-QTOF-IDA-MS/MS (ZenoTOF 7600, AB Sciex GmbH, Darmstadt, Germany) and controlled by SCIEX OS software (AB Sciex GmbH, Darmstadt, Germany). The source operation parameters were as follows: ion spray voltage, −4500 V; ion source gas 1, 60 psi; source temperature 600 °C; ion source gas 2, 70 psi; curtain gas, 35 psi. Instrument tuning and internal mass calibration were performed every 5 samples with the calibrant delivery system applying X500 ESI Calibrant Solution in negative mode tuning (AB Sciex GmbH,

Darmstadt, Germany). Data analysis was performed in SCIEX OS software, and MS-DIAL software (Tsugawa *et al.*, 2015).

Ferrozine iron mobilisation assay

To remove medium residues from the hyphal solution, fungal hyphae (prepared as described above) were washed three times with $MgCl_2$ by centrifugation (5 min at 11,000 xg), and resuspended in fresh $MgCl_2$. Coumarins were supplemented to the culture medium (half strength MS medium without iron, ARE and vitamins (Table S1), 10 mM MES, pH 5.7) to a final concentration of 400 µM. Cultures were inoculated with washed hyphae and grown as described for the 96-well fungal culture assay (22°C, 140 rpm, dark). Samples were collected at 0, 6, and 9 dpi, centrifuged at 3800 rpm for 20 min, the supernatant was transferred into a new 96 well plate and stored at -80 °C until processing.

To assess iron mobilisation, 120 µl sample was transferred into a 96-well plate and supplemented with a final concentration of 0.1 mM $FeCl_3$ and 0.4 mM ferrozine. Absorbance at 562 nm was measured using a TECAN spectrophotometer (Infinite® M Plex, Tecan Trading AG, Switzerland) before and after ferrozine addition. Controls included wells with water, 0.1 mM $FeCl_3$ (negative control), and 0.1 mM FeEDTA (positive control). To quantify total mobilised iron, immobile iron was removed by centrifugation (3800 rpm, 15 min), and the supernatant was transferred to a new 96-well plate. Samples were then incubated with 10 mM HCl and 10 mM ascorbic acid for 20 min in darkness to reduce the mobile iron fraction, followed by absorbance measurement at 562 nm. All values were normalised to FeEDTA samples (before reduction), and $FeSO_4$ calibration curves were used for quantification of mobile iron.

Results

M. phaseolina (F80) enhances iron nutrition in *Arabidopsis* under iron limiting conditions

To test whether fungal endophytes can improve plant iron nutrition, we modified a previously reported gnotobiotic agar-based plant growth assay that allows precise modulation of iron bio-availability and the co-cultivation of *Arabidopsis* plants with root microbiota members (Harbort *et al*., 2020 - STAR protocols). The system relies on half strength MS medium buffered at pH 5.7 with MES and supplemented with either unchelated iron ($FeCl_3$) or chelated iron (FeEDTA), which reflect bio-unavailable iron (unavFe) and bio-available iron (avFe) conditions, respectively. Using this system, we assessed the ability of the fungal root endophyte F80 to enhance the performance of *Arabidopsis* Col-0 wild-type plants under unavFe conditions. F80 was identified previously as part of a culture collection of 41 fungal isolates representative of the *Arabidopsis* root mycobiota (Mesny *et al.*, 2021). Plant performance was evaluated after

two weeks of co-cultivation with fungus or mock treatments using shoot fresh weight (SFW) and shoot total chlorophyll concentration as a proxy for iron status. Three-week-old *Arabidopsis* seedlings exhibited enhanced growth and reduced leaf chlorosis when inoculated with F80 under iron-limiting conditions, closely resembling the avFe phenotype (Figure 2a). Plants grown at unavFe and inoculated with F80 exhibited a significant increase in SFW and shoot chlorophyll concentration compared to mock-treated controls (Figure 2b,c). By contrast, we did not observe F80-mediated plant growth promotion or increased chlorophyll under avFe conditions (Figure 2b,c). Plants inoculated with heat-killed F80 behaved similarly to mock-treated plants (Figure S1), highlighting the importance of live fungus and that putative inoculum-derived iron contamination is negligible. To ascertain whether the observed phenotypes reflect iron status of the plant, the shoot elemental content was measured by HR-ICP-MS (Figure 2d). This analysis showed that F80-inoculated plants accumulated significantly more iron in their shoots under unavFe compared to mock conditions, almost reaching the iron content of plants grown at avFe (Figure 2d). In line with SFW and shoot chlorophyll concentration, no F80-mediated increase in shoot iron content was observed in avFe conditions (Figure 2d). Taken together, these results show that F80 mediates *Arabidopsis* iron nutrition specifically in conditions of limited iron bioavailability. This implies that F80 improves plant access to immobile iron pools in the growth medium.

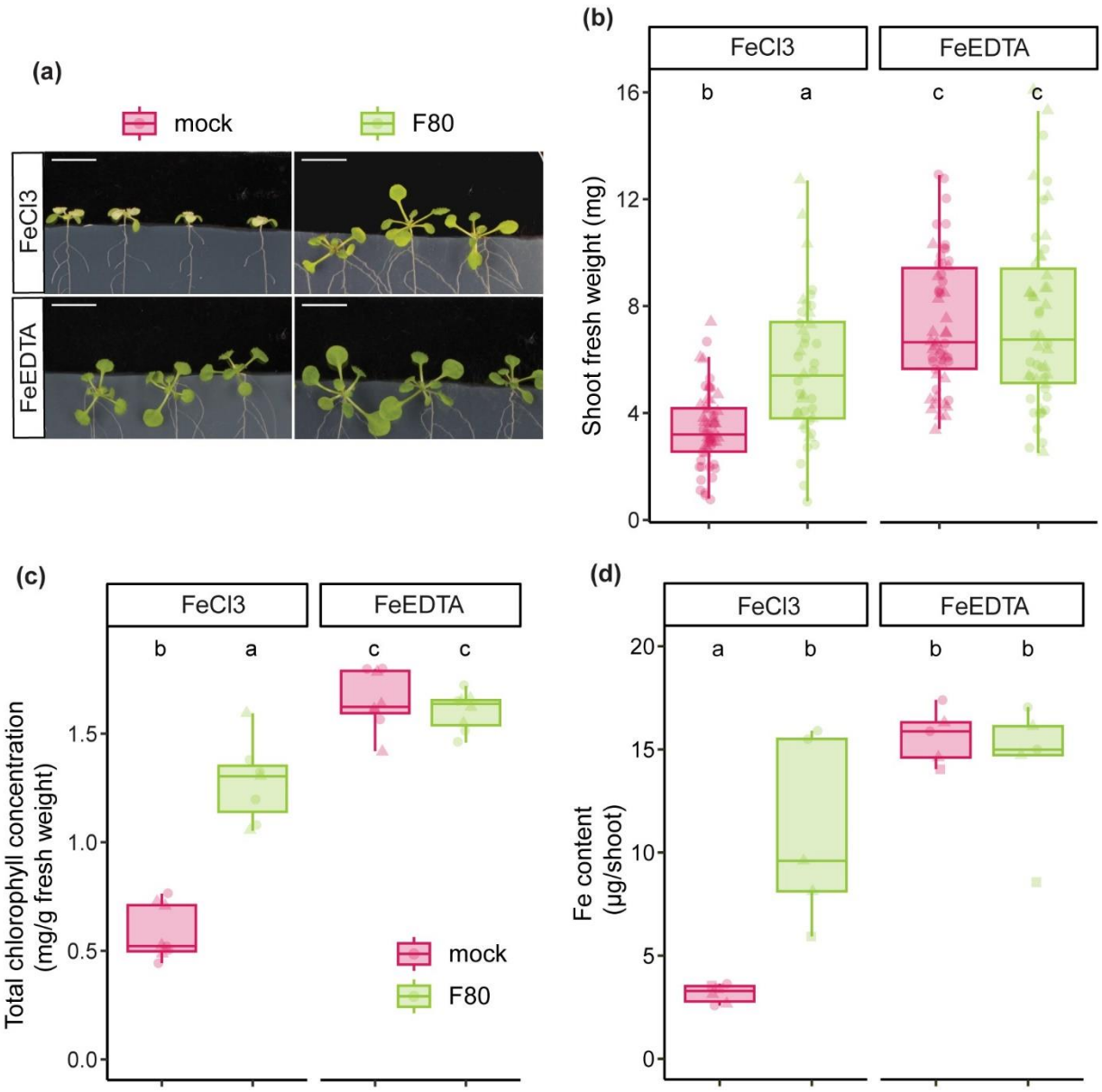

Figure 2. Fungal endophyte *M. phaseolina* (F80) improves *Arabidopsis* iron nutrition under iron limitation.

(a) representative phenotypes, (b) SFW, (c) shoot chlorophyll concentration, and (d) shoot Fe content of Col-0 *Arabidopsis* seedlings. 7-day-old seedlings were transferred to half-strength MS medium and grown for 2 weeks on mock or F80 inoculated plates in unavFe (50µM FeCl3) or avFe (50µM FeEDTA) conditions. Letters indicate significant pairwise differences between groups (p-adj≤0.05) by Dunn pairwise comparison test with Benjamini-Hochberg correction (b,c) or a Tukey's HSD corrected for multiple comparisons (d). Scale bars, 1 cm (a). Data are from two (b,c) or three (d) full factorial replicates (represented by different shapes).

Root-derived scopoletin and host iron-reductive import machinery are essential for F80-mediated plant iron nutrition

Given that F80-mediated plant iron nutrition is specific to iron-limiting conditions and the established link between iron limitation-induced coumarin production and bacterial-mediated improvements in plant iron nutrition (Harbort *et al.*, 2020), we investigated whether F80-mediated improved in iron nutrition of *Arabidopsis* also requires plant-derived coumarins. To this end, we grew the coumarin-deficient *Arabidopsis* mutant *f6'h1* lacking the first step of the coumarin biosynthesis pathway (Kai *et al.*, 2008; Schmidt *et al.*, 2014; Schmid *et al.*, 2014) in unavFe conditions. Compared to Col-0, *f6'h1* plants exhibited reduced ability to tolerate iron deficiency, indicated by their lower SFW and shoot chlorophyll concentration under mock conditions (Figure 3a,b). While F80-mediated rescue of plant iron deficiency was observed in Col-0 plants, F80 failed to improve the performance of *f6'h1* plants, with both SFW and chlorophyll levels remaining below the mean values observed for Col-0 (Figure 3a,b). Consistently, shoot iron content in *f6'h1* plants did not significantly increase upon F80 inoculation and remained comparable to mock-treated controls (Figure 3c).

To examine whether F80 interacts with specific coumarins to facilitate rescue of plant iron deficiency, we used the *s8h* and *cyp82c4* mutant lines which fail to produce fraxetin and sideretin, respectively, yet retain the ability to synthesise scopoletin (Rajniak *et al.*, 2018; Tsai *et al.*, 2018). Inoculation of *s8h* plants with F80 resulted in a significant increase in SFW and shoot chlorophyll concentration, reaching levels comparable to those of F80-inoculated Col-0 plants. This trend was also observed for shoot iron content, as *s8h* plants treated with F80 accumulated similar levels of iron as Col-0 (Figure 3c). Similarly, F80 inoculation improved the performance of *cyp82c4* plants reflected in increased SFW, chlorophyll concentration and shoot iron content compared to mock-treated controls, although levels in *cyp82c4* remained slightly lower than those of Col-0 and *s8h* plants (Figure 3a,b,c). These data show that the fungal root endophyte alleviates plant iron starvation in a coumarin-dependent manner and that the coumarin scopoletin interacts with F80 to rescue host iron deficiency.

To investigate whether F80-mediated plant iron rescue depends on the plant's ability to reduce ferric (Fe^{3+}) and import ferrous (Fe^{2+}) iron, we assessed mutants of *FRO2* and *IRT1*, two key components of the iron acquisition system in *Arabidopsis*. As previously reported, the *fro2* and *irt1* mutants were acutely sensitive to iron limitation, resulting in small and chlorotic plants under unavailable iron conditions (Robinson *et al.*, 1999; Vert *et al.*, 2002; Varotto *et al.*, 2002; Paffrath *et al.*, 2023). F80 failed to effectively increase *fro2* and *irt1* SFW, shoot chlorophyll concentration and shoot iron content (Figure 3a,b,c). This suggests that the F80-mediated rescue involves ferric iron mobilisation and requires downstream Fe^{3+} reduction by FRO2 as well as ferrous iron transport by IRT1. The concentration of other elements in the shoots were

also evaluated for all genotypes by HR-ICP-MS, however no similar trends were observed (Figure S5). The observed differences in F80-mediated plant iron nutrition were not attributed to variation in fungal colonisation, as F80 colonisation levels were similar in all plant genotypes (Figure S2c). Analysis of all plant genotypes at avFe confirmed that F80-mediated rescue is specific to iron deficiency as there were no differences observed in shoot chlorophyll of mock versus F80 inoculated plants (Figure S2a,b). Additionally, presence of FeEDTA completely restored plant growth of all tested coumarin mutants, indicating that coumarins are not required for plant growth at avFe. As anticipated, FeEDTA did not fully restore chlorophyll levels in *fro2* and *irt1*, as iron reduction and uptake are still required under this condition (Figure S2a,b). For all genotypes except *s8h*, an increase in SFW was observed in avFe conditions in the presence of F80, which might reflect a general beneficial effect of the fungus on plant growth. The results suggest that F80-mediated *Arabidopsis* iron acquisition depends on plant coumarin synthesis, especially scopoletin, and requires a functional plant reductive iron transport machinery to facilitate iron uptake.

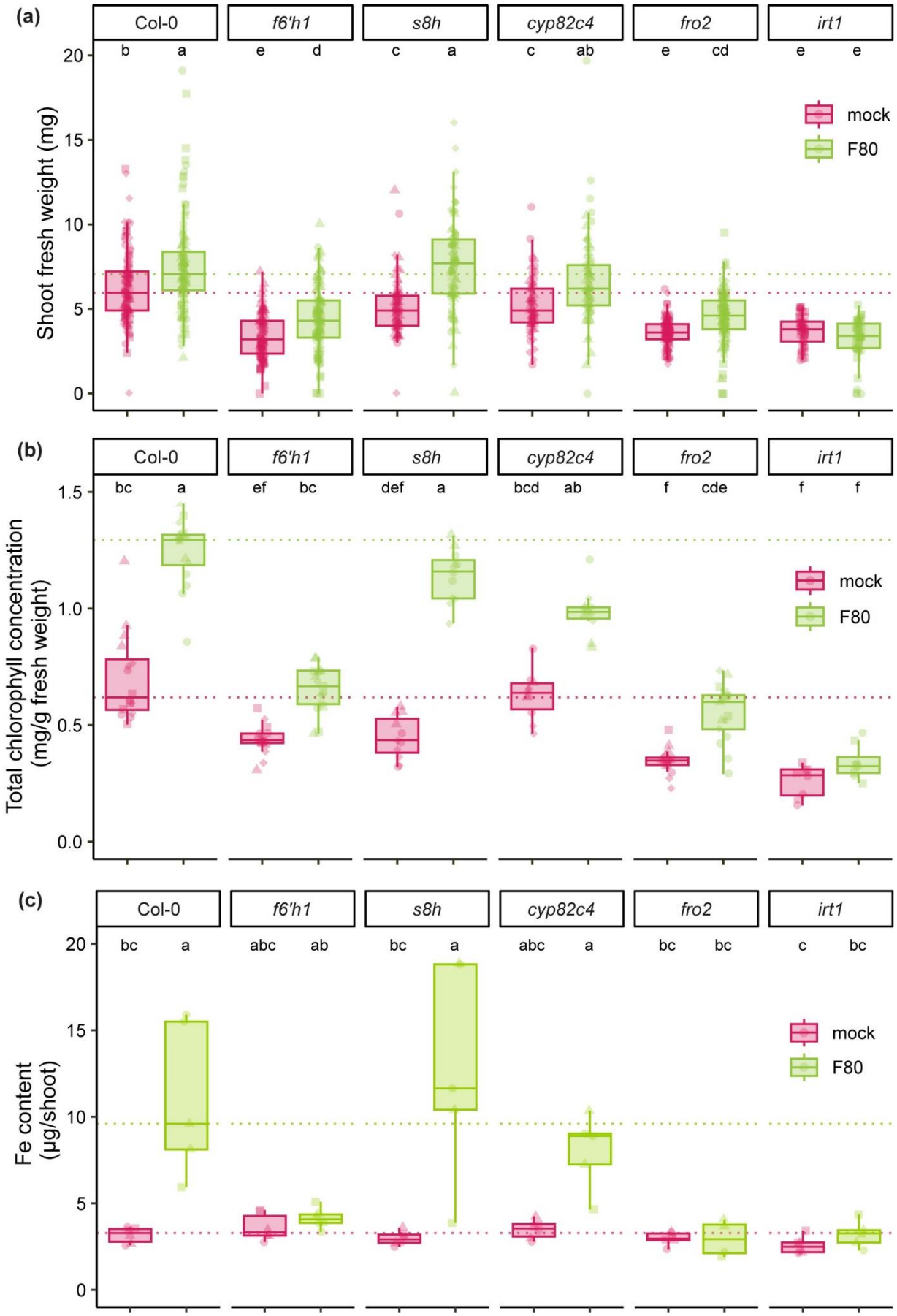

Figure 3. Rescue of iron deficient *Arabidopsis* plants by the fungal root endophyte F80 requires the coumarin scopoletin and the plant's iron reductive import system.

(a) SFW, (b) shoot chlorophyll concentration and (c) shoot Fe content measured by ICP-MS at 2 weeks of growth after transfer of the indicated mutants in the coumarin biosynthesis pathway and the iron reductive import mechanism. 7-day-old seedlings were transferred to half strength MS medium with unavFe (50µM FeCl3) at pH 5.7 mock or inoculated with F80. Dashed line indicates the mean of Col-0.

Letters indicate significant pairwise differences between groups (p-adj≤0.05) by a Dunn pairwise comparison test with Benjamini-Hochberg correction. Statistical significance within genotypes was determined by a Kruskal-Wallis test. Data are from four (a,b) or three (c) full factorial replicates (represented by different shapes).

F80 converts scopoletin into iron-chelating esculetin

Scopoletin is recognised for its selective antimicrobial activity (Sun *et al.*, 2014a; Zamioudis *et al.*, 2014; Lemos *et al.*, 2020; Harbort *et al.*, 2020)). To evaluate the sensitivity of F80 to scopoletin, an *in vitro* time-course assay was performed to monitor the fungal growth in the presence of 2 mM scopoletin in a liquid culture. To additionally assess potential F80-mediated alterations of scopoletin, we tracked scopoletin-derived fluorescence in the cultures over time under long-wave UV (Goodwin & Kavanagh, 1949). Under mock conditions, the expected scopoletin-derived fluorescence remained largely constant, confirming stability of scopoletin in the absence of the fungus. This is consistent with a previous study using mass spectrometry-based quantification of coumarins (Rajniak *et al.*, 2018). In the presence of F80, scopoletin-derived fluorescence decreased rapidly between 3- and 6-days post-inoculation (dpi) (Figure 4a). A scopoletin alteration effect was also indicated by the fungal growth pattern: relative growth of F80 (growth in 2 mM scopoletin/growth in control) decreased from 2 to 5 dpi but recovered from 6 dpi onwards, coinciding with a near-complete disappearance of scopoletin fluorescence (Figure S3b). These data suggest that F80 can evade scopoletin antimicrobial activity by a possible detoxification mechanism that alters scopoletin.

To validate whether F80 alters scopoletin, liquid cultures of the fungus were separated into supernatant and mycelia, and metabolites were profiled by UHPLC-MS/MS. The MS/MS data corroborated the fluorescence-based results in showing a steep decrease in scopoletin levels from 3 to 6 dpi with F80 (Figure 4b, S3d). Notably, a different coumarin molecule, esculetin, was detected in the samples supplemented with scopoletin, and displayed increased abundance from 3 dpi onwards. At the same time, additional degradation products containing hydrolysed lactone rings were observed. Untargeted UHPLC-MS/MS profiling of the samples revealed that the most abundant compound detected, besides scopoletin, was 3-(2,4-dihydroxy-5-methoxyphenyl) propanoic acid ($C_{10}H_{12}O_5$) (Figure 4b, S3d). At 12 dpi, all coumarin compounds, including scopoletin, esculetin, and 3-(2,4-dihydroxy-5-methoxyphenyl) propanoic acid, were nearly undetectable. This suggests that further modification or complete degradation through F80, or compound instability, occurs in this assay. Both, esculetin and the open-lactone structure were detected exclusively in scopoletin-supplemented samples in the presence of the fungus but not in fungal cultures alone (Figure 4b, S3d).

Given that esculetin, an iron-mobilising coumarin (Schmid *et al.*, 2014; Paffrath *et al.*, 2023), was identified as a scopoletin-conversion product, we next tested the interaction of esculetin with F80. First, esculetin stability in F80 cultures supplemented with 2 mM esculetin was

assessed by measuring its levels in the supernatant and fungal pellet over time. Esculetin showed only a slow decline and was still detectable at 12 dpi (Figure 4c, S3e). In parallel, since fraxetin accumulates in the roots of *cyp82c4* plants which support F80-mediated rescue, the stability of fraxetin was evaluated in the presence of F80 in culture (Figure 3a,b,c). Compared to esculetin, fraxetin was more rapidly depleted by the fungus, especially in the supernatant (Figure 4d, S3f). To further investigate the interaction of F80 with these coumarins, relative growth of F80 in the presence of esculetin or fraxetin was evaluated over time. In comparison to F80 cultures supplemented with scopoletin, F80 cultures supplemented with esculetin or fraxetin did not show a decrease in relative growth (Figure S3b,c). The observed F80 conversion of scopoletin to esculetin, a compound that does not affect F80 growth, further supports a fungal detoxification mechanism.

Because our *in planta* data imply a role for F80 in improving plant access to immobile ferric iron through interactions with scopoletin - a coumarin which lacks a catechol moiety and *in vitro* iron mobilising capacity (Figure 3a,b,c) (Schmidt *et al.*, 2014; Rajniak *et al.*, 2018; Paffrath *et al.*, 2023) - we hypothesised that F80-mediated alteration of scopoletin is the cause of iron mobilisation to the plant. To test this, we made use of a spectrophotometric assay which quantifies mobile iron based on the ferrozine-Fe(II) complex. Fraxetin and esculetin were included in the analysis because esculetin was detected in the F80-scopoletin cultures (Figure 4b, S3d) and fraxetin produced in F80-rescued *cyp82c4* plants might also interact with the fungus. As expected, the catecholic coumarins fraxetin and esculetin, but not scopoletin, mobilised iron under mock conditions (Figure 4e). However, when F80 was cultured with these coumarins, differential effects on total iron mobilisation were observed. In F80 cultures supplemented with scopoletin, there was an increase in mobilised iron at 6 and 9 dpi (Figure 4e), perhaps due to the conversion of scopoletin to esculetin by F80 (Figure 4b). Conversely, total iron mobilisation in cultures supplemented with fraxetin or esculetin in the presence of the fungus decreased significantly at 6 and especially 9 dpi (Figure 4e). The results suggest that F80 affects iron mobilisation differently depending on the coumarin substrate it encounters. While scopoletin likely serves as a precursor to iron-chelating compounds such as esculetin, fraxetin and esculetin participate directly in iron-binding dynamics.

These findings show that an interaction between F80 and scopoletin yields synergistic amounts of mobilised iron. Put together with F80's capability to convert scopoletin to the catechol coumarin esculetin, we reasoned that increased iron mobility might be due to the presence of esculetin. This could explain the observed F80-mediated *Arabidopsis* iron nutrition.

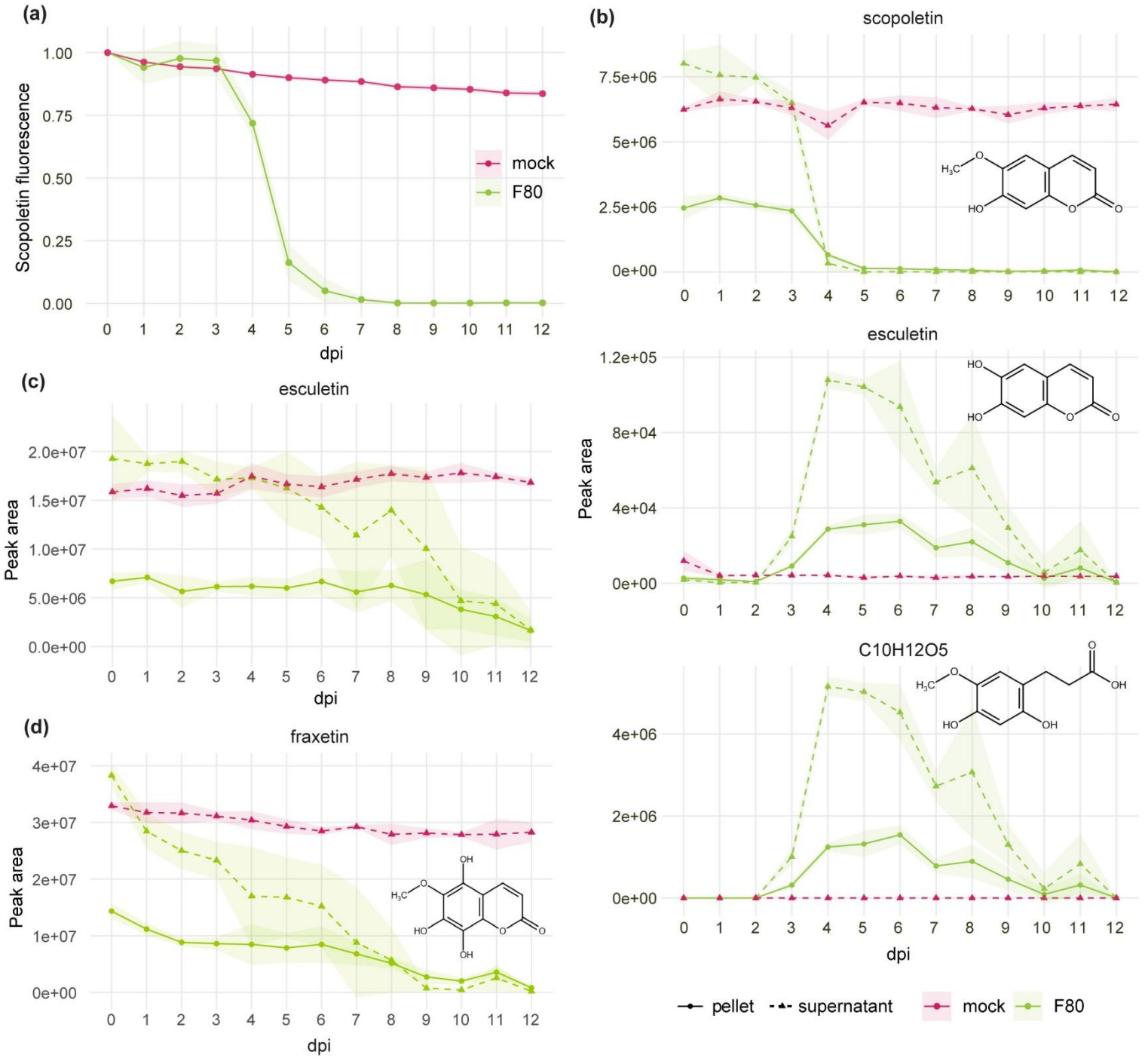
(a)
Scopoletin fluorescence
1.00
0.75
0.50
0.25
0.00
0 1 2 3 4 5 6 7 8 9 10 11 12
dpi
mock
F80
(b)
scopoletin
7.5e+06
5e+06
2.5e+06
0e+00
esculetin
1.2e+05
8e+04
4e+04
0e+00
Peak area
C10H12O5
4e+06
2e+06
0e+00
dpi
pellet
supernatant
mock
F80
(c)
esculetin
2.0e+07
1.5e+07
1.0e+07
5.0e+06
0.0e+00
Peak area
dpi
(d)
fraxetin
4e+07
3e+07
2e+07
1e+07
0e+00
Peak area
dpi

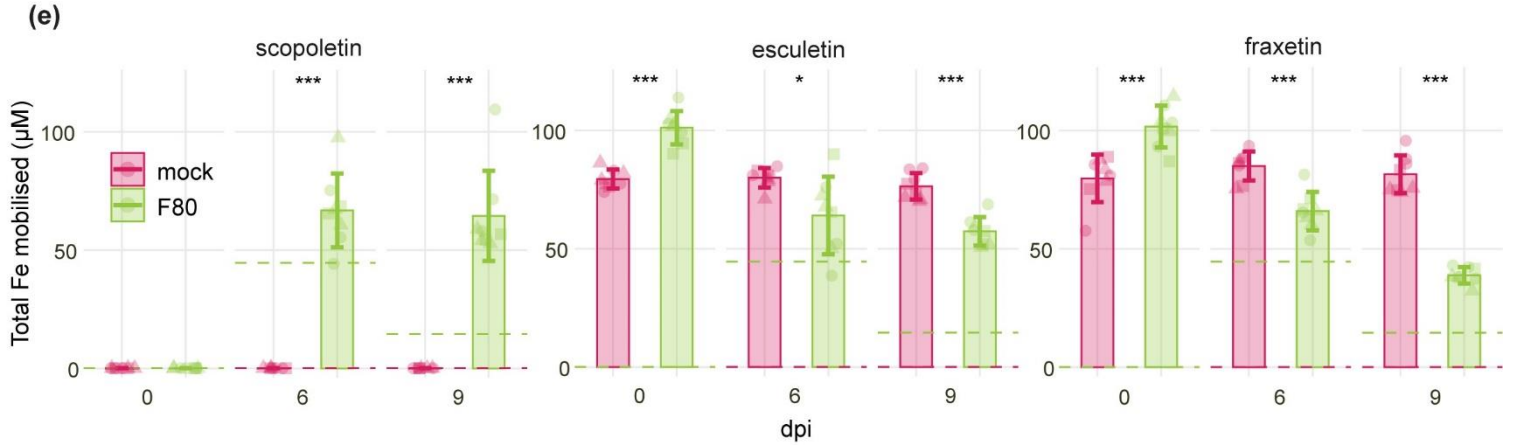
(e)
scopoletin
esculetin
fraxetin
Total Fe mobilised (µM)
100
50
0
mock
F80
***
*
0 6 9
dpi

Figure 4. The fungal endophyte F80 converts scopoletin into esculetin and further degradation compounds.
(a) Time course of 0-12 dpi displaying specific scopoletin fluorescence measured in *in vitro* mock and F80 cultures supplemented with 2mM scopoletin (excitation at 385nm and emission detected at 470nm). Data combined from 3 biological replicates. The curve-shade indicates the standard error. The Area Under the Curve of graph (a) is shown in Figure S3a. (b) MS-QTOF-IDA-MS/MS peak area of scopoletin, esculetin and 3-(2,4-dihydroxy-5-methoxyphenyl) propanoic acid (C10H12O5) in F80 culture supernatant (dashed line) and the fungal pellet (full line) grown for 0-12 dpi supplemented with 2mM scopoletin. Curve-shade indicates mean ± SD. Absolute concentration values are presented in Figure S3d. (c) MS-QTOF-IDA-MS/MS peak area of esculetin in F80 culture supernatant (dashed line) and the fungal pellet (full line) grown for 0-12 dpi supplemented with 2mM esculetin. Curve-shade indicates mean ± SD. Absolute concentration values are presented in Figure S3e. (d) MS-QTOF-IDA-MS/MS peak area of fraxetin in F80 culture supernatant (dashed line) and the fungal pellet (full line) grown for 0-12 dpi supplemented with 2mM fraxetin. Curve-shade indicates mean ± SD. Absolute concentration values are presented in Figure S3f. (e) Total amount of iron mobilised from poorly soluble $FeCl_3$ (0.1 mM) in the F80 culture supernatant or axenic medium (mock) supplemented with scopoletin, fraxetin, or esculetin (final concentration of 0.4 mM) at 0, 6, or 9 dpi. Mobilised iron was assessed spectrophotometrically based on a Fe(II)-ferrozine assay. Control values for treatments without fungus (red) or without coumarins (green) are included as dashed lines. Error bars represent mean ± SD, statistical differences between treatments were assessed using *t*-tests for normally distributed residuals or, otherwise, Wilcoxon rank-sum tests. Significance levels are indicated by asterisks with *p<0.05, **p<0.01, and ***p<0.001. All panels represent data from three biological replicates (represented by different shapes).

F80 and scopoletin cooperate to mobilise ferric iron in the rhizosphere

To assess whether F80 interaction with coumarins observed in culture translate into iron mobilisation effects *in planta*, we conducted coumarin supplementation assays using the coumarin-deficient *f6'h1* mutant. This approach provided a coumarin-free plant background, enabling evaluation of the importance and sufficiency of specific coumarins for plant physiological fitness and growth under iron limitation. Based on the positive interaction of F80 and scopoletin in enhancing iron mobilisation and growth recovery of *f6'h1* plants at avFe (Figure S2a,b), we hypothesised that combinatorial treatment of the plant growth medium with F80 and scopoletin would result in increased mobile ferric iron and, in turn, restore iron limiting plant growth of *f6'h1*. Addition of 10 µM scopoletin to the plant growth medium under mock (non-F80) conditions did not significantly increase SFW or chlorophyll concentration in *f6'h1* to levels observed in Col-0 inoculated with F80 (Figure 5a,b). When combined with F80 inoculation, scopoletin supplementation restored F80-mediated rescue, with both SFW, chlorophyll and shoot iron concentrations being similar to Col-0 inoculated with F80 (Figure 5a,b, S5). Strikingly, the cooperative effect of F80 and scopoletin resembled the mock phenotypes of 10 µM fraxetin or esculetin supplementations, which increased SFW and chlorophyll concentration to levels comparable to Col-0 with F80 (Figure 5a,b). Supplementation of fraxetin or esculetin in the presence of F80 resulted in slightly reduced SFW and chlorophyll levels compared to the corresponding mock conditions (Figure 5a,b), in line with the fungal culture supernatant iron mobilisation data (Figure 4e).

To further understand the role of F80 in the iron import pathway of *Arabidopsis* plants, scopoletin, fraxetin or esculetin were added to the growth medium of *fro2* mutant plants. Importantly, none of these compounds significantly enhanced SFW or chlorophyll concentration in *fro2*, either alone or in combination with F80 (Figure S4a,b). This underscores the necessity of a functional FRO2 for F80-mediated alleviation of plant iron deficiency. It also supports the notion that F80 cooperatively interacts with scopoletin to mediate ferric iron mobilisation in the rhizosphere. To critically test the impact of chemical iron mobilisation on *f6'h1* and *fro2* mutants, 10 µM NaEDTA (a synthetic iron chelator) was added to the medium. In *f6'h1* plants, NaEDTA supplementation almost fully rescued the iron-deficiency phenotype under mock and F80-inoculated conditions (Figure S4c,d). This aligns with a previous study showing that iron chelators like NaEDTA can bypass the requirement for microbial interactions by artificially increasing iron solubility (Jin *et al.*, 2006). By contrast, no significant NaEDTA-mediated rescue was observed in *fro2* mutants (Figure S4c,d). This result reinforces the conclusion that FRO2 is essential for the iron uptake pathway when bio-available ferric iron is present in the form of Fe(III)-chelates (Figure S4c, S3d). F80 colonisation of roots remained consistent across all experimental conditions, indicating that differences in rescue phenotypes were not due to variation in fungal colonisation (Figure S4e).

To test whether F80 can also use plant-synthesised scopoletin, we quantified differences in scopoletin concentration in root exudates of Col-0 plants grown over 7 d in the presence or absence of F80. HRLC-MS/MS analysis revealed that the presence of F80 strongly decreased scopoletin levels in the agar medium in both unavFe and avFe conditions (Figure 5c). Levels of scopolin and scopoletin quantified inside root tissues from this experiment revealed no significant differences between treatments (Figure S4f). Altogether, the data suggest that F80 and scopoletin interact cooperatively in the rhizosphere to mediate ferric iron mobilisation upstream of the FRO2-IRT1 reductive import module.

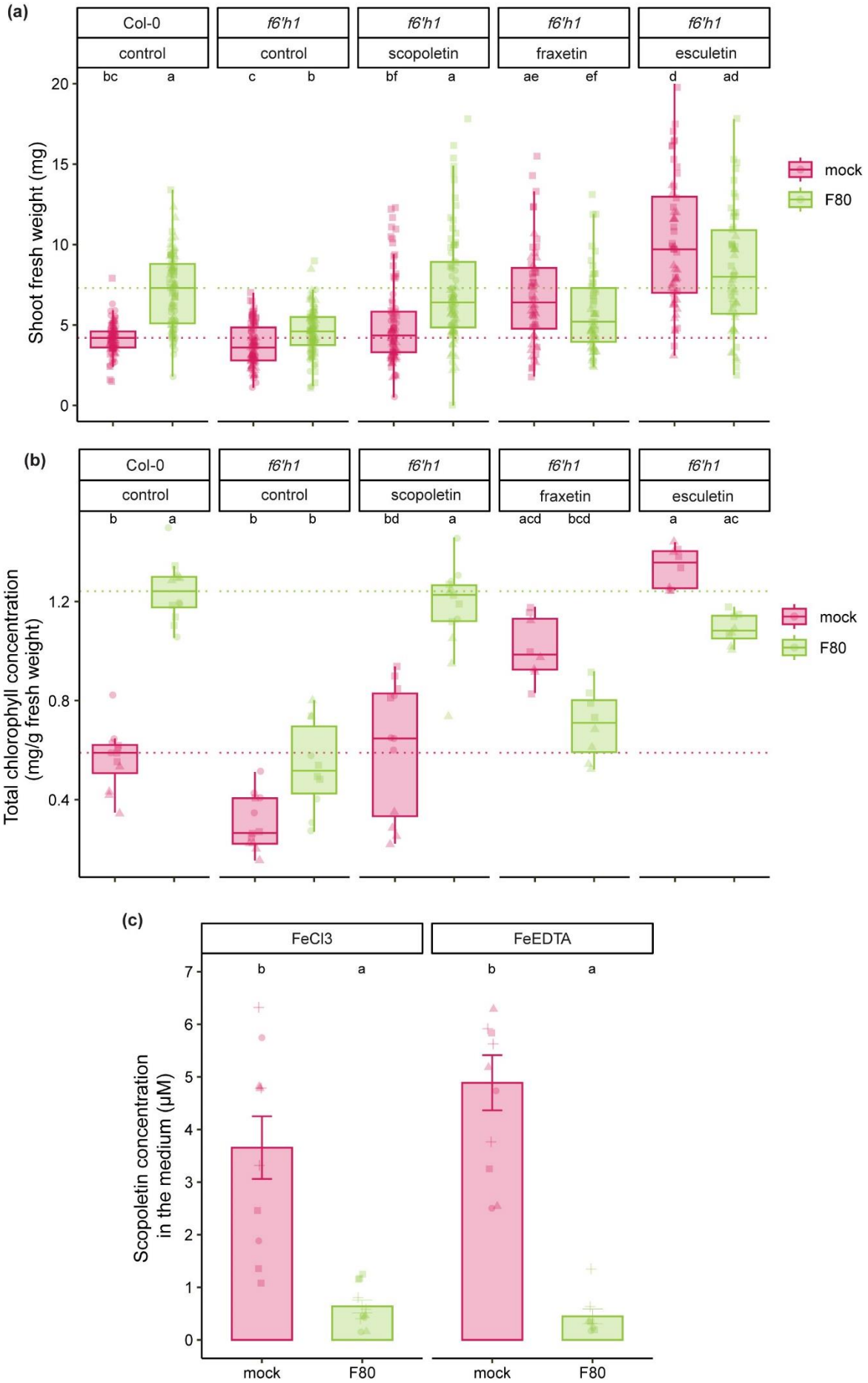

Figure 5. Interaction between the fungal endophyte F80 and scopoletin rescues the coumarin-deficient mutant *f6'h1*. (a) SFW and (b) shoot chlorophyll content of Col-0 and *f6'h1* plants 2 weeks past inoculation. 7-day-old seedlings were transferred to half-strength MS medium with unavailable iron (50 µM FeCl3) at pH 5.7, supplemented with 10 µM of the indicated coumarins or an equal amount of DMSO for the control, and mock or inoculated with F80. Dashed line indicates the mean of Col-0. Letters

indicate significant pairwise differences between groups (*p*-adj≤0.05) by a Dunn pairwise comparison test with Benjamini-Hochberg correction. Data are from three full factorial replicates (represented by different shapes). (c) The concentration of scopoletin exuded after 1 week in the medium of 9-day-old seedlings transferred to half-strength MS medium with unavailable (50 µM FeCl3) or available (50 µM FeEDTA) iron at pH 5.7 mock or inoculated with F80. Metabolites were extracted from approximately 50 ml of the medium and analysed with MS-QTOF-IDA-MS/MS. Bars represent the mean from 4 biological replicates (n=2-3) with standard error bars. Letters indicate significant pairwise differences between groups (*p*-adj≤0.05) by a Tukey's HSD corrected for multiple comparisons.

Discussion

Coumarins are crucial for plant iron uptake in conditions of low iron availability. Scopoletin is one of the most abundant coumarins in root exudates of *Arabidopsis* plants grown under iron-limiting conditions (Sisó-Terraza *et al.*, 2016; Rosenkranz *et al.*, 2021), despite its inability to chelate and mobilise iron. Scopoletin is mainly described for its selective antimicrobial activity against fungi and commensal bacteria (Ba *et al.*, 2017; Harbort *et al.*, 2020; Yu *et al.*, 2021), but its potential role in plant iron nutrition remains undefined. Here, we show that scopoletin and the fungal root endophyte *Macrophomina phaseolina* F80 cooperate to provide mobile Fe^{3+} for subsequent import via the plant reductive import module consisting of the ferric chelate reductase FRO2 and the ferrous iron importer IRT1 (Figure 6). Our results support a pivotal role of scopoletin in the intricate interplay between F80 and its host plant, whereby scopoletin production and interaction with F80 in the rhizosphere enables the rescue of iron-deficient *Arabidopsis*.

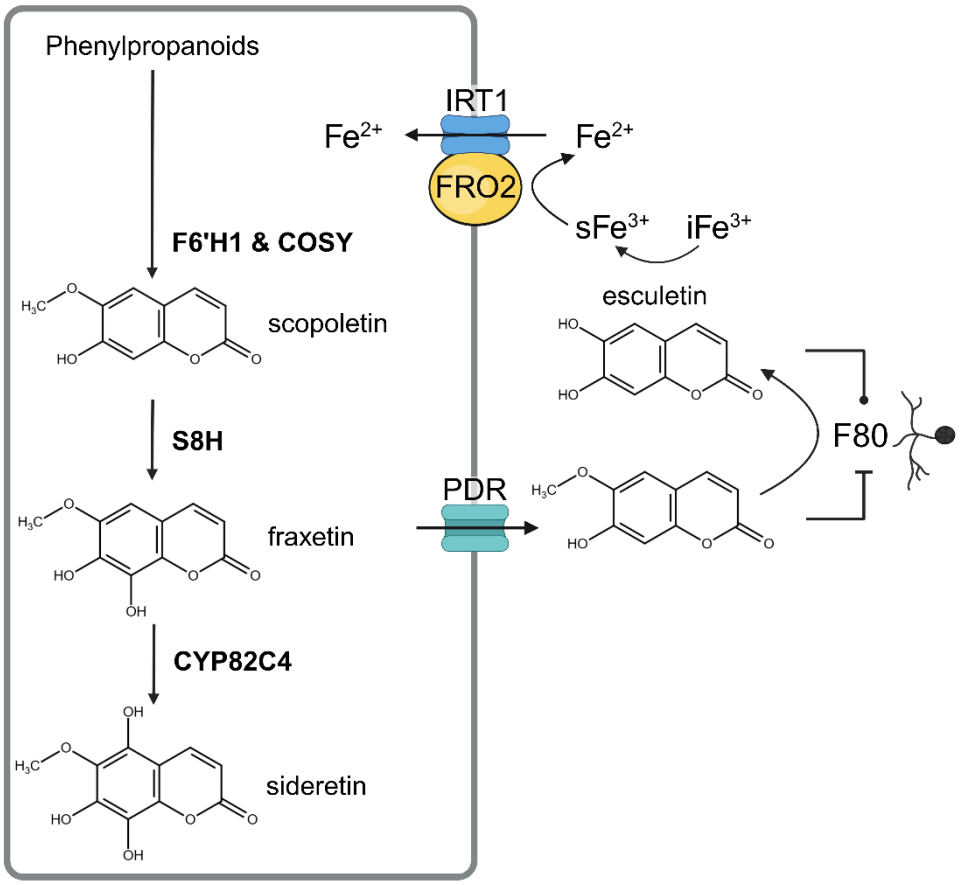

Figure 6. Model for the interaction of the fungal root endophyte *M. phaseolina* F80 with root-derived scopoletin to mediate iron nutrition in *Arabidopsis*
Iron stress promotes coumarin biosynthesis and exudation in *Arabidopsis* roots. The first steps in coumarin biosynthesis are catalysed by F6'H1 and COSY leading to the production of scopoletin. Subsequent conversion to fraxetin and sideretin occurs through the activity of S8H and CYP82C4, respectively. Coumarins are secreted into the rhizosphere by transporters from the PDR family. Once secreted to the rhizosphere, coumarins assist plants in iron acquisition from the soil environment. The catechol coumarins fraxetin, sideretin and esculetin can directly mobilise iron. Our model proposes a cooperative interaction between the fungal root endophyte F80 and the coumarin scopoletin, which enhances ferric iron mobilisation in the rhizosphere, upstream of the plant's FRO2-IRT1 reductive iron uptake system. *Ex planta* data suggest that F80 mediates the conversion of scopoletin into the catechol coumarin esculetin, facilitating iron solubility and rescuing iron-deficient plant growth. (Figure made with Biorender)

Our data suggest that ferric iron mobilisation is conferred through fungal conversion of the F80-inhibitory non-catechol coumarin scopoletin to a non-inhibitory catechol coumarin esculetin which is a potent Fe^{3+} chelator (Figure 4, S3, 6) (Schmidt *et al.*, 2014; Schmid *et al.*, 2014; Paffrath *et al.*, 2023). Because fungal mediated scopoletin conversion also occurs in the rhizosphere during plant colonisation (Figure 5c), it is likely to represent a key mechanism by which the fungus enhances iron availability. The scopoletin to esculetin transition not only enhances iron solubility but might also represent a "win–win" scenario benefiting both the fungal endophyte and its host: the fungus mitigates scopoletin antimicrobial inhibitory effects while the plant gains access to more bioavailable iron. This scenario is supported by i) *ex-planta* time-course experiments that showed decreasing abundance of scopoletin coupled with esculetin generation in the presence of F80 and ii) cooperative iron mobilisation by scopoletin and F80 yielding similar levels of mobilised iron as those provided by esculetin alone (Figure 4). Host rescue from limiting iron was entirely dependent on coumarin production as no rescue was observed in the coumarin-deficient *f6'h1* mutant (Figure 3). By contrast, *s8h* mutants which produce scopoletin but lack fraxetin and sideretin supported fungal-mediated rescue of iron deficiency (Figure 3). Thus, scopoletin appears to be necessary and sufficient for plant iron nutrition in the presence of this fungal root endophyte. A role of scopoletin in iron mobilisation was further confirmed by chemical complementation experiments. Scopoletin supplementation restored F80-mediated rescue of *f6'h1* plants to similar levels of catechol coumarins or the synthetic iron chelator EDTA in mock conditions (Figure 5). Collectively, these findings highlight a new type of plant-microbe interaction in which a fungal endophyte repurposes a plant-derived coumarin precursor to generate bioavailable iron-chelating compounds.

Coumarin production and exudation are highly induced upon iron starvation (Fourcroy *et al.*, 2014; Schmid *et al.*, 2014; Sisó-Terraza *et al.*, 2016; Tsai *et al.*, 2018; Paffrath *et al.*, 2023). Current literature suggests that fraxetin and sideretin are the primary coumarins responsible for iron acquisition (Rajniak *et al.*, 2018; Tsai *et al.*, 2018; Robe *et al.*, 2021c; Paffrath *et al.*, 2023). Based on their exudation profiles and ability to chelate and reduce iron in varying pH conditions, fraxetin appears to be more important at alkaline pH whereas sideretin primarily

functions at more acidic pH (Paffrath *et al.*, 2023). Scopoletin, although not an efficient iron mobiliser is, together with the redox-active sideretin the most abundant coumarin detected in *Arabidopsis* root exudates under acidic conditions (Sisó-Terraza *et al.*, 2016; Rosenkranz *et al.*, 2021; Paffrath *et al.*, 2023). Thus, a chief role of scopoletin in shaping the rhizosphere microbiome was thought to be through its inhibitory properties (Stringlis *et al.*, 2018b). Our results demonstrate that scopoletin can also contribute indirectly to iron nutrition as a precursor for iron-chelating coumarins generated by microbial conversion.

F80 was isolated from apparently healthy *Arabidopsis* plants in natural populations sampled in Europe (Durán *et al.*, 2018; Thiergart *et al.*, 2020). Previous studies demonstrated that this fungal strain alleviated phosphate starvation in agar-plate assays (Mesny *et al.*, 2021), suggesting that F80 may also be relevant in mitigating other forms of nutrient stress. These and our data reinforce the notion that F80 can exist as a neutral or beneficial endophyte associated with *Arabidopsis* roots. Conversely, *M. phaseolina* strains are well-documented plant pathogens responsible for charcoal rot, a disease affecting over 500 plant species including crops such as maize, soybean, and canola (Su *et al.*, 2001; Bandara *et al.*, 2018; Sinha *et al.*, 2022). The ability of *M. phaseolina* F80 to degrade scopoletin might have ecological implications, for example, in promoting plant iron nutrition in certain environments and/or conferring microbial competition for niche establishment. Esculetin, for example, was found to inhibit certain fungal pathogens (Beesley *et al.*, 2023). Notably, scopoletin has been implicated in plant defence as its increased accumulation was associated with enhanced resistance against pathogens (Zamioudis *et al.*, 2014). Therefore, fungal-mediated degradation of scopoletin could benefit pathogens by mitigating plant defence (Sun *et al.*, 2014a; Gao *et al.*, 2024). At this stage, it remains unclear whether scopoletin conversion by *F80* is driven by a specific enzymatic activity. Alternatively, the fungus might generate a physicochemical environment that facilitates non-enzymatic oxidation and demethylation to esculetin, as previously observed during coumarin-mediated iron-oxide dissolution at the surface of iron minerals (Baune *et al.*, 2020). Scopoletin was found to be degraded in four different unsterilised soils, indicating that this trait might be ecologically relevant and prevalent (Galán-Pérez *et al.*, 2021).

Microbe-assisted nutrient acquisition is an emerging concept in plant nutrition, with many studies focusing on bacterial siderophores as key contributors to plant iron uptake (Kramer *et al.*, 2019). In this context, the role of fungal endophytes remains largely unexplored. To our knowledge, this study provides the first mechanistic basis for an endophytic fungus directly enhancing plant iron nutrition through its interaction with a plant-derived coumarin. It therefore represents a significant advance in our understanding of how commensal fungal associations can strengthen plant nutritional resilience and productivity. Given the widespread occurrence

of endophytes in natural and agricultural ecosystems and scopoletin-secreting dicot plants, future research might identify similar coumarin transformations in other plant-microbe associations.

In conclusion, we reveal here a fungal endophyte contribution to plant iron nutrition. By demonstrating that *M. phaseolina* (F80) converts scopoletin into bioactive iron-chelating coumarins, this study expands our understanding of how plant–microbe interactions influence nutrient acquisition. Fungal endophytes such as F80 could be valuable allies in enhancing plant resilience to nutrient stress, particularly in iron-deficient soils. Alongside the role of bacteria in iron nutrition (Harbort *et al.*, 2020) our findings highlight the cross-kingdom significance of coumarins in microbiota-mediated plant iron acquisition. The insights gained might have implications for developing sustainable agricultural practices that leverage beneficial microbial partnerships to enhance plant nutrition and stress resilience.

Acknowledgements

The research was funded by Deutsche Forschungsgemeinschaft SPP 2125 DECRyPT to JEP. We thank Jaqueline Bautor (Max Planck Institute for Plant Breeding Research) for experimental support, Yudelsy A. Tandron Moya (Leibniz Institute of Plant Genetics and Crop Plant Research) for conducting ICP-MS analysis, and Paul Schulze-Lefert for helpful discussions.

Competing interests

The authors declare no competing interests.

Author contributions

LVD conceived the study with AP and JEP. LVD designed and performed the experiments and analysed the data. CH performed and analysed the ferrozine iron mobilisation assay. DE performed and analysed metabolite profiling. MM provided materials, analytical tools and experimental advice. RFHG supervised the ICP-MS analyses. GUB and AT supervised metabolite profiling. LVD and JEP wrote the paper with inputs from all authors.

Data availability

Data supporting the findings of this study are available in Figures S1–S5 and Table S1.

3 Chapter 3

Fraxetin is essential for fungal root endophyte-meditated iron mobilisation for *Arabidopsis* growth at circum-neutral pH

Lara Van Dijck[1], Charlotte Hülsmann[1], Milena Malisic[1], Anthony Piro[1], Jane E. Parker[1]

[1] Department of Plant Microbe Interactions, Max Planck Institute for Plant Breeding Research, 50829 Cologne, Germany

Abstract

In calcareous soils, iron solubility and uptake become limiting, yet root-secreted coumarins can chelate and mobilise iron. Here, we show that *Macrophomina phaseolina* (F80) and *Truncatella angustata* (F73) each rescue iron deficiency in *Arabidopsis* mono-association at pH 7.3, but only when the plant's endogenous iron reduction and uptake machinery and coumarin biosynthesis/export pathways are intact. *Arabidopsis* mutants lacking fraxetin secretion remain iron-deficient despite fungal inoculation, demonstrating that fraxetin is the key metabolite driving fungal-assisted iron acquisition at circum-neutral pH. Both endophytes also degrade antimicrobial scopoletin, suggesting dual roles in coumarin turnover. *Ex planta* co-culture assays further reveal fungus- and pH-specific modulation of coumarin-mediated iron mobilisation: F80 enhances ferric iron mobilisation and reduction with scopoletin at both pH 5.7 and 7.3, whereas F73 shows no activity at acidic pH but promotes iron mobilisation independently of coumarins at pH 7.3. Together, these data establish fraxetin-dependent and fungus-specific mechanisms for endophyte-facilitated plant growth in iron-limiting circum-neutral pH environments.

Introduction

Iron is a vital micronutrient for plants, indispensable for key biological processes including respiration, chlorophyll biosynthesis, and DNA synthesis (Abadia & Terry, 1986). Yet, despite its abundance in soils, iron is often poorly available to plants due to its low solubility under aerobic and neutral to alkaline conditions, where it primarily exists as insoluble ferric (Fe^{3+}) oxides and hydroxides (Lindsay & Schwab, 1982; Cornell & Schwertmann, 2003). This challenge affects nearly 30% of the world's arable land and severely limits crop productivity and nutritional quality (Morrissey & Guerinot, 2009).

To acquire iron, plants have evolved two major strategies. Grasses use "strategy II," secreting phytosiderophores to chelate and uptake Fe^{3+}, whereas non-grass species like *Arabidopsis thaliana* use "strategy I," which involves acidifying the rhizosphere through AHA2-mediated proton extrusion, reducing Fe^{3+} via FERRIC REDUCTION OXIDASE 2 (FRO2), and transporting ferrous iron (Fe^{2+}) through IRON-REGULATED TRANSPORTER 1 (IRT1) (Yuan

et al., 2008; Santi & Schmidt, 2009). However, the effectiveness of strategy I is reducing as environmental pH increases, prompting plants to deploy additional mechanisms to improve iron uptake.

A key adaptation in *Arabidopsis* under iron-limited conditions is the biosynthesis and secretion of coumarins—phenylpropanoid-derived secondary metabolites that aid in iron mobilisation and shape the root microbiome (Schmidt *et al.*, 2014; Rajniak *et al.*, 2018). Coumarin biosynthesis is initiated by the transcription factor FIT (FER-LIKE IRON DEFICIENCY-INDUCED TRANSCRIPTION FACTOR) (Jakoby *et al.*, 2004; Yuan *et al.*, 2008), which induces yet another transcription factor MYB72 (Palmer *et al.*, 2013). This in turn activates the enzyme FERULOYL-CoA 6'-HYDROXYLASE1 (F6'H1), leading to the production of scopoletin. Scopoletin can be further hydroxylated by SCOPOLETIN 8-HYDROXYLASE (S8H) to form fraxetin, a potent Fe^{3+} chelator and reducer especially active under alkaline conditions (Kai *et al.*, 2008; Siwinska *et al.*, 2018). Fraxetin can be further converted into sideretin by the CYTOCHROME P450 82C4 enzyme CYP82C4 (Rajniak *et al.*, 2018; Tsai *et al.*, 2018). Coumarins are secreted into the rhizosphere by ATP-binding cassette transporters like PLEIOTROPIC DRUG RESISTANCE 9 (PDR9) (Fourcroy *et al.*, 2014), where they contribute to both iron acquisition and microbial community modulation.

Beyond their role in iron mobilisation, coumarins possess antimicrobial properties that selectively shape the root microbiome. Scopoletin, for example, disrupts microbial membrane integrity and promotes oxidative stress, inhibiting pathogens while facilitating beneficial associations (Harbort *et al.*, 2020; Stassen *et al.*, 2021). These dual functions—nutrient mobilisation and microbiome structuring—underscore the ecological significance of coumarins in plant health and resilience.

While recent studies have highlighted the role of root-associated bacteria in fraxetin-mediated iron mobilisation, much less is known about how fungal endophytes interact with coumarins or contribute to iron acquisition, especially under more alkaline conditions. Previous research identified the fungal endophyte *Macrophomina phaseolina* (F80) as capable of enhancing *Arabidopsis* iron nutrition in under iron-limited acidic conditions, through scopoletin conversion to iron-chelating coumarins (Chapter 2; (Van Dijck *et al.*, 2025)).

In this chapter, we introduce and investigate a second fungal isolate, *Truncatella angustata* (strain F73), which was identified through fungal screening as being tolerant to scopoletin (Anthony Piro, unpublished).

This study explores whether these fungal strains—*M. phaseolina* (F80) and *T. angustata* (F73)—can support plant iron acquisition under more challenging circum-neutral conditions (pH 7.3), where coumarins play an increasingly critical role. Using *Arabidopsis* mutants

impaired in coumarin biosynthesis (*f6'h1*) and export (*prd9*), only producing scopoletin (*s8h*) or lacking the ability to hydroxylate scopoletin (*cyp82c4*), we assess the importance of specific coumarins in fungal-mediated iron mobilisation. *Ex planta* culture assays further investigate how fungal endophytes influence coumarin-mediated mobilisation and reduction of iron from unavailable iron pools.

Our results show that both fungal strains can improve *Arabidopsis* iron status indicators under circum-neutral iron-limiting conditions, but this benefit depends on the presence of fraxetin rather than scopoletin. Notably, the positive effects are observed in *cyp82c4* mutants, which accumulate higher levels of fraxetin, but not in *f6'h1* mutants unless fraxetin is supplemented. Scopoletin supplementation does not rescue plants at pH 7.3, further reinforcing the key role of fraxetin in this interaction.

By characterising the role of fungal endophytes in coumarin-dependent iron mobilisation, this research contributes to our understanding of plant-microbe interactions in nutrient-limited environments. These insights have the potential to inform strategies for enhancing crop nutrition and resilience in more alkaline soils through microbiome-informed approaches and metabolic engineering.

Material and methods

Plant and fungal material

Experiments were performed with the following *Arabidopsis* genotypes: Columbia-0 wildtype (Col-0), *f6'h1-1* AT3G13610; SALK_132418C (*f6'h1*), *s8h-1* AT3G12900; SM_3_27151 (*s8h*), *cyp82c4-1* AT4G31940; SALK_001585 (*cyp82c4*), *pdr9-2* AT3G53480; SALK_050885 (*pdr9*), *frd1-1* AT1G01580; N3777 (*fro2*), and *irt1-1* AT4G19690; SALK_024525 (*irt1*). The two fungal strains used in this study were isolated from the roots of wild *Arabidopsis* populations as part of a microbial culture collection (Durán *et al.*, 2018): *Macrophomina phaseolina* MPI-SDFR-AT-0080 (F80) (Mesny *et al.*, 2021), *Truncatella angustata* MPI-SDFR-AT-0073 (F73).

Growth conditions

Arabidopsis seeds were surface sterilised for 15min with 70% EtOH + 0.1% Tween-20, subsequently for 2min in 95% EtOH, dried and stratified at 4°C in sterile distilled water for 2 days. Seeds were germinated on 0.5xMS medium (vitamins, 0.5 g/l MES, pH 5.7, 0.5% sucrose, 1% BD DIFCO™ Agar) square plates and grown vertically for 7 days in a growth chamber (10 h light/14 h dark, 21 °C/19 °C). Fungi were revived from -80°C glycerol stocks and grown on PDA at 22°C for approx. 2 weeks. Fungal mycelium was harvested, diluted to 100 mg/ml in 10 mM $MgCl_2$ and ground for 5 min by adding metal beads (SK550 1.1, Fast &

Fluid Management BV, Netherlands). The fungi were heat-killed (HK) by incubating samples at 99°C for 1 h.

Gnotobiotic agar-plate system

Arabidopsis seedlings (7-day-old) were transferred to iron-free 0.5xMS medium (750 µM $MgSO_4$, 625 µM KH_2PO_4, 10.3 mM 138 NH_4NO_3, 9.4 mM KNO_3, 1.5 mM $CaCl_2$, 55 nM $CoCl_2$, 53 nM $CuCl_2$, 50 µM H_3BO_3, 2.5 µM KI, 139 50 µM $MnCl_2$, 520 nM Na_2MoO_4, 15 µM $ZnCl_2$, and 9.4 mM KCl, with 1% BD DIFCO™ Agar, 140 Bacteriological) made from stock solutions, supplemented with 10 mM MES and 50 µM FeCl3 or FeEDTA for pH 5.7 or 5 mM MOPS and 100 µM FeCl3 or FeEDTA for pH 7.3. The medium was inoculated with 50 µg/ml fungal hyphae or an equal amount of $MgCl_2$. Coumarins (in DMSO) were added to 100 µM for the coumarin supplementation experiments. Plates were sealed, positioned vertically, and incubated for 2 weeks in a growth chamber.

Shoot fresh weight and total chlorophyll analysis

Plants were harvested 2 weeks after transfer, the shoot fresh weight (SFW), and total shoot chlorophyll content was determined. Chlorophyll was extracted following the protocol previously described (Harbort et al., 2020 and Hiscox & Israelstam, 2011). 5-7 shoots were pooled and chlorophyll was extracted with 1 ml DMSO per 30 mg tissue, absorbance was measured at 652 nm on a Nanodrop spectrophotometer (Thermo Fisher Scientific).

Fungal load analysis

To quantify the fungal load two weeks post-transfer, roots were collected in Lysing Matrix E tubes (MP Biomedicals, USA) and crushed for 30 s at 6200 rpm. After adding 980 µl sodium phosphate buffer and 122.5 µl MT-buffer (MP Biomedicals, USA), samples were crushed two more times (30 s, 6200 rpm), then centrifuged for 15 min at 13,000 rpm. 50 µl binding matrix (MP Biomedicals, USA) per sample was added to a 96-well plate. A filter plate (Acroprep Advance, 0.2 µm Supor filter, Pall) was placed on top, and 150 µl supernatant from each sample was loaded onto the filter plate and centrifuged (20 min, 1500 rpm). The flow-through was mixed with the binding matrix by shaking for 3 min, thereafter 190 µl was transferred to a second filter plate and washed twice with 150 µl SEWS-M (MP Biomedicals, USA) by centrifuging for 5 min at 1500 rpm and the centrifuging step was repeated to dry the samples. DNA was eluted with 30 µl of ddH2O by centrifuging at 1500 rpm for 5 min, and stored at -20 °C. Fungal colonisation was measured by qPCR as described (Mesny *et al.*, 2021) using ITS1F/ITS2 for fungal ITS1 and UBQ10F/UBQ10R for *Arabidopsis* Ubiquitin10. Reactions used iQ™ SYBR® Green Supermix, primers, and 1 µl DNA. qPCR was performed on a BioRad CFX Connect: 95 °C (3 min), 39 cycles of 95 °C (15 s), 60 °C (30 s), 72 °C (30 s). Colonisation index = $2^{-Cq(ITS1)/Cq(UBQ10)}$.

96-well fungal culture assay

Medium was prepared to mimic the plant root environment in the gnotobiotic agar-plate plant assays, 0.5xMS medium supplemented with artificial root exudates (ARE) vitamins and different pH buffering conditions: pH 5.7 (10 mM MES) and pH 7.3 (10 mM MOPS). The full composition of the medium can be found in Table S1. Before inoculation the medium was sterile filtered (0.22 µm) and supplemented with scopoletin to a final concentration on 2 mM or an equal amount of DMSO, subsequently, 190 µl medium was added per well. The wells were inoculated with 10 µl of fungal hyphal solution (final concentration 5mg/ml) or 10 µl of 10 mM $MgCl_2$ as a blank control. Cultures were grown for 12 days at 22 °C with shaking (140 rpm), daily around the same time OD600 and scopoletin fluorescence (excitation 385 nm, emission 470 nm) was measured using a TECAN spectrophotometer (Infinite® M Plex). Scopoletin fluorescence values were normalised to the OD600 and to the fluorescence values at the start of each experiment (day 0), to minimise variation between independent experiments. To be able to detect small differences in growth, the relative fungal growth was calculated by dividing the OD600 in the presence of scopoletin to the OD600 in the control (DMSO) wells.

Ferrozine iron mobilisation and reduction assay

To evaluate if F80 and F73 affect the ability of scopoletin, fraxetin and esculetin to mobilise and reduce iron at pH 5.7 and 7.3, an in vitro spectrophotometric assay was developed based on Yi & Guerinot, (1996). Ferrozine, a compound that can bind specifically to ferrous Fe^{2+} and forms a coloured complex with an absorbance at 662 nm, was used. The coumarins (in DMSO) were added to the fungal culture medium described above (Table S1) to a final concentration of 10, 50 or 400 µM. Wells of a 96-well plate with 190 µl of medium were inoculated with 10µl of washed mycelium (to remove any medium residues, harvested mycelium was washed three times for this assay) or 10 µl of $MgCl_2$ (mock). Plates were incubated at 22 °C in the dark with shaking (140 rpm), and OD600 was measured daily to monitor fungal growth. At 0, 6, and 9 days post-inoculation (dpi), samples were centrifuged (3800 rpm, 20 min), and supernatants were stored at −80 °C.

Iron reduction was assessed by adding 0.1 mM $FeCl_3$ and 0.4 mM ferrozine to 120 µl of sample and measuring absorbance at 562 nm before and after ferrozine addition (TECAN Infinite® M Plex). Iron reduction was measured every 10 min over 10 h. Controls included water, $FeCl_3$ with 0.3 mM ascorbic acid (positive) or 0.3 mM NaEDTA (negative), and FeEDTA for estimating total mobilised iron. A $FeSO_4$ dilution series (starting at 0.1 mM) was used to generate standard curves for reduced iron quantification. To measure total mobilised iron, the immobile iron fraction was removed by centrifugating the same samples (3800 rpm, 15 min). Supernatants were incubated with 10 mM HCl and 10 mM ascorbic acid to reduce all iron still present. After 20 min in darkness, absorbance at 562 nm was measured. For calculating the total amount of

mobilised iron, absorbance was blanked against FeEDTA controls (prior to reduction with HCL and ascorbic acid), and $FeSO_4$ standard curves were used to quantify mobilised iron.

Statistical analysis

Statistical analyses were conducted in R (version 4.4.0). For comparisons across more than two treatment groups where normality and homogeneity of variance assumptions were fulfilled, means were compared using ANOVA followed by a Tukey's post hoc test. If the assumptions were not met, data were analysed using Kruskal–Wallis tests followed by Dunn's post hoc test with Benjamini–Hochberg correction to control for false discovery rate. Iron reduction and mobilisation assays, which compared primarily two conditions within each group, were assessed with pairwise tests. A Student's t-test was applied when data met normality assumptions; otherwise, a non-parametric Wilcoxon rank-sum test was used. Significance thresholds were set at $p < 0.05$ for all tests. Results were presented as means ± standard deviation, unless otherwise stated and all statistical procedures were clearly reported in figure legends.

Results

F80 and F73 enhance *Arabidopsis* growth in unavailable iron conditions at circum-neutral pH

In this chapter we wanted to extend the scope to two different phylogenetically diverse endophytic fungi, building on the findings in chapter 2. Here, we introduce *Truncatella angustata* (F73) an Ascomycete part of the same *Arabidopsis* culture collection as F80 (Durán *et al.*, 2018). To investigate how the fungal endophytes F80 and F73 affect plant iron nutrition at circum-neutral pH, wild-type Col-0 *Arabidopsis* seedlings were grown in contrasting iron conditions in the gnotobiotic agar plate system buffered at pH 7.3 (1/2MS agar, 5 mM MOPS). Fe^{3+} was supplemented to the system at 100 µM: poorly soluble $FeCl_3$ mimicking conditions of iron unavailability (unavFe) or pre-chelated Fe-EDTA (avFe) which is soluble and therefore readily available to the plant. As an indication of plant performance and as a proxy for iron nutritional status, SFW and shoot chlorophyll content were measured. First, the ability of F73 to improve plant growth under iron limitation at acidic pH was tested as described in chapter 2. Interestingly, F73, in contrast to F80 was not able to improve SFW nor chlorophyll content of plants grown in unavFe (Figure 7a,b). At circum-neutral pH in unavFe mock conditions, the plants showed clear signs of iron starvation, such as chlorosis and decreased chlorophyll content as well as SFW compared to avFe mock conditions (Figure 7). In contrast to mock conditions, inoculation with F80 or F73 resulted in a significant increase in SFW and chlorophyll content of the plants grown in unavFe (Figure 7c,d). Furthermore, an active colonisation by living fungi is needed for fungal-mediated improvement of iron status indicators, as the

inoculation with both heat-killed fungi had a mock-like phenotype (Figure S6). This also confirmed that rescue in not caused by iron residues present in the inoculum. Notably, neither F80 nor F73 was able to fully rescue iron-starved wild-type *Arabidopsis* seedlings to levels comparable to avFe conditions in the two weeks past inoculation period at circum-neutral pH (Figure 7c,d). On average, seedlings were smaller in at circum-neutral pH compared to acidic pH (Figure 7a,c), reflecting results of plants grown in more alkaline iron poor soils (Schmidt et al 2014). Taken together, F80 and F73 have the potential to improve *Arabidopsis* iron nutrition, however F73 only at circum-neutral pH suggesting that the underlying mechanisms might be different at different pH conditions.

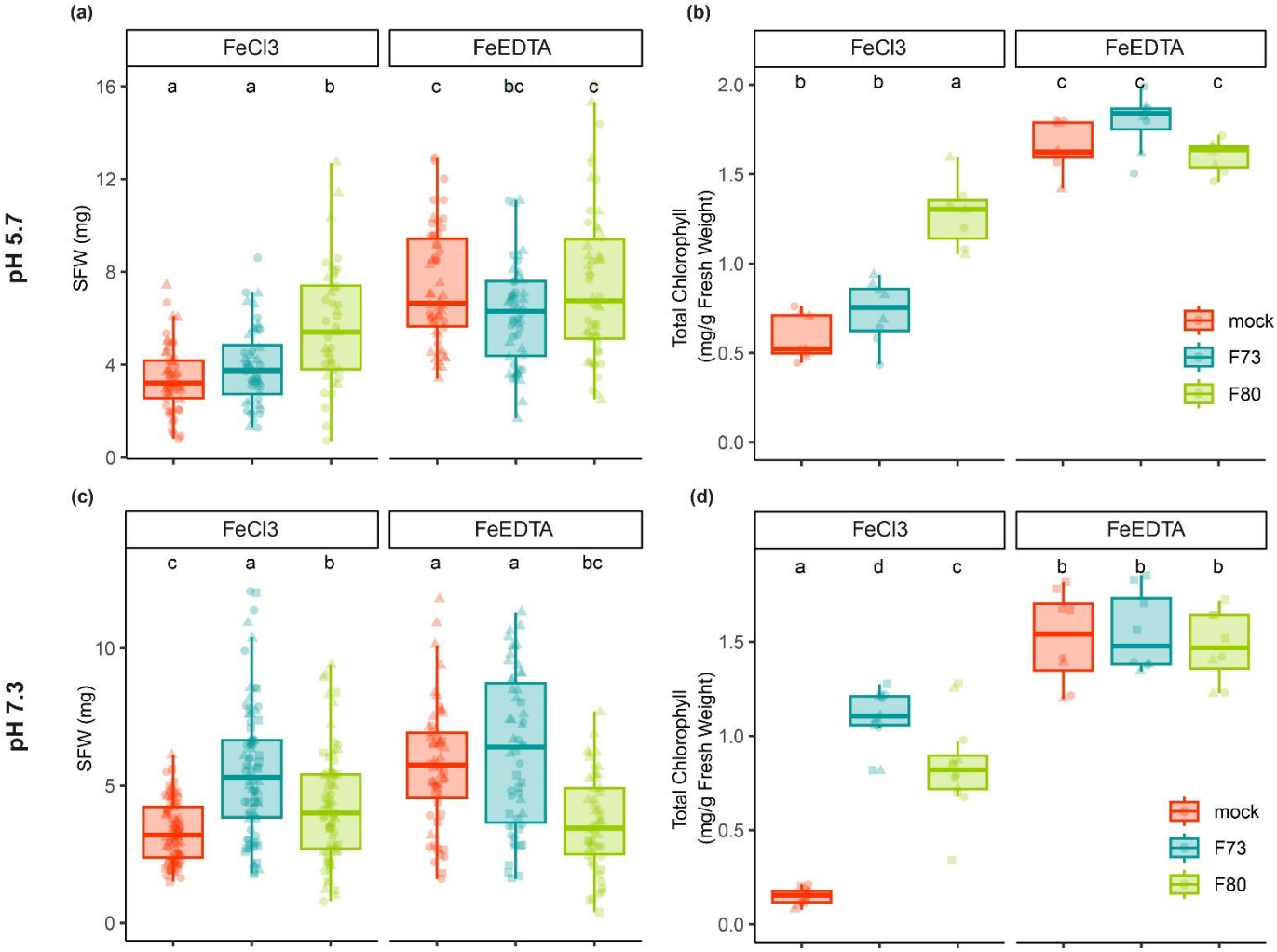

Figure 7. Fungal endophyte-mediated enhancement of *Arabidopsis* iron status indicators at pH 5.7 and 7.3. (a,c) SFW and (b,d) shoot chlorophyll content of Col-0 *Arabidopsis* seedlings, 7-day old seedlings were transferred to 0.5MS medium grown for 2 weeks on mock, F73 or F80 inoculated plates (a,b) at pH 5.7 (10mM MES) in unavFe (50µM FeCl3) or avFe (50µM FeEDTA) and (c,d) at pH 7.3 (10mM MOPS) in unavFe (100µM FeCl3) or avFe (100µM FeEDTA). Letters indicate significant pairwise differences between groups (p-adj≤0.05) by Dunn pairwise comparison test with Benjamini-Hochberg correction (a,c) or a Tukey's HSD corrected for multiple comparisons (b,d). Data are from two (a,b) or three (b,c) biological replicates (represented by different shapes).

Coumarin biosynthesis and exudation are essential for F80- and F73-mediated enhancement of plant growth under iron limitation at pH 7.3

In chapter 2 the presence of scopoletin was shown to be essential for F80-mediated *Arabidopsis* iron nutrition at acidic pH. To further develop our mechanistic understanding of fungal endophyte iron nutrition enhancement, we tested if coumarins are similarly required at circum-neutral pH. *Arabidopsis* mutants defective in coumarin biosynthesis (*f6'h1*, *s8h*, *cyp82c4*) or export (*pdr9*) were grown in the contrasting iron conditions. Unlike Col-0, coumarin deficient *f6'h1* mutants failed to exhibit any increase in shoot chlorophyll content following inoculation with F73 or F80 (Figure 8a,b), highlighting the importance of coumarins at circum-neutral pH. Next to *f6'h1*, *s8h* and *cyp82c4* mutants impaired in fraxetin and sideretin production, respectively, and the coumarin export *pdr9* mutant were tested (Schmidt *et al.*, 2014; Rajniak *et al.*, 2018; Tsai *et al.*, 2018; Harbort *et al.*, 2020). Under unavFe mock conditions, all genotypes, as observed in wild-type Col-0, exhibited chlorotic young leaves with chlorophyll content and SFW significantly reduced compared to avFe mock conditions (Figure 8a,b). An approximate 80% decrease in chlorophyll content under unavFe conditions, confirmed severe iron deficiency. Interestingly, *s8h* plants only producing scopoletin did not show any improvement by either fungus (Figure 8a,b), suggesting a different mechanism as found for acidic pH for F80. The fungi only improved chlorophyll content and SFW in *cyp82c4* mutants, which produce scopoletin and fraxetin but lack sideretin (Rajniak *et al.*, 2018). Furthermore, neither F80 nor F73 enhanced plant performance in *pdr9* mutants (Figure 8a,b), the functional export of coumarins via PDR9 appears to be essential for fungal-mediated improvement of iron status indicators at pH 7.3. To determine whether the genotype- and coumarin-specific effects on plant performance resulted from differential fungal root colonisation, we quantified F80 and F73 colonisation levels in *Arabidopsis* roots using qPCR. No significant differences in F73 colonisation were observed between Col-0 and the coumarin biosynthesis mutants (Figure S7c). Similarly, F80 colonisation levels were comparable across most genotypes, except for *f6'h1* and *s8h* mutants, where colonisation was slightly increased relative to Col-0 (Figure S7d).

Taken together, these findings suggest that fraxetin plays a crucial role in fungal-assisted improvement of plant performance under iron unavailability, as scopoletin biosynthesis in *s8h* mutants was insufficient to restore fungal-mediated rescue at pH 7.3. This places fraxetin at the centre of microbe-assisted iron acquisition at circum-neutral pH, as fraxetin and its secretion have been found to be essential for bacterial-mediated plant iron nutrition at circum-neutral pH (Harbort *et al.*, 2020).

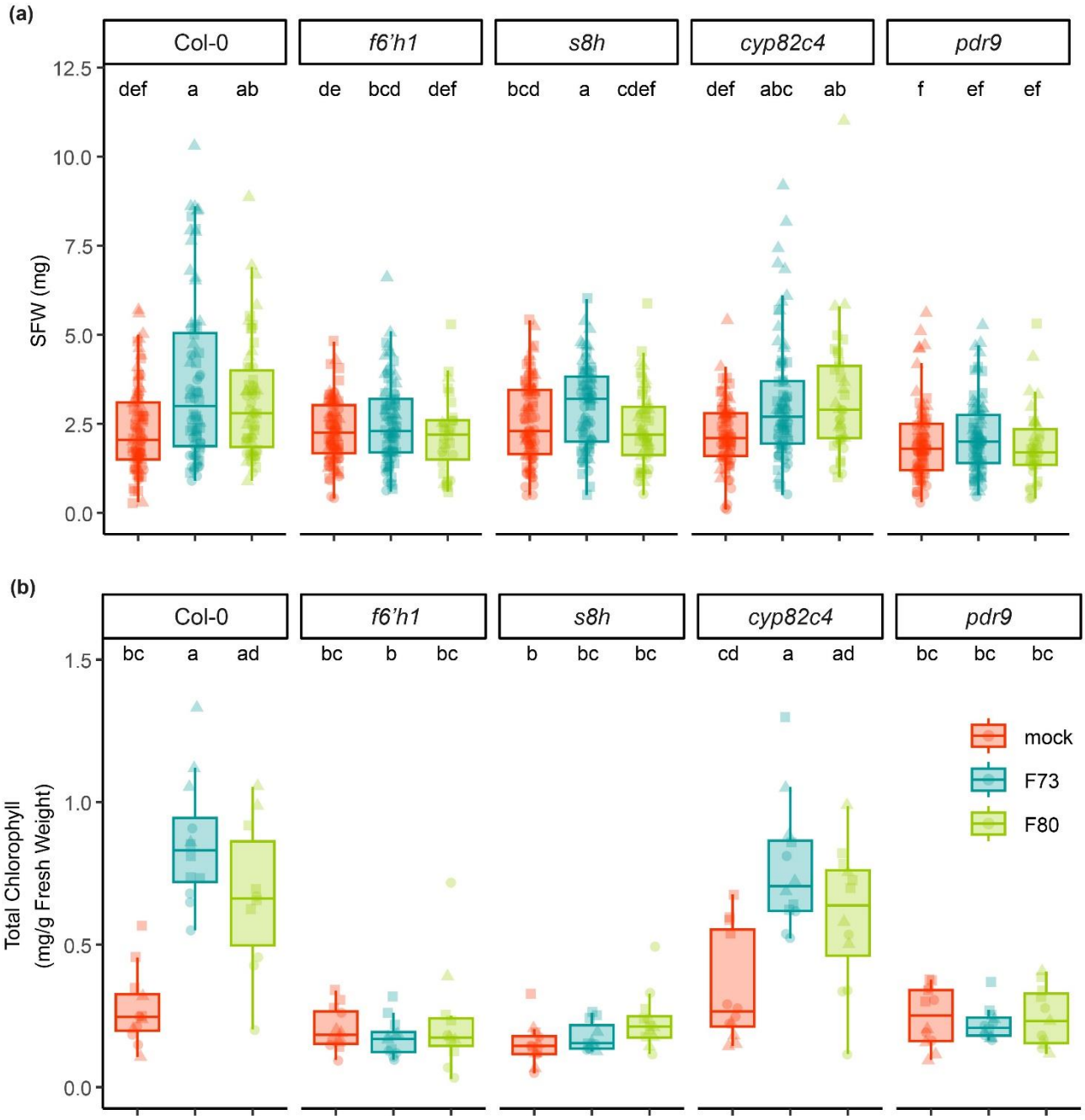

Figure 8. Fungal endophyte-mediated enhancement of *Arabidopsis* growth in unavFe at pH 7.3 requires fraxetin biosynthesis and secretion. (a) SFW and (b) shoot chlorophyll content of Col-0, *f6'h1*, *s8h*, *cyp82c4*, and *pdr9* seedlings (germinated 7 days) grown for 2 weeks in unavFe 0.5 MS medium (100 µM FeCl3, 10mM MOPS) mock or inoculated with fungal hyphae (50 µg/ml). Data are from 3 biological replicates (represented by different shapes), letters indicate significant pairwise differences between groups (p-adj≤0.05) by Dunn pairwise comparison test with Benjamin-Hochberg correction.

F80- and F73-mediated enhancement of plant performance in unavFe at pH 7.3 relies on the hosts ferric chelate reduction by FRO2 and uptake by IRT1

Iron mobilisation was found to be the key to iron nutrition improvement by F80 at acidic pH (Chapter 2; (Van Dijck *et al.*, 2025)) and likely how bacteria-fraxetin cooperation leads to plant rescue (Harbort *et al.*, 2020). After the mobilisation of iron, it still needs to be reduced before uptake into roots. To investigate whether iron reduction and uptake by the plant is still required for F80 and F73 to promote plant iron nutrition at pH 7.3, we analysed *Arabidopsis* mutants deficient in ferric chelate reduction (*fro2*) and iron uptake (*irt1*). Under unavFe mock conditions, the shoot chlorophyll content and SFW of *fro2* and *irt1* mutants were comparable to those of Col-0 (Figure 9a,b). However, unlike Col-0, neither *fro2* nor *irt1* exhibited increased shoot chlorophyll content or SFW when inoculated with F80 or F73 (Figures 9a,b). Furthermore, there were no differences in colonisation observed between Col-0, *fro2*, and *irt1* for both fungi (figure S8c,d). This suggests that fungal-mediated enhancement of iron status indicators is dependent on the plant's endogenous iron reduction and uptake system and likely involves iron mobilisation. Both mutants displayed higher chlorophyll content in avFe compared to unavFe, irrespective of the presence or absence of fungi. However, their chlorophyll levels remained lower than those of Col-0 under avFe, with shoots still showing signs of chlorosis (Figure S8a,b). These observations confirm that *Arabidopsis* experiences iron deficiency without functional FRO2 or IRT1, even when the chemical FeEDTA chelator is supplemented to the medium. In conclusion, these findings demonstrate that the beneficial effects of F80 and F73 on plant growth at pH 7.3 are contingent on the plant's ability to reduce Fe^{3+} via FRO2 and import Fe^{2+} via IRT1. This highlights the necessity of functional plant iron homeostasis mechanisms for fungal-assisted iron acquisition.

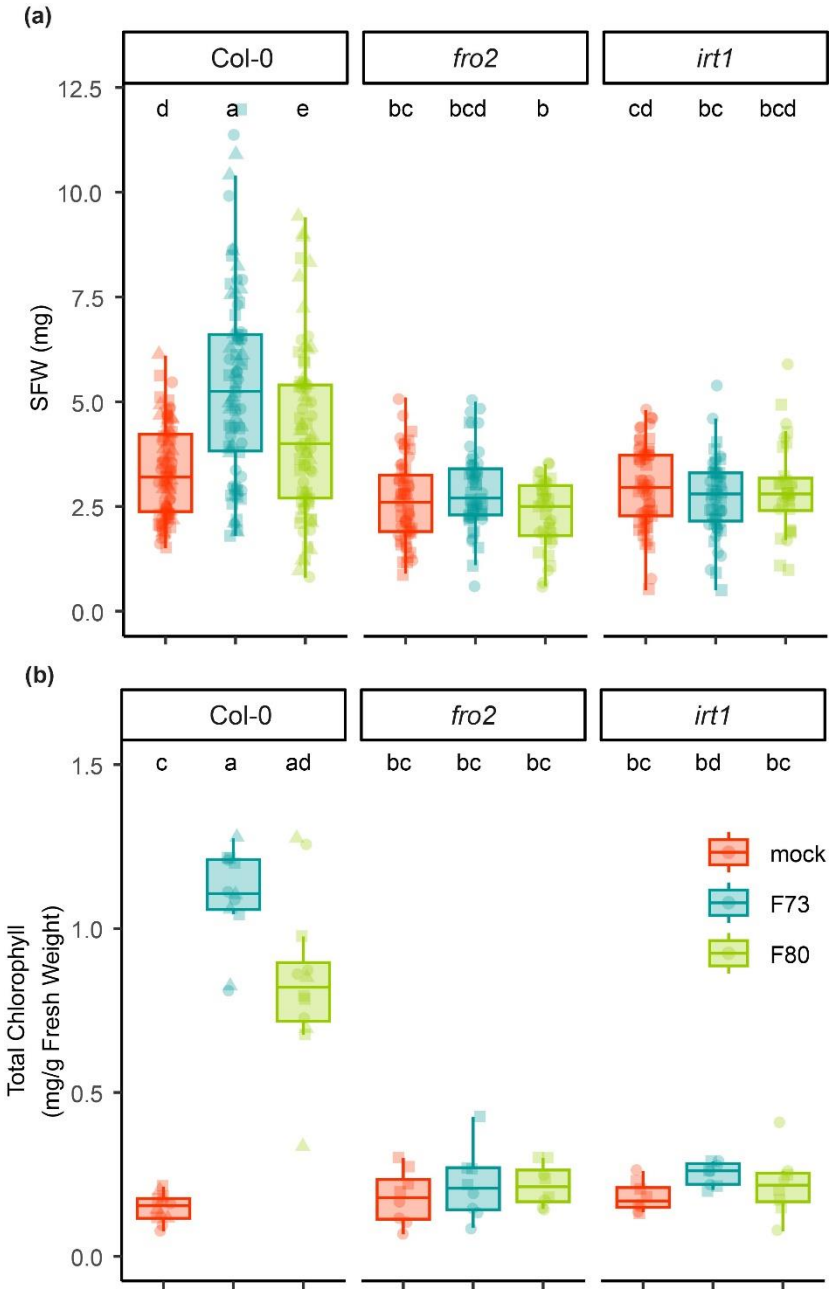

Figure 9. Fungal endophyte-mediated enhancement of *Arabidopsis* growth in unavFe at pH 7.3 relies on plant ferric iron reduction and uptake. (a) SFW and (b) shoot chlorophyll content of Col-0, *fro2*, and *irt1* seedlings (germinated 7 days) grown for 2 weeks in unavFe 0.5 MS medium (100 µM FeCl3, 10mM MOPS) mock or inoculated with fungal hyphae (50 µg/ml). Data are from 3 biological replicates (represented by different shapes), letters indicate significant pairwise differences between groups (p-adj≤0.05) by Dunn pairwise comparison test with Benjamin-Hochberg correction.

Coumarin supplementation can restore F80- and F73-mediated enhancement of plant iron status indicators in *f6'h1* mutants at pH 7.3

Cyp82c4 mutants were rescued by both fungi, this mutant can produce both scopoletin and fraxetin. Although the biosynthesis of esculetin is yet to be discovered, its presence has been reported in low concentration in *s8h* and *cyp82c4* mutants (Paffrath *et al.*, 2023). In order to find the specific coumarin required for each fungus to exert plant rescue or to find possible coumarins cooperating for rescue, we conducted chemical coumarin supplementation assays. The *f6'h1* mutant, lacking all coumarins, was used as an entirely coumarin-deficient background, and supplemented with 100 µM scopoletin, fraxetin, esculetin, or combinations in unavFe. Scopoletin supplementation had no significant effect on shoot chlorophyll content or SFW in *f6'h1* plants across all conditions (mock, F80, and F73), except for a minor increase in SFW when inoculated with F73 (Figure 10a,b). Scopoletin is not an efficient iron mobilising compound, because it lacks a catechol group to chelate iron. In contrast, fraxetin supplementation restored the ability of F80 and F73 to increase chlorophyll content and SFW in *f6'h1* plants under unavFe conditions (Figure 10a,b). Yet, F73-fraxetin interaction resulted in higher shoot chlorophyll content compared to F80 with fraxetin, suggesting a more efficient fraxetin-mediated iron mobilisation in the presence of F73. Esculetin supplementation, unlike the other coumarins, significantly improved chlorophyll content in *f6'h1* plants even under mock conditions, thereby indicating a direct involvement in iron mobilisation. For plants inoculated with fungi, esculetin increased chlorophyll content and SFW of F80-inoculated *f6'h1* plants, but had no such effect on F73-inoculated plants (Figure 10a,b). These findings indicate a fungus-specific interaction with esculetin, whereas fraxetin elicits functionally redundant effects across both fungi at pH 7.3. We also tested combinatorial coumarin supplementation of scopoletin with fraxetin and scopoletin with esculetin, but we did not identify any additive effects. This suggests that the fungi might not increase iron mobilisation by interacting with the tested coumarins together. In the last treatment, EDTA was supplemented and lead to an increased SFW and Chlorophyll content in the presence of both fungi. This indicated that the fungi can also interact with a structurally distinct chemical chelator to mobilise iron.

To further explore the dependency of fungal-mediated iron acquisition on plant iron homeostasis mechanisms, we supplemented *fro2* mutants with the different coumarins or EDTA in unavFe (Figure S9). Regardless of the treatment, *fro2* plants exhibited severe iron starvation across all mock and fungus-treated conditions, as indicated by low SFW and chlorophyll content (Figure S9a,b). These results suggest that the fungal-mediated enhancement of plant performance in unavFe at pH 7.3 likely involves iron mobilisation and relies on both coumarin biosynthesis and FRO2-dependent iron reduction.

To assess whether the supplementation of coumarins to the medium led to a differential root colonisation, the colonisation index was also determined here. For both *f6'h1* and *fro2* scopoletin, fraxetin and esculetin supplementation did not have an impact on F73 and F80 colonisation and levels were similar to Col-0 (Figure S10a,b,c,d). However, *f6'h1* plants without coumarins supplemented, exhibited a slight increase in F80 colonisation levels compared to Col-0 and all coumarin supplementation conditions (Figure S10b). Overall, no major differences in fungal root colonisation were observed across genotypes or coumarin supplementation conditions. These findings indicate that the fungal-mediated, genotype-specific enhancement of *Arabidopsis* growth under iron limitation is not primarily driven by differences in root colonisation, but rather by coumarin-mediated modifications in iron availability.

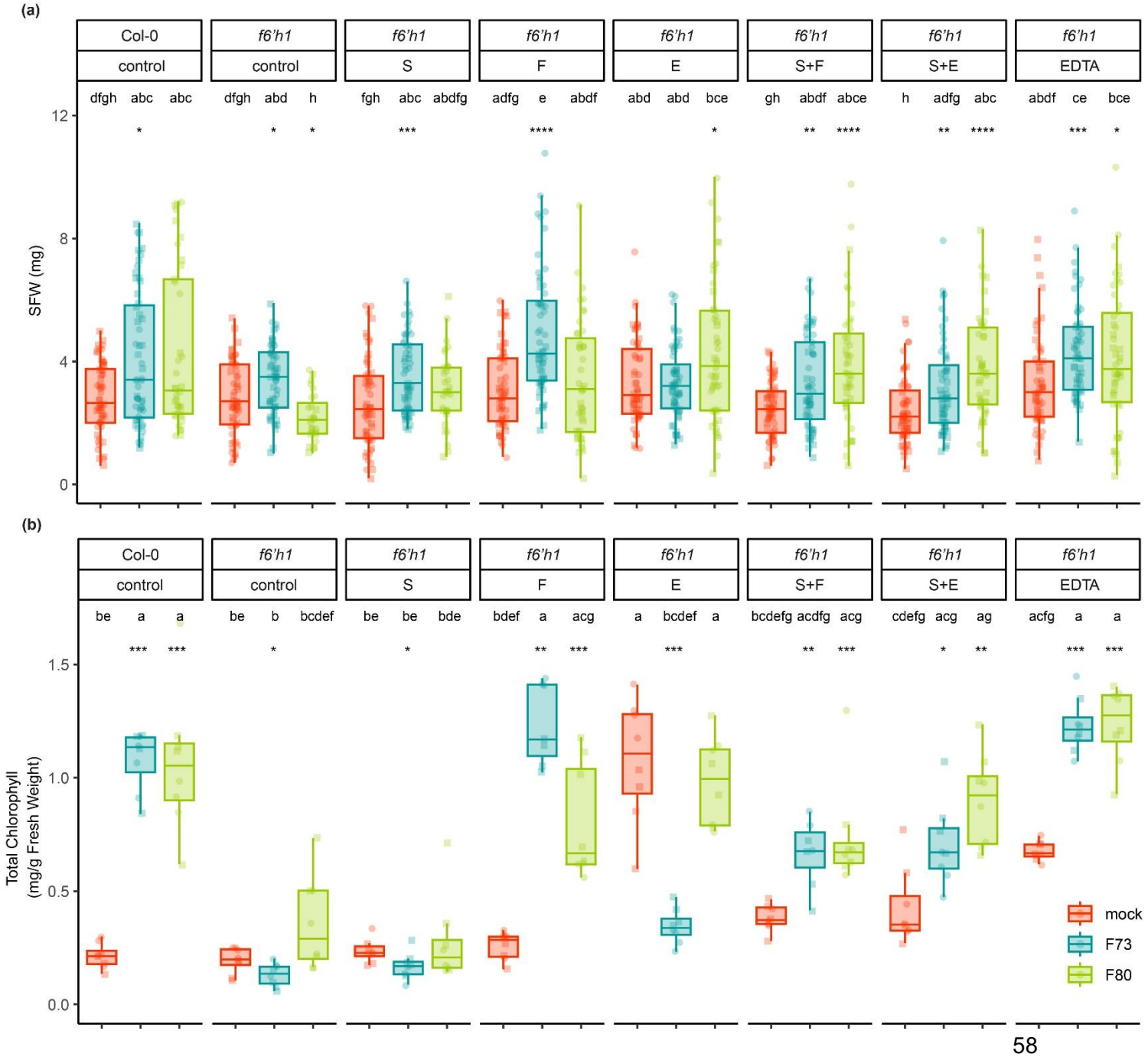

Figure 10. Fraxetin supplementation restores fungal endophyte-mediated enhancement of *Arabidopsis* iron status indicators at pH 7.3. (a) SFW and (b) shoot chlorophyll content of Col-0 and *f6'h1* seedlings (germinated 7 days) grown for 2 weeks in unavFe 0.5 MS medium (100 µM FeCl3, 10mM MOPS) mock or inoculated with fungal hyphae (50 µg/ml) supplemented with 100 µM scopoletin (S), fraxetin (F), esculetin (E), Na_2EDTA (EDTA) or scopoletin combined with fraxetin (S+F) and esculetin (S+E) or an equal amount of DMSO (control). Data are from 2 biological replicates (represented by different shapes), letters indicate significant pairwise differences between groups (p-adj≤0.05) by Dunn pairwise comparison test with Benjamini-Hochberg correction. Pairwise comparisons between fungi-treated and mock-treated samples within each genotype were assessed using the Wilcoxon rank-sum test, with *p < 0.05, **p < 0.01, ***p < 0.001, and ****p < 0.0001 indicating significance.

F80 and F73 degrade scopoletin in acidic and circum-neutral pH conditions

The fungal endophyte-mediated enhancement of plant growth in unavFe at pH 7.3 relies on the biosynthesis of root-secreted coumarins. Coumarins, particularly scopoletin, are known to inhibit the growth of certain soil-borne fungi (Stringlis *et al.*, 2018a; Harbort *et al.*, 2020). In chapter 2 we show that F80 can degrade high concentrations of scopoletin (2 mM) at pH 5.7 in liquid cultures. To investigate whether F73 can degrade scopoletin and evaluate potential differences in degradation capacities between F80 and F73 in different pH conditions, both fungi were cultivated in 1/2 MS medium buffered at pH 5.7 or 7.3, and supplemented with 2 mM scopoletin. Scopoletin fluorescence was monitored daily over a 12-day period. In mock conditions, scopoletin fluorescence remained stable throughout the experiment in both pH's, indicating scopoletin is stable in this system also at a more alkaline pH. In both pH conditions cultures inoculated with F80 or F73, a decrease in scopoletin fluorescence was observed (Figure 11a,b). This confirmed the F80 results from Chapter 2 and revealed a very similar effect on scopoletin by F73. Moreover, both fungi degraded scopoletin a little faster at circum-neutral pH with fluorescence levels reaching 0 at 4 dpi compared to 5 dpi in acidic pH. In both pH conditions, F73 started to degrade scopoletin more rapidly than F80. (Figure 11a,b).

To evaluate the impact of scopoletin on fungal growth, OD600 of the fungi co-cultured with 2 mM scopoletin was normalised to the OD600 of fungi grown without scopoletin. At pH 5.7, F80 and F73 exhibited a decrease in normalised growth from 0-4 dpi for F73 and 3-7 dpi for F80 (Figure S11c). At circum-neutral pH, the relative growth of both F73 and F80 decreased when co-cultured with scopoletin until 4 dpi (Figure S11d). For F73, the decline in normalised growth was followed by an increase, stabilising at 8 dpi (Figure S11d). Interestingly, at pH 7.3, the increase in normalised growth of F80 at 3 dpi did not stabilise but was followed by a second growth decrease starting at 7 dpi (Figure S11d). Overall, the observations at pH 7.3 were largely consistent with those at pH 5.7 (Figure S11). These findings collectively suggest that fungal growth is not inhibited by scopoletin after 3 to 5 days of co-culture at either pH 5.7 or

pH 7.3, correlating with the fungi's ability to degrade scopoletin. The observed recovery in fungal growth may be attributed to the degradation of the growth-inhibiting substrate, scopoletin.

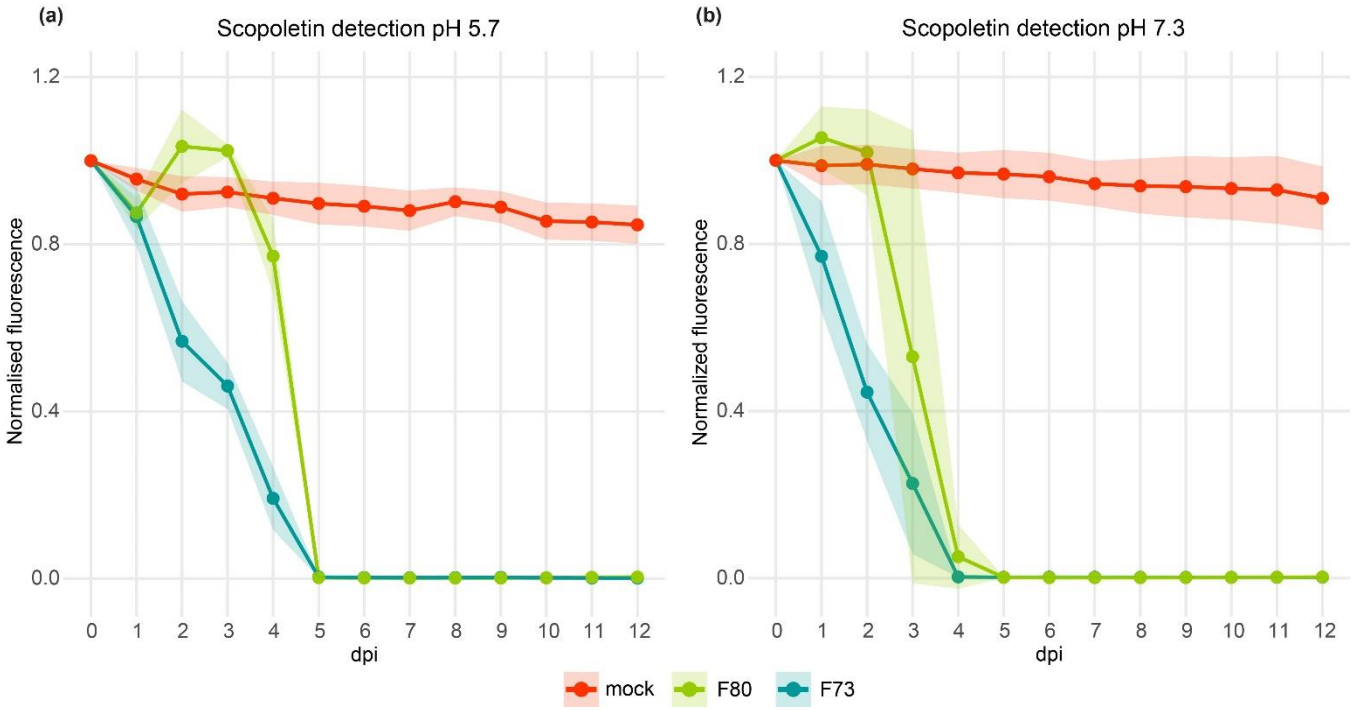

Figure 11. Fungal endophytes F80 and F73 degrade scopoletin at pH 5.7 and 7.3. fungal hyphae were grown for a time course of 12 days in medium buffered (a) at pH 5.7 (10 mM MES) or (b) 7.3 (10 mM MOPS) supplemented with scopoletin (final concentration of 2 mM). Scopoletin fluorescence (exciting at 385nm and emission detected at 470nm) was normalised to fungal growth (OD600) and to the fluorescence at day 0. Data from 3 independent experiments are shown, the curve shade indicates the standard deviation, the Area Under the Curve of graph (a) and (b) can be found in Figure S11a,b.

pH- and coumarin-dependent iron mobilisation in F80 and F73 culture supernatants

Plant iron deficiency is exacerbated under neutral to alkaline conditions due to the low solubility of Fe^{3+} and reduced efficiency of FRO2-mediated ferric iron reduction (Connolly *et al.*, 2003). Coumarins play a crucial role in iron acquisition by mobilising Fe^{3+} into soluble complexes and, under some conditions, reducing Fe^{3+} to Fe^{2+} (Schmidt *et al.*, 2014). The efficiency of iron mobilisation and reduction by coumarins is highly pH- and buffer-dependent (Paffrath *et al.*, 2023). To investigate how fungal interactions influence these processes, we conducted *ex planta* culture studies assessing iron mobilisation in the culture supernatant of F80 and F73 supplemented with three distinct coumarins (scopoletin, fraxetin, esculetin) at contrasting pH conditions.

F80 and F73 were grown in iron-free medium, buffered at pH 5.7 or pH 7.3 and supplemented with coumarins. At 0 dpi, 6 dpi, and 9 dpi, supernatants were collected and incubated with 100

µM $FeCl_3$, inducing ferric iron hydroxide ($Fe(OH)_3$) precipitation. Iron mobilisation was quantified spectrophotometrically based on (Fe^{2+})-ferrozine complex formation. The total amount of reduced iron in the culture supernatants was assessed as well, however (Kang *et al.*, 2023) show that ferrozine can facilitate the reduction of iron from iron-coumarin complexes. Therefore, these results could be an overestimation of the amount of iron reduced. As the *in planta* experiments point to a fungal-mechanism involving iron mobilisation relying on the ferric reductase FRO2, we will mainly focus on the iron mobilisation results here. Our experimental setup allowed us to assess the fungus- and pH-specific effects on iron mobilisation across different coumarins, highlighting how fungal-coumarin interactions modulate iron solubility under varying conditions.

Iron mobilisation at pH 5.7

At pH 5.7, scopoletin did not mobilise iron under mock conditions at any concentration or time point (Figures 12a,b, S12a,b). However, in culture with F80, the total iron mobilised increased significantly, particularly at higher initial scopoletin concentrations (Figure S12a). At 6 dpi, 400 µM scopoletin supplemented to F80 culture led to the mobilisation of approximately 70-90% of the precipitated iron. By 9 dpi, 70% iron remained mobilised, indicating sustained mobilisation activity (Figure 12a). While F80 in absence of coumarins was capable of mobilising iron (indicated by the dashed line), the presence of scopoletin enhanced this effect, particularly at higher concentrations (Figure S12a). In contrast, F73 cultures exhibited minimal iron mobilisation, with only ~20% at 9 dpi, regardless of scopoletin supplementation (Figures 12b, S7b). This suggests that scopoletin-driven iron solubilisation is fungus-dependent and significantly more pronounced in F80 than in F73 culture supernatant. Unlike scopoletin, esculetin and fraxetin were highly effective in mobilising iron under mock conditions, with nearly 100% at 0 dpi. This level remained stable at 6 and 9 dpi, indicating that fraxetin and esculetin maintain iron solubility under acidic conditions (Figure 12a,b). In F80 cultures grown in the presence of esculetin the total iron mobilised decreased slightly over time compared to mock, with ~60% at 9 dpi (Figure 12a). In F80-fraxetin cultures iron mobilisation decreased from 100% at 0 dpi to ~40% at 9 dpi, suggesting some fungal alteration of fraxetin-bound iron (Figure 12a). In contrast, F73 cultures exhibited a different pattern: iron mobilisation decreased from similar levels as mock at 0 dpi to nearly 0 at 6dpi and recovered to ~30% by 9 dpi for both esculetin and fraxetin (Figure 12b). This effect, however, seemed to be independent of the amount of coumarin supplemented (Figure S12b), indicating that iron solubilisation in F73 cultures is primarily fungus-driven rather than coumarin-dependent. The *ex-planta* iron mobilisation results could explain why we did not observe a plant growth enhancement by F73 at pH 5.7, as we detected little mobile iron in its supernatant, whereas we did for F80.

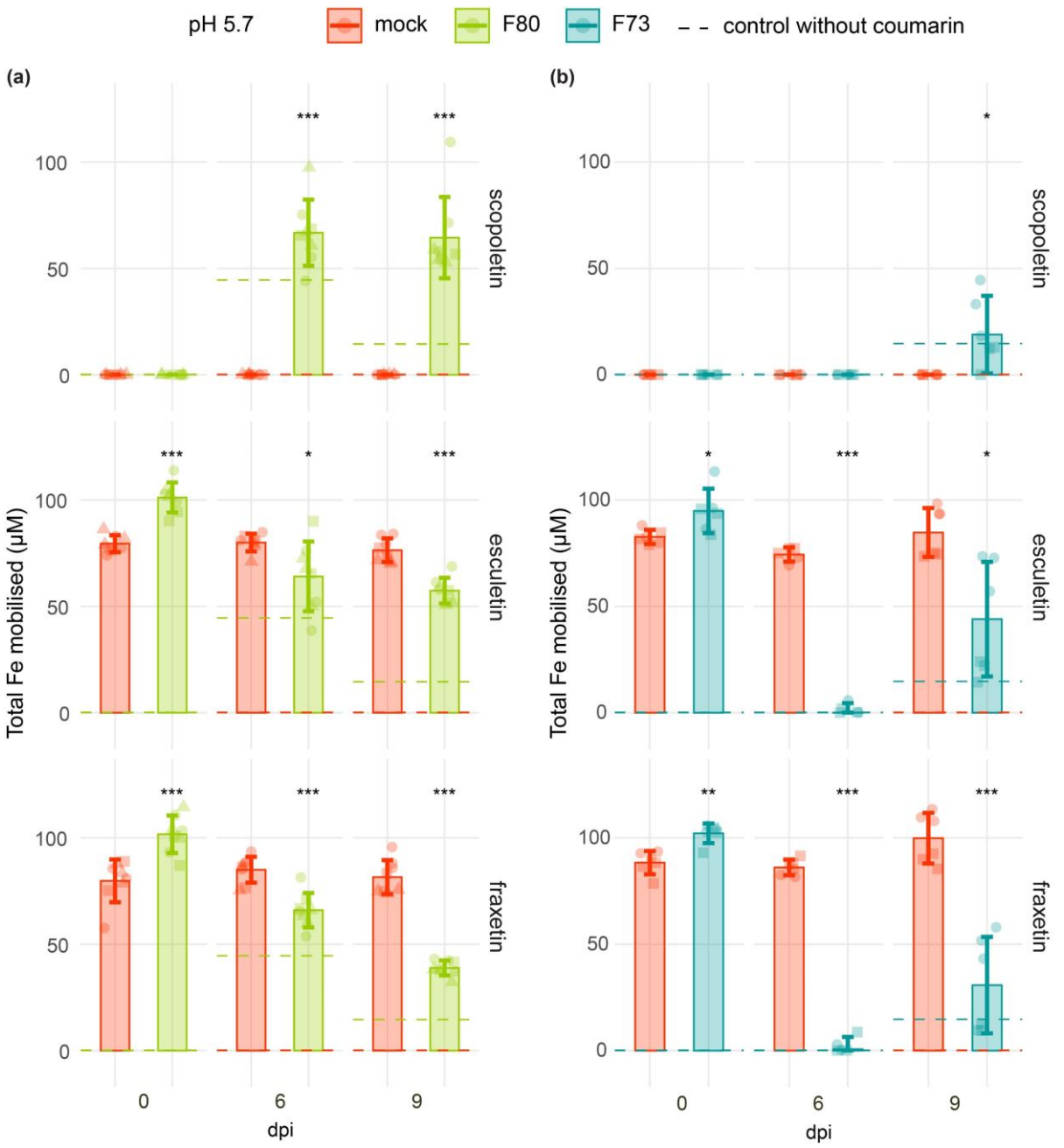

Figure 12. Total iron mobilisation in F80 and F73 cultures supplemented with scopoletin, fraxetin, and esculetin at pH 5.7. The total iron (Fe) mobilised in (a) F80, (b) F73 or mock (MgCl2, indicated with the red dashed lines) supernatant of cultures grown with scopoletin, fraxetin, esculetin (final concentration of 0.4 mM), or an equal amount of DMSO (control indicated with the green/blue dashed lines) at 0, 6, or 9 dpi at pH 5.7 (10 mM MES). Mobile iron was measured spectrophotometrically based on the formation of Fe^{2+}-ferrozine complexes, mean ± SD of 3 (a) and 2 (b) biological replicates are shown (represented by different shapes), significance levels shown for comparisons when applicable. Statistical differences between treatments were assessed using t-tests for normally distributed residuals or, otherwise, Wilcoxon rank-sum tests, significance levels are indicated by asterisks with *p <0.05, **p < 0.01, and ***p < 0.001. (Panel (a) generated from data presented in chapter 2 (Van Dijck *et al.*, 2025))

Iron mobilisation at pH 7.3

Scopoletin under mock conditions did not mobilise iron at pH 7.3, resembling the results at acidic pH (Figure 13a,b, S13a,b). Yet, in F80 culture, 400 µM scopoletin significantly enhanced iron mobilisation, reaching 70-90% at 6 dpi and remaining ~70% at 9 dpi (Figure 13a). This suggests that F80 sustains scopoletin-mediated iron solubilisation under circum-neutral conditions. F73-scopoletin cultures displayed a slower raise in iron mobilisation, with ~20% at 6 dpi and ~70% at 9 dpi (Figure 13b). Iron solubility in F73 cultures grown in the absence of coumarins (indicated by the dashed line) was nearly as high, suggesting the main driver is fungal activity rather that scopoletin interaction. At 0 dpi, 400 µM esculetin mobilised approximately 70% in mock conditions at pH 7.3, but declined to 25% by 9 dpi, indicating a loss of iron-mobilising capacity (Figure 13). Fraxetin mock was less efficient, solubilising only 30–40% of iron at 0 dpi, strongly declining over time, with no mobile iron detected by 6 dpi (Figure 13). This result confirms what has been previously found, fraxetin's stability in the absence of iron at circum-neutral pH is very low, due to a high susceptibility to oxidative degradation (Kang *et al.*, 2023). When F80 was cultured with esculetin, iron mobilisation remained stable at ~60% throughout the experiment, suggesting that F80 counteracts the decline in esculetin-mediated iron solubilisation at circum-neutral pH (Figure 13a). Similarly, in F80 cultures with fraxetin, the amount of mobilised iron remained more stable (~30–40% from 0 to 9 dpi) compared to mock, suggesting that fungal interactions stabilised fraxetin's activity at circum-neutral pH (Figure 13a). F73 cultures with esculetin and fraxetin followed a similar pattern to those observed with scopoletin. Iron mobilisation decreased at 6 dpi but increased again at 9 dpi (~60%), regardless of coumarin supplementation (Figure 13b). This further supports the idea that iron solubilisation in F73 cultures is primarily fungus-driven rather than coumarin-dependent.

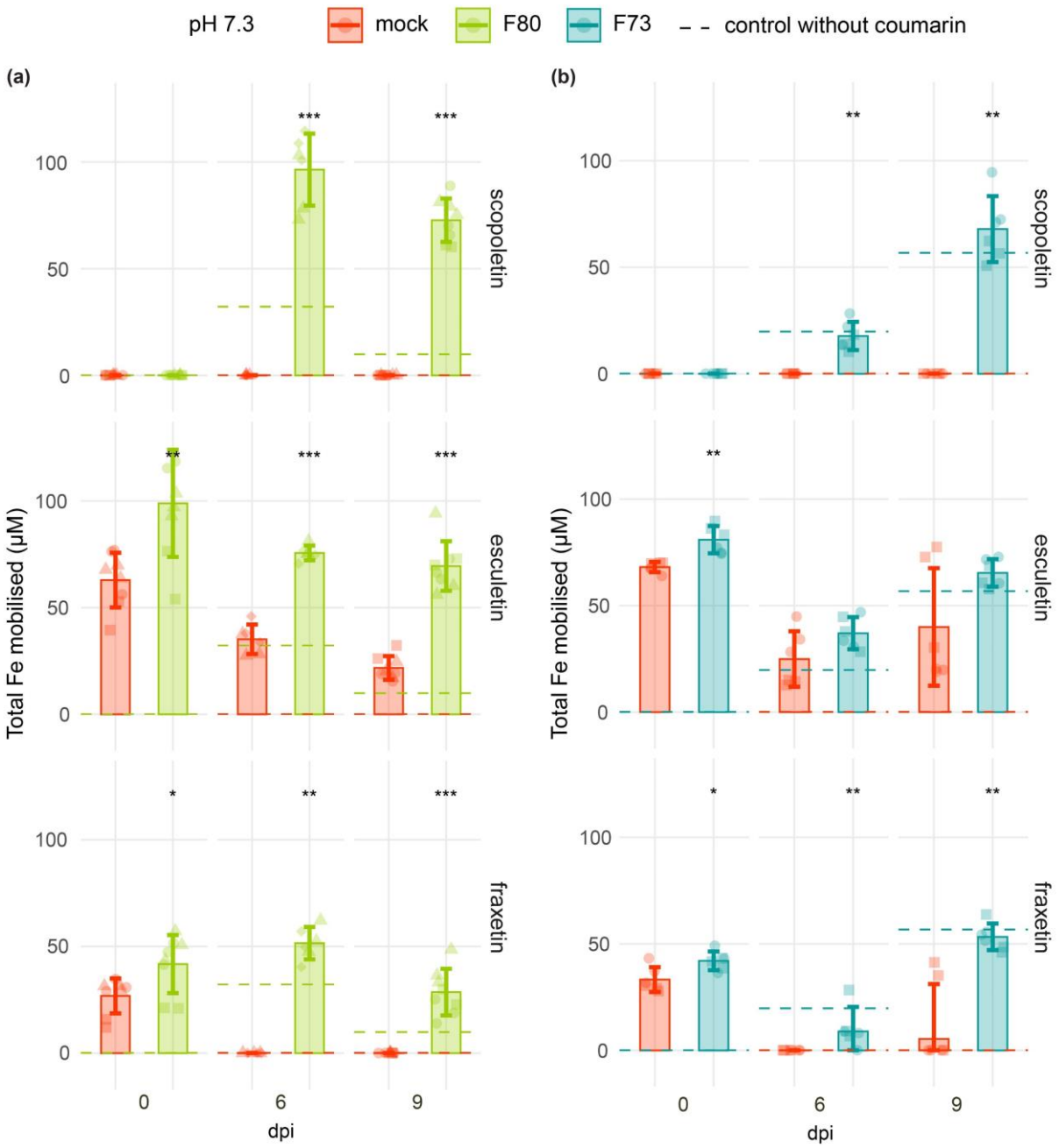

Figure 13. Total iron mobilisation in F80 and F73 cultures supplemented with scopoletin, fraxetin, and esculetin at pH 7.3. The total iron (Fe) mobilised in (a) F80, (b) F73 or mock (MgCl2, indicated with the red dashed lines) supernatant of cultures grown with scopoletin, fraxetin, esculetin (final concentration of 0.4 mM), or an equal amount of DMSO (control indicated with the green/blue dashed lines) at 0, 6, or 9 dpi at pH 7.3 (10 mM MOPS). Mobile iron was measured spectrophotometrically based on the formation of Fe^{2+}-ferrozine complexes, mean ± SD of 3 (a) and 2 (b) biological replicates are shown (represented by different shapes), significance levels shown for comparisons when applicable. Statistical differences between treatments were assessed using t-tests for normally distributed residuals or, otherwise, Wilcoxon rank-sum tests, significance levels are indicated by asterisks with *p <0.05, **p < 0.01, and ***p < 0.001.

Collectively these results highlight that the capacity of coumarins to mobilise iron is strongly influenced by pH, fungal presence, and the duration of interaction in culture. Fraxetin and esculetin mobilised iron effectively under mock conditions (pH 5.7), while scopoletin required fungal interaction. F80 significantly enhanced iron mobilisation for all three coumarins, particularly at pH 7.3, whereas F73 exhibited a delayed but eventual increase in iron mobilisation, independent of coumarin supplementation. These findings highlight the complex interactions between coumarins and fungi in facilitating iron mobilisation and suggest that specific fungal associations may enhance iron availability in different soil conditions.

Iron reduction was assessed alongside iron mobilisation, but due to the potential overestimation caused by ferrozine-facilitated reduction of iron-coumarin complexes (Kang *et al.*, 2023), these results should be interpreted with caution. In general, iron reduction was minimal under mock conditions for scopoletin and esculetin in both pH's, indicating that these coumarins alone did not significantly contribute to iron reduction (Figures S14, S15). Fraxetin is known to be a strong iron reducing agent at acidic pH (Kang *et al.*, 2023), which was reflected in our results and again highlighting the difference in stability depending on the pH (Figures S14, S15). At pH 7.3, iron reduction was consistently lower across all conditions compared to pH 5.7 (Figures S14, S15), underscoring the widespread limitation of iron availability under more alkaline conditions. In F80 cultures, iron reduction was most pronounced in the presence of scopoletin, particularly at 6dpi and pH 5.7, at 9 dpi reduction activity persisted despite a strong decline (Figure S14a). Fraxetin and esculetin exhibited some iron reduction activity in F80 cultures at pH 5.7 (Figure S14a), but this effect was weaker compared to iron mobilisation, and even less at pH 7.3 (Figure S15a). In F73 cultures, iron reduction was in general very low, with no strong coumarin-specific effects observed (Figures S14, S15). Overall, these results suggest that fungal activity, particularly for F80, plays a more significant role in iron reduction than coumarin supplementation alone, and that iron reduction may not be the primary mechanism driving iron availability in these systems.

In addition, to determine whether the above reported results could be influenced by coumarins affecting the fungi, we evaluated fungal growth in the iron mobilisation and reduction assays. The normalised OD600 (to OD600 in DMSO control) of F80 and F73 in the cultures supplemented with coumarins was calculated. As the highest concentration of coumarins used in this experimental set-up (400 µM) is still quite low, we did not find any significant differences in growth of the fungal cultures in all conditions tested (Figure S16a,b). Therefore, we can conclude that the iron mobilisation and reduction are the result of the interaction or cooperation of the fungi with the different coumarins.

Discussion

Root exudation of specialised metabolites represents a central strategy by which plants adapt to nutrient deficiencies and shape the composition of their rhizosphere microbiota (Hacquard *et al.*, 2015; Voges *et al.*, 2019; Robe *et al.*, 2021b). In the present study, we demonstrate that the fungal endophytes F80 and F73 confer enhanced *Arabidopsis* growth under iron-limited conditions at a more alkaline pH (pH 7.3), and that this benefit is contingent upon the biosynthesis of root-exuded coumarins. Indeed, coumarin-deficient *f6'h1* mutants did not exhibit improved growth upon inoculation with F80 or F73, underscoring the necessity of coumarin biosynthesis for fungal-mediated iron acquisition (Figure 8, S7). Among coumarin biosynthetic mutants, only *cyp82c4*—which accumulates scopoletin and elevated levels of fraxetin—benefited from fungal inoculation, implicating fraxetin as a key mediator. Exogenous application of fraxetin, but not scopoletin, restored the capacity of F80 and F73 to promote iron status indicators in *f6'h1* plants (Figure 10), highlighting an interaction between fungal endophytes and fraxetin at pH 7.3.

Fraxetin is consistently the most highly induced coumarin when *Arabidopsis* faces iron limitation at elevated pH and it exhibits efficient Fe^{3+} chelation capacities under these conditions (Schmidt *et al.*, 2014; Rajniak *et al.*, 2018; Vélez-Bermúdez & Schmidt, 2022a; Paffrath *et al.*, 2023). Moreover, fraxetin secretion is indispensable for bacterial rescue of iron-starved *Arabidopsis* at circum-neutral pH (Harbort *et al.*, 2020). Our data thus extend this interplay to fungal endophytes, suggesting a potential mechanism by which fraxetin enables diverse microbial partners to overcome the iron solubility bottleneck in neutral to alkaline soils. Fungal enhancement of plant performance also required functional iron uptake pathways in the plant. Neither F80 nor F73 improved plant growth in *fro2* or *irt1* mutants at pH 7.3, indicating a reliance on the plant's endogenous Fe^{3+} reduction and Fe^{2+} uptake mechanisms. This finding aligns with prior reports that fraxetin and commensal bacteria enhance iron nutrition only when FRO2 and IRT1 are functional (Harbort *et al.*, 2020; Paffrath *et al.*, 2023). This convergence underscores fraxetin's physiological importance and suggests that further dissection of fraxetin–microbe interactions may uncover broadly conserved strategies for enhancing plant iron nutrition in challenging environments.

In addition to fraxetin, esculetin has also been implicated in iron mobilisation at high pH (Rodríguez-Celma *et al.*, 2013b,a; Schmidt *et al.*, 2014; Fourcroy *et al.*, 2014). In the current study, esculetin supplementation at pH7.3 improved total chlorophyll content in *f6'h1* plants under both mock and F80 conditions, but not with F73 inoculation. However, no differences in shoot fresh weight (SFW) were detected between mock and F73 treatment. The differential chlorophyll effect is not attributable to variation in fungal colonisation, suggesting a possible interference of F73 with esculetin availability or activity. Although esculetin's iron mobilisation

properties were unaffected at this pH by F73 in culture, its degradation *in planta* remains a possibility. Degradation of related compounds such as esculin by fungi has been documented as a detoxification mechanism (Bchini *et al.*, 2024), raising the hypothesis that F73 may modify or catabolise esculetin exuded by plant roots.

Comparison of these findings with previous data at pH 5.7 revealed pH-dependent specificity in fungal–coumarin interactions. While both F80 and F73 enhanced plant iron status indicators via a fraxetin-dependent mechanism at pH 7.3, only F80 was effective at pH 5.7, and this effect was associated with scopoletin, not fraxetin (Chapter 2, (Van Dijck *et al.*, 2025)). Given scopoletin's known antifungal properties (Stringlis *et al.*, 2018a; Harbort *et al.*, 2020), these observations prompted further investigation into fungal degradation of scopoletin. In fungal cultures, both F80 and F73 were capable of degrading 2 mM scopoletin at pH 5.7 and pH 7.3, with F73 exhibiting a more rapid degradation rate (Figure 11). The decrease in scopoletin fluorescence correlated with increased fungal biomass, suggesting a detoxification mechanism (Figure S11). Although these assays do not capture the complexity of plant-fungal interactions *in planta*, the data suggest that scopoletin degradation is unlikely to explain the pH-dependent differential plant performance observed with F73.

To dissect how F80 and F73 influence coumarin-driven Fe^{3+} mobilisation, we measured soluble iron released from precipitated $FeCl_3$ in supernatants of the fungi grown with coumarins at both acidic (pH 5.7) and circum-neutral (pH 7.3) conditions. **At pH 5.7**, fraxetin alone mobilised all available Fe^{3+}, while esculetin released substantial Fe^{3+} but less than fraxetin; scopoletin showed no activity on its own. These results are consistent with previously published data (Schmid *et al.*, 2014; Rajniak *et al.*, 2018; Paffrath *et al.*, 2023). In culture with F80, fraxetin's mobilisation was attenuated over time—likely reflecting partial fungal modification—yet F80 alone still released more iron than mock, indicating both direct and coumarin-enhancing roles. Remarkably, scopoletin acquired significant mobilisation ability when paired with F80, consistent with its microbial conversion into catecholic derivatives (chapter 2, (Van Dijck *et al.*, 2025)). In contrast, F73 markedly suppressed fraxetin- and esculetin-mediated iron release and did not confer iron mobilisation with scopoletin, mirroring its inability to rescue plant growth at pH 5.7 *in planta*. **At pH 7.3**, both fraxetin and esculetin rapidly lost iron-mobilising power in mock assays—reflecting instability in more alkaline conditions (Kang *et al.*, 2023). However, F80 presence restored and even enhanced iron release from all three coumarins, and showed pronounced mobilisation activity with scopoletin. It supports a fungal stabilisation and/or transformation of these compounds into effective chelators. This trait might be very important in a natural environment, where rapid degradation or complexation with soil components can affect coumarin stability and activity (Sisó-Terraza *et al.*, 2016; Rosenkranz *et al.*, 2021; Galán-Pérez *et al.*, 2021). By contrast, F73 increased iron release only after prolonged incubation

and did so irrespective of added coumarin, suggesting a coumarin-independent mechanism such as the secretion of siderophores (Boukhalfa & Crumbliss, 2002; Baakza *et al.*, 2004).

Although *ex planta* iron mobilisation trends at pH 5.7 closely paralleled *in planta* phenotypes (Figure 2 & Chapter 2), the responses at pH 7.3 proved more nuanced. F80 promoted iron mobilisation most strongly in culture with scopoletin, yet also required fraxetin for *in planta* rescue. As scopoletin-producing *s8h* mutants remained iron-deficient when inoculated with F80, and scopoletin supplementation failed to reinstate rescue in the *f6'h1* background. These findings suggest that while F80 alone can generate some mobile iron from scopoletin at high pH, the quantity or timing of release is insufficient to meet the plant's needs in the rhizosphere. One plausible explanation is that effective iron mobilisation by F80 under circum-neutral conditions requires both scopoletin and fraxetin. The F80-scopoletin interaction may boost local iron availability, and when combined with F80's stabilisation of fraxetin's chelating activity, could achieve sufficient iron solubilisation in the rhizosphere. However, our coumarin-supplementation experiments did not reveal synergistic effects of scopoletin and fraxetin—perhaps because the concentrations used exceeded the optimal window, as high levels of exogenous coumarins can inhibit root growth (Graña *et al.*, 2017).

The discrepancies in our results likely reflects key differences between the simplified assay conditions and the complex rhizosphere: coumarin concentrations, fungal biomass, and coumarin interconversion all fluctuate dynamically at the root surface, whereas the *ex planta* assays capture only a static snapshot of one metabolite–microbe pairing. This underscored the need for integrated *in situ* approaches that capture real-time coumarin fluxes, fungal conversion kinetics, and plant uptake dynamics to fully understand fungal-mediated plant iron nutrition. Collectively, our data suggest that effective fungal-mediated plant growth rescue at high pH depends on both the presence and stabilisation of fraxetin, in concert with the plant's FRO2/IRT1 machinery.

Conclusions and future perspectives

This work highlights a novel, cross-kingdom synergy in which plant secondary metabolites and fungal endophytes co-operate to overcome the iron-solubility bottleneck imposed by high pH. In this chapter, we reveal that the root endophytes F80 and F73 boost *Arabidopsis* iron status indicators under circum-neutral, iron-limited conditions by exploiting plant-secreted coumarins. Both fungi require a functional plant iron reduction and uptake system (FRO2/IRT1) and the plant's ability to synthesise and export fraxetin.

Looking forward, unravelling the fungal mechanism(s) that underlies the cooperation with scopoletin and fraxetin will be critical. Comparative genomics and targeted mutagenesis in F80 and F73 offer promising avenues to identify the genetic factors responsible for coumarin

interaction. Moreover, time-resolved metabolite profiling in soil microcosms could map the dynamic fate of multiple exuded coumarins. Furthermore, testing these endophyte–coumarin partnerships in multispecies microbial communities and in field-relevant calcareous soils will reveal whether the synergies observed in cultures and in gnotobiotic assays translate to complex agricultural settings. Since both F80 and F73 were found to promote plant performance under phosphate limitation (Mesny *et al.*, 2021), it would be interesting to investigate whether coumarins influence phosphorus acquisition. Elucidating the regulatory networks governing these interactions will enhance our understanding of how plants integrate nutritional and microbial signals to optimise growth under environmental stress. Finally, dissecting how the dual roles of coumarins in nutrient mobilisation and defence shape the balance between mutualism and antagonism will deepen our understanding of plant–microbe interactions. Such insights could inform strategies to engineer root exudate profiles or inoculate crops with tailored microbial consortia, ultimately improving plant resilience and productivity in nutrient-poor soils.

Author contributions

LVD conceived the study with AP and JEP. LVD and CH designed and performed the experiments and analysed the data. CH performed and analysed the ferrozine iron mobilisation and reduction assay. MM provided materials, analytical tools and experimental advice.

4 Chapter 4

Transcriptional changes in *M. phaseolina* (F80) in presence of scopoletin

Introduction

Plants secrete the coumarin scopoletin into the rhizosphere, where it exerts selective antimicrobial activity against soil-borne fungi (Carpinella *et al.*, 2005; Ba *et al.*, 2017; Stringlis *et al.*, 2018b; Beyer *et al.*, 2019; Zhao *et al.*, 2022). Scopoletin inhibits growth of necrotrophic pathogens such as *Botrytis cinerea* by disrupting cell walls and membranes, triggering broad detoxification responses in exposed fungi (Yuan *et al.*, 2024). Notably, the *Botrytis cinerea* scopoletin alteration factor 1 (Bcsaf1) was the first fungal gene identified to encode an enzyme capable of degrading scopoletin by reducing the double bond linking C3-C4, leading to hydrolysis of the δ-lactone ring (Piro *et al.*, in prep).

In Chapter 3, we showed that the endophytes *M. phaseolina* (F80) and *T. angustata* (F73) are less sensitive to scopoletin and can alter or degrade it in culture-based systems. Chapter 2 described the F80-mediated conversion of scopoletin into iron-chelating compounds (e.g. esculetin), and that this activity underpins F80's ability to rescue *Arabidopsis* iron nutrition. Yet the underlying fungal genes and pathways responsible for scopoletin conversion remain unknown.

To uncover these mechanisms, we performed RNA-sequencing on F80 mycelia grown in liquid culture with 2 mM scopoletin and sampled at the onset of degradation, as monitored by scopoletin fluorescence assays. Principal component analysis confirmed that scopoletin treatment accounted for ~79% of transcriptional variance, indicating a robust fungal response to the compound. Functional annotation with eggNOG-mapper revealed that many differentially expressed genes were part of the Clusters of Orthologues Genes (COG) category: secondary metabolism and detoxification. Among the highly induced candidates are several monooxygenases, oxidoreductases, and dehydrogenases. In this chapter, we describe the selection and heterologous expression of the seven top candidates, their evaluation in *Saccharomyces cerevisiae*, and the insights and limitations these experiments provide in pinpointing the genetic drivers of fungal-mediated coumarin transformation.

Material and methods

F80 RNA-Sequencing

For each replicate experiment, ten F80 cultures containing 200 µl 1/2MS medium as described for the 96-well fungal culture assay (chapter 2) were grown at 22°C (140rpm) supplemented with 2mM scopoletin or an equal volume of DMSO. Scopoletin fluorescence was monitored

and the cultures were harvested when there was a fluorescence decrease of approximately 30%. Hyphae were collected in tubes using Miracloth filters and flash frozen in liquid nitrogen. Two 3.175 mm and five 1.3 mm stainless steel beads were added to each tube, and samples were homogenised in a Qiagen TissueLyzer II for two 1-minute cycles at 30 Hz. To extract RNA, 800 µl TRIzol and 160 µl Chloroform were added to each tube, samples were vortexed briefly, and centrifuged for 10 minutes at 20000 x g (4°C). Thereafter, 100 µl of the aqueous (upper) phase was added to 35 µl of isopropanol in a new tube and vortexed for 5 seconds. The Promega Reliaprep kit was used for RNA purification. Library preparation, PolyA enrichment and RNAseq (2^7 reads, 150 bp paired end reads) were performed by Novogene.

Raw RNA-seq reads were trimmed using Trimmomatic v0.38 with the parameters LEADING:3 TRAILING:3 SLIDINGWINDOW:4:20 MINLEN:51. Trimmed reads were then aligned to the *Macrophomina phaseolina* reference genome (GCA_020744275.1) using HISAT2 v2.2.1. HISAT2 indexes were built from the reference genome, and known splice sites were extracted from the corresponding GTF annotation. Read counting was conducted with HTSeq v0.13.5, to generate raw count tables for each sample. The resulting count tables were combined into a single matrix for downstream expression analysis. Differential gene expression analysis was performed using DESeq2 v1.24.0 in R. EggNOG-mapper was used to extract the functional annotations of genes (Cantalapiedra *et al.*, 2021).

Heterologous expression in yeast and scopoletin degradation assay

Yeast expression vectors were derived from Yeast 2-Hybrid vector pGBKT7 (Louvet *et al.*, 1997) by PCR amplification using primers nAP1069/nAP1070 to replace the Gal4 AD with a yeast Kozak sequence and FLAG tag. F80 open reading frames (ORFs) were amplified from cDNA generated from RNA extracted using the my-Budget Plant RNA kit from scopoletin-treated cultures. RNA (1 µg) was DNase I-treated (30 min, 37 °C) and reverse-transcribed using the RevertAid First Strand cDNA Kit with Oligo dT primers. ORFs were amplified with primers adding 15–18 bp overlaps to the pGBKT7 vector (primers are listed in Table S2). PCR products were purified and assembled via In-Fusion (Takara) into DpnI-digested pGBKT7, then transformed into *E. coli* DH10b. Transformants were selected on LB-Kan (25 mg/L), screened by SpeI-HF digestion, and verified by Sanger sequencing. A FLAG-only control was constructed by amplifying pGBKT7 with nAP1069/nAP1071 and assembled similarly. Vectors were transformed into *S. cerevisiae* MaV203 *S. cerevisiae* MaV203 (MATα, *leu*2-3,112, *trp*1-901, *his*3Δ200, *ade*2-101, *gal*4Δ, *gal*80Δ, *SPAL*10*::URA*3, *GAL*1::*lacZ*, *HIS*3UAS GAL1*::HIS*3@*LYS*2, *can*1R, *cyh*2R) grown on YPAD (Per 1 L: 10 g Bacto Yeast Extract, 20 g Tryptone/peptone ex casein, 20 g Glucose, 40 mg Adenine, 20 g Difco Agar), or in liquid YPAD (lacking agar) by lithium acetate/PEG transformation, and transformants were selected and cultured on Standard Defined medium lacking tryptophan (SD-W) (Per 1 L: 6.7 g Yeast

Nitrogen Base without amino acids, 0.74 g SD-W nutrient mix, 20 g Difco Agar, 50 ml 40% glucose added after autoclaving), or in liquid SD-W (lacking agar).

To test the candidates for scopoletin degradation, a similar 96-well plate assay was used as described above. Overnight yeast cultures (30 °C, 250 rpm) were diluted to OD600= 0.25 in SD-W medium containing 0.5 mM scopoletin or an equal amount of DMSO. 180 µl per well was inoculated with 20 µl of culture in 96-well plates and incubated at 30 °C with shaking. Fluorescence (λ_ex 385 nm / λ_em 470 nm) and OD600 was measured at the start and after 24h with a Tecan plate reader.

The expression of the proteins in the yeast cultures was confirmed with immunoblotting. Aliquots equivalent to 0.5 OD600 were harvested, washed in water, and resuspended in 0.5 ml ice-cold water. Samples were treated with 75 µl of 2 N NaOH and 1.15 M β-mercaptoethanol on ice for 15 min, with repeated vortexing. For precipitation, 75 µl of 55% trichloroacetic acid was added, samples were incubated on ice for 15 min with repeated vortexing, and pelleted (20,000 × g, 4 °C, 20 min). The pellets were resuspended in 25 µl HU buffer (200 mM Sodium Phosphate pH 6.8, 8 M Urea, 5% (w/v) sodium dodecyl sulphate, 1 mM EDTA, 100 mM dithiothreitol, and 1% (w/v) bromophenol blue), incubated at 65°C for 15 min for denaturation, and cleared by centrifugation (1 min, 20,000 × g). 8 µl of each sample was run by SDS-PAGE on BioRad anyKD gels at 150V. Proteins were transferred to nitrocellulose membranes, blocked for 1 h in 5% milk in TBST (20 mM Tris pH 7.5, 150 mM NaCl, 0.1% Tween-20), and probed overnight at 4 °C with 1:5000 anti-FLAG rabbit polyclonal IgG (Merck F7425) or 1:4000 anti-GAPDH mouse monoclonal IgG (Thermo MA5-15738) in 2% fat-free dry milk in TBST. The membranes ware washed three times with TBST (5 min), and secondary antibodies were applied for 1 h (1:5000 anti-rabbit or anti-mouse IgG-HRP, respectively, in 2% fat-free dry milk TBST). Membranes were washed three times with TBST (5 min) and once with TBS (20 mM Tris pH 5,7, 150 mM NaCl), and developed using Clarity ECL substrate (Bio-Rad) on a ChemiDoc MP system.

Results and discussion

Our goal was to characterise the genome-wide transcriptional changes of F80 in the presence of scopoletin. To identify genes in F80 that respond to scopoletin exposure, we performed RNA-seq on F80 cultures supplemented with 2 mM scopoletin. Fluorescence monitoring confirmed the onset of scopoletin degradation before mycelial harvest and RNA extraction. Principal component analysis (PCA) of the processed transcriptomes showed that 79 % of the variance separated scopoletin from control samples, whereas only 13 % reflected differences between biological replicates (Figure 14). This clear partitioning validates the experimental design and indicates a robust transcriptional response to scopoletin challenge.

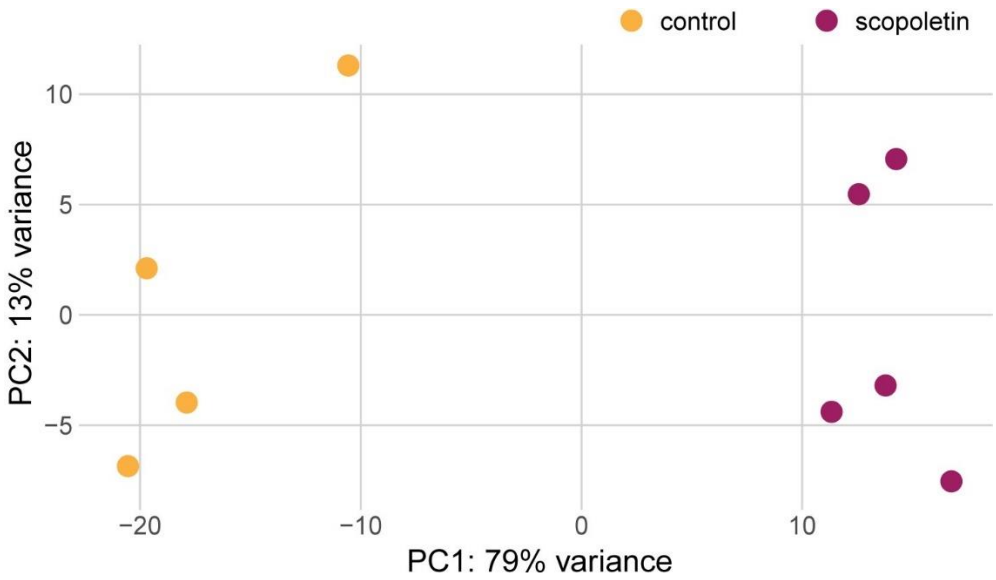

Figure 14. Principal Component analysis plot. Principal component analysis of gene expression from RNAseq in scopoletin (purple) versus DMSO control (yellow) F80 cultures.

Functional annotation using eggNOG-mapper highlighted limited genome coverage, as previous studies of closely related strains notified that the *M. phaseolina* genome remains under-annotated (Islam *et al.*, 2012; Burkhardt *et al.*, 2019). Consequently, many of the differentially expressed genes (DEGs) that we identified remain to be characterised. However, COG categories which group proteins into broad functional classifications, provided more general annotations and were used to plot the overall changes following scopoletin treatment (Figure 15). Among the COG categories, 'secondary metabolites biosynthesis, transport and catabolism' contained the highest total number of DEGs, while 'nucleotide transport and metabolism' had the lowest. The largest disparities between up- and down-regulated genes were found for: lipid metabolism; inorganic ion transport and metabolism; secondary metabolites biosynthesis, transport and catabolism; carbohydrate transport and metabolism (Figure 15). Unfortunately, the functions of the majority of up- and down-regulated genes remain unknown (Figure 15). Notably, most COG categories showed a higher downregulated gene count, only four categories (translation, ribosomal structure and biogenesis; replication and repair; cell cycle control and mitosis; cytoskeleton) exhibited net up-regulation, suggesting a broad reallocation of resources under scopoletin stress. This likely reflects scopoletin's antifungal activity against both filamentous fungi and yeasts, where it compromises membrane integrity and disrupts biofilm formation (Carpinella *et al.*, 2005; Gnonlonfin *et al.*, 2012; Sun *et al.*, 2014b; Lemos *et al.*, 2020; Yuan *et al.*, 2024)

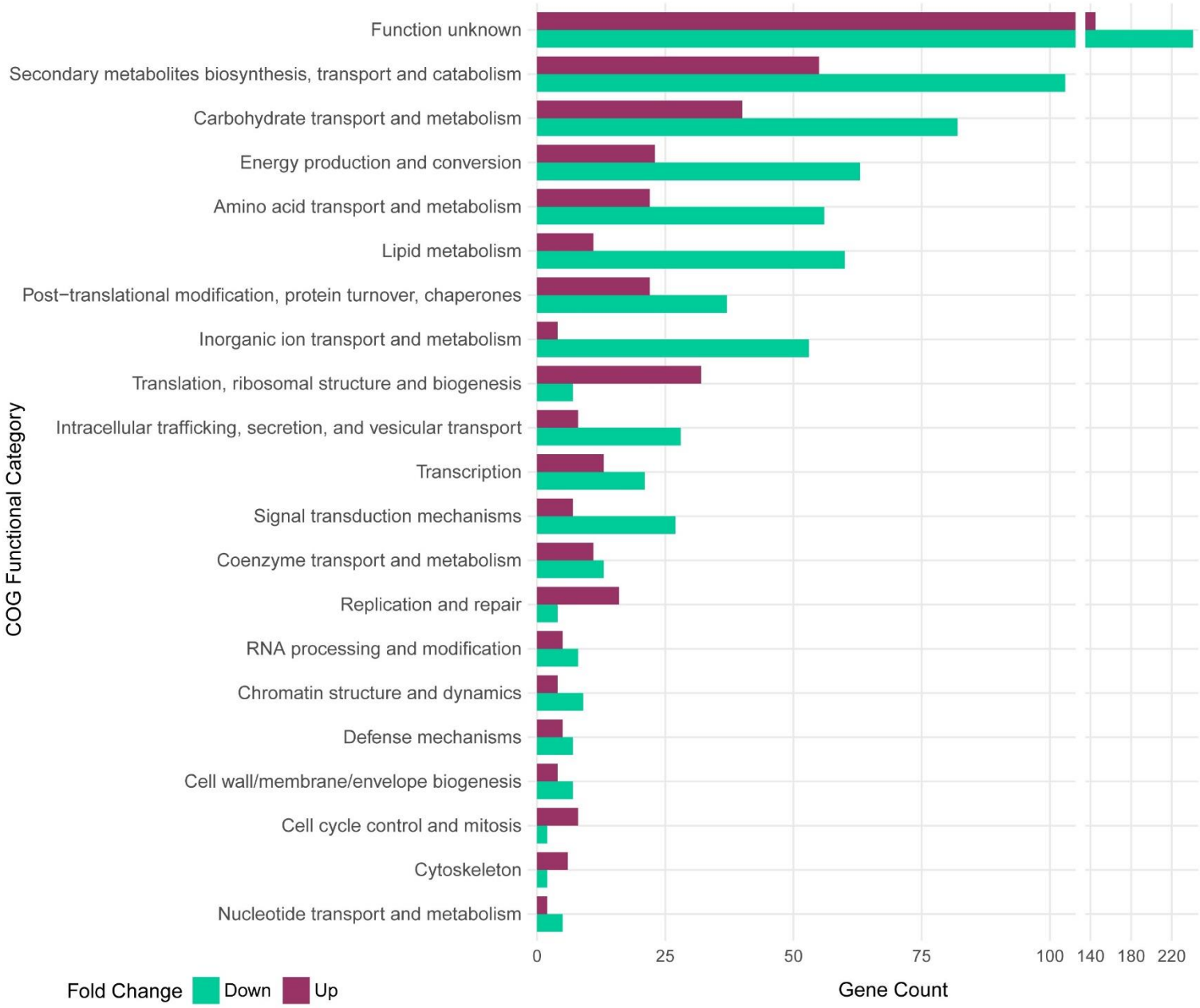

Figure 15. Gene count in COG functional categories. RNAseq in F80 in culture with 2 mM scopoletin, relative to (DMSO) controls. The amount of up and downregulated F80 genes in the different Clusters of Orthologues Genes (COG) categories annotated with EggNOG-mapper. Blue and purple bars represent genes significantly (p-adj≤0.05) downregulated or upregulated Log2fold ≥ 1, respectively. Data from 5 independent experiments with 10 replicate cultures each.

We next focused on the top up-regulates genes (Figure 16, Table 1). Fungal detoxification of plant toxins often involves monooxygenases and oxidoreductases, as found for *Botrytis cinerea* (You *et al.*, 2024) and other basidiomycetes (Syed *et al.*, 2010) and ascomycetes (Francis *et al.*, 2012). Fungal P450 monooxygenases are renowned for their versatility in both primary and secondary metabolism, detoxication, and enabling adaptation to environmental

stresses (Durairaj *et al.*, 2016). Accordingly, our volcano plot (Figure 16) revealed several highly up-regulated genes encoding cytochrome P450 monooxygenases (p450) (candidates 1 and 2), an FAD-linked oxidoreductase (FAD OR) (candidate 4), and an alcohol dehydrogenase (candidate 7) (Table 1). Candidate 7 also contains a predicted enoyl reductase domain (ENR), reminiscent of the *B. cinerea* scopoletin-alteration factor Bcsaf1, which also carries an enoyl reductase domain (Piro *et al.*, in prep). BcsSaf1 catalyses the catalyses the reduction and hydrolysis of scopoletin to 3-(2,4-dihydroxy-5-methoxyphenyl)propanoic acid (Piro *et al.*, in prep), a compound we also detected in the metabolite profile of F80-scopoletin cultures (Chapter 2, (Van Dijck *et al.*, 2025)). The induction of these enzymes suggests a detoxification response aimed at modifying or mineralising scopoletin.

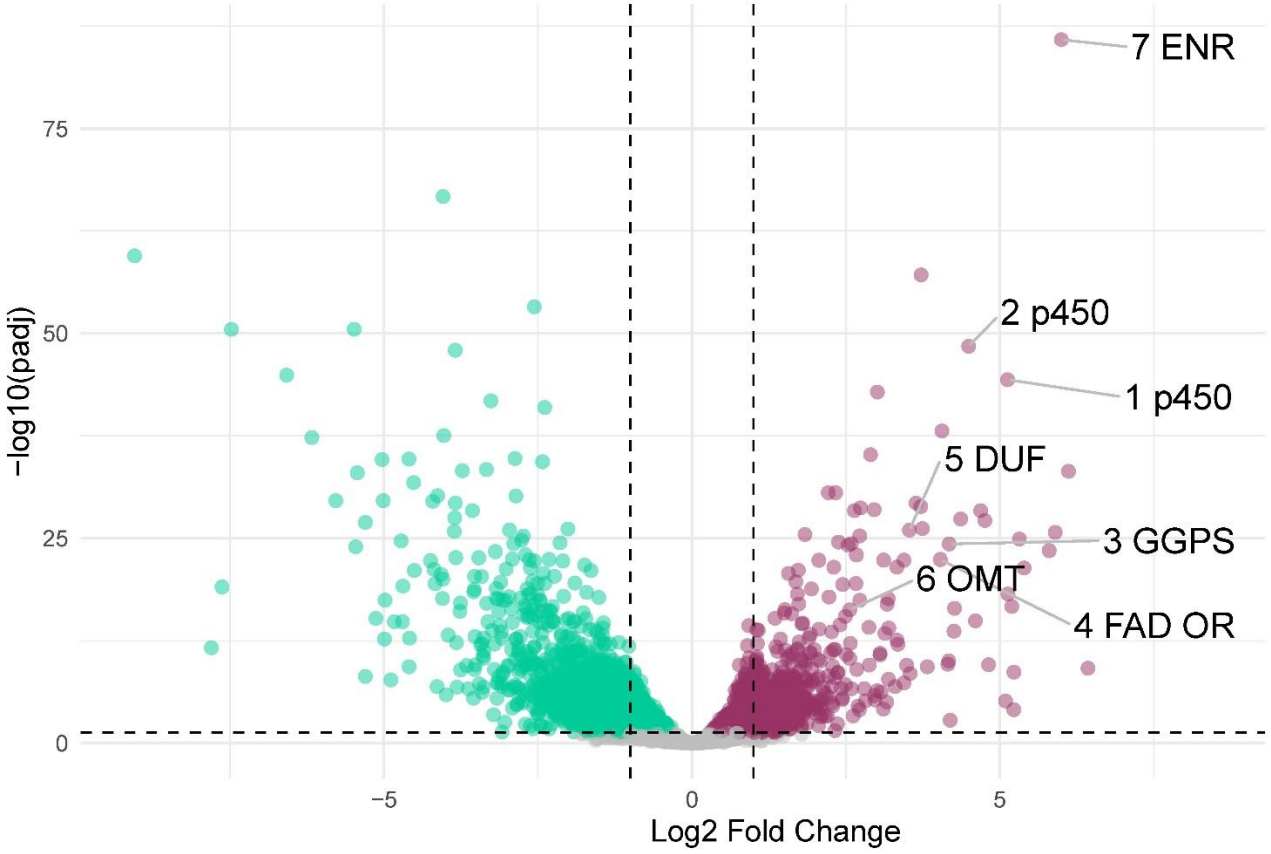

Figure 16. F80 RNA-Seq volcano-plot. RNAseq in F80 in culture with 2 mM scopoletin, relative to (DMSO) controls. Blue and purple dots represent genes significantly (padj $\leq$ 0.05) downregulated or upregulated $\geq$ 2-fold, respectively. Labeled genes are candidates selected for expression in yeast. Data from 5 independent experiments with 10 replicate cultures each.

Candidates 1 - 4 co-localise in a predicted biosynthetic gene cluster (BGC) identified via FunBGCeX (BGC7) (Tang & Matsuda, 2024). The above considerations, along with the tendency for fungal secondary-metabolite genes to occur in genomic clusters (Robey *et al.*, 2021), led us to prioritise these loci as candidate genes.

Figure 17. BGC7 *M. phaseolina*. FunBGCeX predicted biosynthetic gene cluster (BGC) 7 contains candidates 1-4, location indicated. (Scaffold JAGTJR010000012, position: 467806-503701, length 35896 bp)

To prioritise *in planta* relevance, we cross-referenced F80 DEGs with an *Arabidopsis* root RNA-Seq dataset enriched for genes differentially regulated in roots colonised by F80 (Mesny *et al.*, 2021). Five of seven top candidates (1, 2, 4, 5, and 6) were also induced in F80-colonised roots (Table 1), underscoring their potential role in the rhizosphere. Candidate 5, containing a domain of unknown function (DUF) 3328 domain, and candidate 6, a putative O-methyltransferase (OMT) (Figure 16, Table 1), may participate in coumarin modification or sequestration, as similar enzymes have been linked to microbial adaptation to host-derived phenolics (Jalkanen *et al.*, 2020; Venkatesagowda & Dekker, 2021).

Table 1. List of selected F80 gene candidates. For each candidate their protein ID, annotated description and log2 Fold Change in F80-scopoletin and the *Arabidopsis* (*in planta*) RNA-seq (Mesny *et al.*, 2021).

Candidate	Protein ID	Description	log2FoldChange	log2FoldChange *in planta*
1	78534	Cytochrome P450 monooxygenase activity	5.12	9.43
2	78543	Cytochrome P450 monooxygenase activity	4.49	4.83
3	662146	geranylgeranyl pyrophosphate synthase	4.18	X
4	710584	FAD linked oxidoreductase	4.03	6.20
5	745907	DUF3328	3.53	4.11
6	703228	O-methyltransferase	2.56	6.65
7	692377	Alcohol dehydrogenase	6.00	X

We expressed each candidate as an N-terminal FLAG fusion in *Saccharomyces cerevisiae* to assay scopoletin-degradation activity, using Bcsaf1 from *B. cinerea* as a positive control. Despite successful cloning and heterologous expression, none of the candidates matched Bcsaf1's scopoletin-degrading efficiency (Figure 18). Several candidates impaired yeast

growth (Figure S17), hinting at potential toxicity or improper folding in the heterologous system. Candidate 7 did not inhibit the growth of the yeast, and its proper expression a western blot analysis was performed, indicating a high expression of the candidate 7 protein in the yeast system (Figure S18). The inability to pinpoint a single scopoletin-degrading enzyme may reflect (i) transient or low-abundance expression peaks not captured at our sampling timepoint, (ii) the requirement for co-expression of multiple BGC genes, or (iii) non-enzymatic oxidation facilitated by fungal reactive oxygen species, as observed during coumarin-mediated iron-oxide dissolution (Baune *et al.*, 2020).

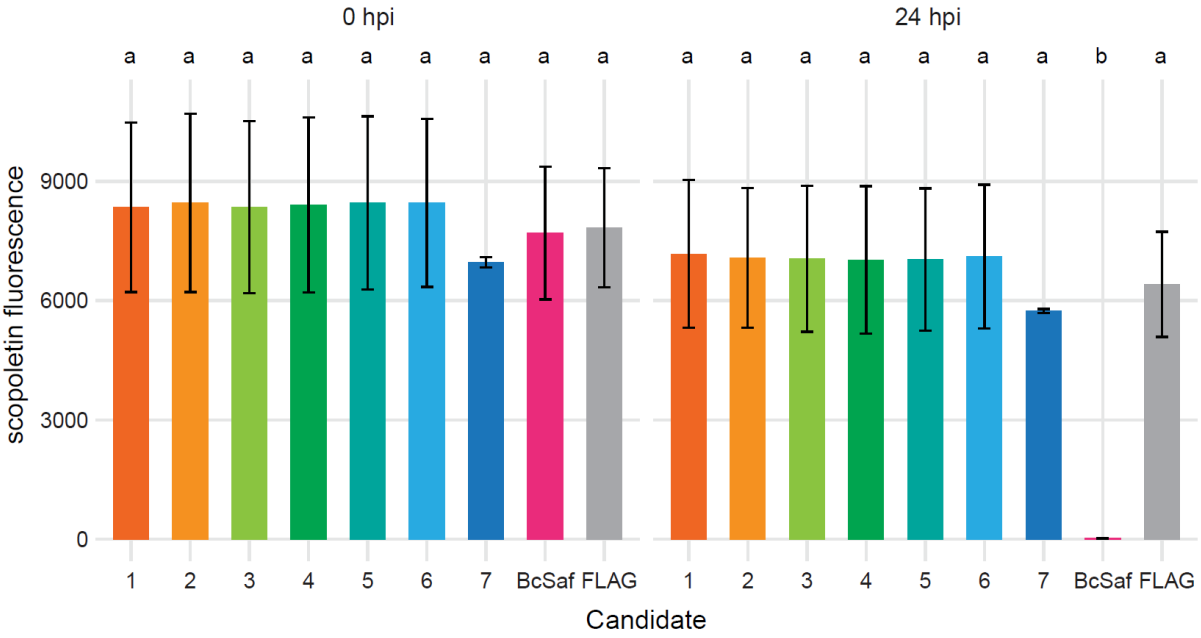

Figure 18. Fluorsecence-based scopoletin degradation assay in *S. cerevisiae* expressing F80 candidate genes. The candidate genes 1-7 were cloned and expressed in *S. cerevisiae* as N-terminally FLAG-tagged proteins and grown in culture with 0.5 mM scopoletin to assess their scopoletin-degradation capacity. Fluorescence was measured at the start and 24 hours past inoculation (hpi) (exciting at 385nm and emission detected at 470nm). BcSaf1 was used as a positive control (BcSaf) and an empty FLAG-vector as negative control (FLAG). Bars represent the mean ± SD, Letters indicate significant pairwise differences between groups (p-adj≤0.05) by a pairwise t-test with Bonferroni correction. Data are from two biological replicates (3 technical replicates each).

Collectively, our data illuminate a broad detoxification and secondary-metabolite response to scopoletin in F80, characterised by the induction of monooxygenases, oxidoreductases, and potential BGC-associated enzymes. Future work could employ time-course transcriptomics to capture dynamic expression peaks, CRISPR/Cas9-mediated gene knockouts in F80 to test candidate function *in situ*, and co-expression of entire BGCs in heterologous hosts. Integrating metabolite flux analysis in soil microcosms will further clarify whether enzyme-mediated conversion or abiotic oxidation drives scopoletin transformation, ultimately revealing how endophytic fungi harness plant secondary metabolites to enhance iron acquisition.

5 Main discussion

Over the course of this thesis, we have uncovered a multifaceted role for root-secreted coumarins and their interactions with fungal endophytes in supporting *Arabidopsis* iron nutrition under both acidic and circum-neutral pH. In Chapter 2, we demonstrated that scopoletin—despite its own inability to directly chelate iron—serves as a microbial precursor: the fungal endophyte *Macrophomina phaseolina* (F80) converts scopoletin into the potent catechol coumarin esculetin, thereby cooperatively mobilising Fe^{3+} upstream of the plant's FRO2-IRT1 reductive import machinery (Figure 19). Chapter 3 extended these findings to circum-neutral pH, revealing that both F80 and *Truncatella angustata* (F73) require the plant-derived coumarin fraxetin to alleviate iron starvation (Figure 19). Fraxetin, highly induced under more alkaline iron-limiting conditions, emerged as a central mediator across bacterial and fungal interactions. Finally, Chapter 4 employed transcriptomics to explore the fungal genetic basis for scopoletin degradation, but did not pinpoint a single enzyme, suggesting that coumarin conversion may involve a broader detoxification response or non-enzymatic mechanisms. Collectively, these studies uncover a novel, cross-kingdom mechanism by which plants and fungal endophytes collaborate via coumarin chemistry to alleviate iron limitation.

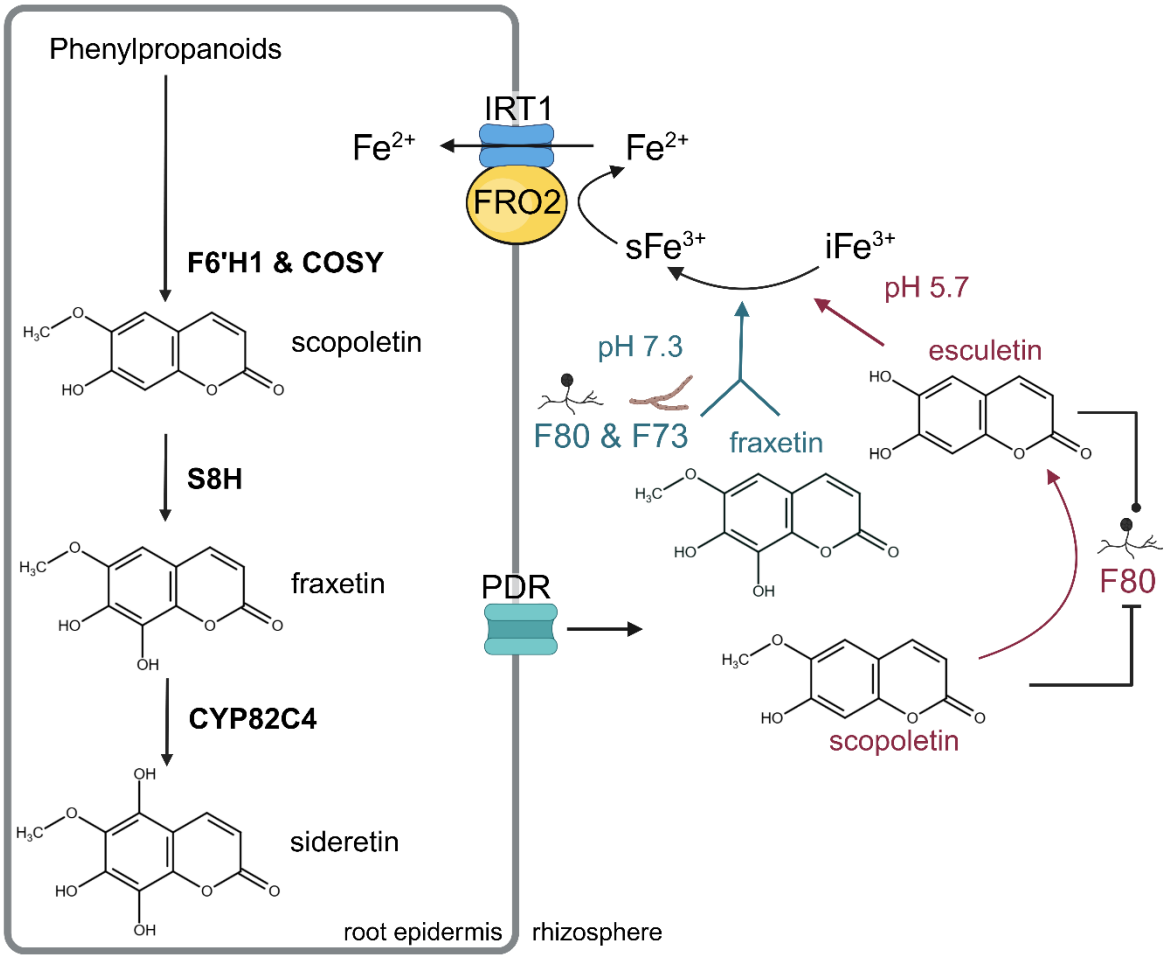

Figure 19. Model of root fungal endophytes cooperating with distinct coumarins at acidic and circum-neutral pH to mediate iron nutrition in *Arabidopsis*. In *Arabidopsis*, iron deficiency induces the biosynthesis and exudation of coumarins, with F6'H1 and COSY initiating the pathway to generate scopoletin, and subsequent conversion occurs via S8H and CYP82C4 into fraxetin and sideretin, respectively. These compounds are secreted into the rhizosphere via ABC-type PDR transporters, where catechol coumarins such as fraxetin, sideretin, and esculetin chelate ferric iron to support uptake via the FRO2–IRT1 system. Our results suggest a cooperative mechanism in which F80 converts scopoletin into esculetin, enhancing iron solubility and supporting plant iron acquisition at pH 5.7 (in magenta). At pH 7.3 F80 and F73 cooperate with fraxetin to alleviate iron starvation symptoms upstream of the plant's FRO2-IRT1 reductive iron uptake system (blue). (Figure made with Biorender)

5.1 Scopoletin–fungal cooperation mobilises Fe^{3+} resulting in plant rescue under iron limiting acidic conditions (Chapter 2)

Despite its inability to chelate Fe^{3+}, scopoletin is one of the most abundant coumarins exuded by iron-starved *Arabidopsis* roots under acidic conditions (Schmid *et al.*, 2014; Sisó-Terraza *et al.*, 2016; Rajniak *et al.*, 2018; Rosenkranz *et al.*, 2021; Paffrath *et al.*, 2023). Chapter 2 revealed that F80 degrades scopoletin in *in vitro* and *in planta* assays, converting it to the catechol coumarin esculetin—a potent Fe^{3+} chelator—thereby resolving the Fe^{3+} solubility bottleneck (Schmidt *et al.*, 2014; Schmid *et al.*, 2014; Paffrath *et al.*, 2023). This "win–win" scenario benefits the fungus by detoxifying scopoletin's antimicrobial activity (Sun *et al.*, 2014b; Stringlis *et al.*, 2018b; Yuan *et al.*, 2024) and the plant by generating bioavailable iron. Genetic evidence supports scopoletin's central role. Specifically, coumarin-deficient *f6'h1* mutants were not rescued by F80, whereas F80 restored proper iron nutrition to *s8h* mutants (which accumulate scopoletin but lack fraxetin/sideretin). Furthermore, chemical complementation with scopoletin restored F80-mediated rescue of *f6'h1* plants, firmly establishing scopoletin's necessity and sufficiency when partnered with F80.

5.2 Fraxetin as a keystone coumarin for *Arabidopsis* nutrition at circum-neutral pH (Chapter 3)

Under circum-neutral conditions (pH 7.3), Strategy I mechanisms such as rhizosphere acidification, become insufficient for effective iron acquisition (Santi & Schmidt, 2009; Tsai & Schmidt, 2017, 2020). Chapter 3 demonstrated that both F80 and the unrelated endophyte F73 can improve *Arabidopsis* growth under iron limitation at pH 7.3, but only when fraxetin biosynthesis and export are intact. The *cyp82c4* mutant, which produces scopoletin and accumulates fraxetin, was uniquely rescued by both fungi, whereas *f6'h1* and *pdr9* (impaired in fraxetin export) were not (Kai *et al.*, 2008; Ziegler *et al.*, 2017). Exogenous fraxetin—but not scopoletin—restored fungal-mediated rescue of *f6'h1*, pinpointing fraxetin as the critical chelator at circum-neutral pH. These results parallel bacterial studies showing that commensal

communities rescue iron-starved *Arabidopsis* in a fraxetin-dependent manner under circum-neutral conditions (Harbort *et al.*, 2020). In axenic assays, fraxetin is the major coumarin exuded at high pH, with robust iron mobilising activity (Fourcroy *et al.*, 2014; Schmid *et al.*, 2014; Sisó-Terraza *et al.*, 2016; Tsai *et al.*, 2018; Paffrath *et al.*, 2023). The present findings extend fraxetin's role from purely plant- and bacterial-mediated processes to fungal partnerships, suggesting a conserved, cross-kingdom strategy for overcoming iron starvation at circum-neutral pH.

5.3 Fungal scopoletin degradation: a complex stress response (Chapter 4)

Chapter 4 sought to identify the genetic basis of scopoletin degradation in F80 by RNA-sequencing of F80 cultures exposed to scopoletin. Although multiple monooxygenase and oxidoreductase genes were induced—consistent with a general detoxification response to antimicrobial toxins—no clear single candidate was found via scopoletin degradation assays by heterologous expression in yeast. Possible explanations include timing of peak expression, requirement for entire biosynthetic clusters, non-enzymatic oxidative reactions, or the influence of rhizosphere microenvironments. Notably, the detection of esculetin in chapter 2 is consistent with oxidative demethylation of scopoletin described in coumarin-mediated iron-oxide dissolution (Baune *et al.*, 2020). In this study, non-enzymatic coumarin oxidation products are discussed, however, oxidative demethylation has also been described to be executed by cytochrome P450 enzymes (Hagel & Facchini, 2010), which we frequently detected among the highly scopoletin-upregulated genes in F80. The fact that no single scopoletin degradation gene was identified, underscores the need for broader metabolomic and genetic screens, perhaps leveraging mutagenesis or co-expression analyses, to elucidate potential enzymatic machinery.

5.4 Broader implications and future directions

5.4.1 Cross-kingdom convergence on coumarin cooperation

The demonstration that both bacteria (Harbort *et al.*, 2020) and fungi employ coumarin-dependent mechanisms to facilitate iron mobilisation underscores the centrality of root-derived coumarins in these plant – microbe interactions. This convergence opens up questions regarding how these interactions would influence plant growth under nutrient limitations in a community context. In natural, iron-limited (alkaline) soils, Harbort *et al.* (2020) showed that *Arabidopsis f6'h1* mutants exhibit reduced SFW and chlorophyll content, while cyp82c4 plants perform comparable to wild type when soil microbiota are present. These observations imply that the simplified, binary interactions we describe with F80 and F73 likely persist within complex microbial communities, underscoring the ecological relevance of coumarin-mediated iron mobilisation across microbial kingdoms. Moreover, *Arabidopsis* and other plants exude a

variety of non-catechol coumarins (Kai *et al.*, 2006; Sisó-Terraza *et al.*, 2016; Pan *et al.*, 2017), raising the possibility that root-associated microbes similarly convert these precursors into iron-chelating compounds.

5.4.2 Expanding to other nutrients and microbiome functions

It would be worth investigating whether coumarin – microbiota interactions also drive the uptake of additional nutrients. Given that F80 and F73 also enhance *Arabidopsis* performance under phosphate limitation (Mesny *et al.*, 2021), it is plausible that coumarin–endophyte cooperation extends to additional micronutrients. Testing whether coumarin-biosynthesis mutants alter P uptake, or whether other phenylpropanoid derivatives (e.g., flavonoids, phenolics) serve similar cross-nutrient roles, represents a rich avenue for future research.

More broadly, plants secrete diverse secondary metabolites—anthocyanins, alkaloids, terpenoids—in response to nutrient stress. Systematic screens of fungal culture collections isolated from plant roots may reveal novel plant-growth-promoting fungi (PGPFs) that interact with these compounds. Outside of well-studied groups such as AMF and *Trichoderma* species (Govindarajulu *et al.*, 2005; Chaverri *et al.*, 2015; Lehmann & Rillig, 2015; Martínez-Medina *et al.*, 2017; Zhao *et al.*, 2020; Vyas *et al.*, 2024), the nutrient-mobilisation potential of most fungal endophytes remains uncharacterised. Leveraging high-throughput metabolomic and microbiome profiling could identify new PGPFs, opening opportunities to enhance crop nutrition and resilience across a range of soil types.

5.4.3 Mechanistic elucidation of fungal scopoletin degradation

In order to further elucidate the mechanism by which these coumarin-fungal interactions take place, it would be worth to perform additional RNA-seq experiments at additional timepoints, increasing the chance of finding the genetic determinant responsible for the scopoletin conversion. If a specific fungal enzyme or BGC is responsible, generating fungal gene knock-out mutants would further resolve the mechanism of scopoletin-conversion, and could be used *in planta* to further demonstrate the importance of fungal-mediated coumarin-derivatives in plant iron nutrition. Additionally, monitoring coumarin exudation in combination with possible microbial conversions, would help to further understand the dynamics in the rhizosphere of plants under nutrient limitations. To be able to map all of these reactions, working with more complex synthetic communities could help to dissect cooperative vs competitive interactions. Such approaches will reveal whether microbial partners share conserved coumarin conversion pathways or have evolved distinct enzymatic solutions.

5.4.4 Ecological and agricultural relevance

F80 and F73 were isolated from the roots of healthy *Arabidopsis* plants growing in European soils (Durán *et al.*, 2018), and related *M. phaseolina* strains are known pathogens causing

charcoal rot across 500+ species (Su *et al.*, 2001; Marquez *et al.*, 2021; Shirai & Eulgem, 2023). The lack of disease symptoms in *Arabidopsis* suggests that F80 may be a more host-adapted strain with reduced virulence. Emerging research highlights that fungal endophytes, especially those in long-term associations with specific hosts, can undergo evolutionary shifts towards mutualism—often driven by gene loss or modulation in pathogenicity factors to favour compatibility (Ma *et al.*, 2010; Reinhardt *et al.*, 2021). This is supported by research on plant–fungus co-evolution: endophytic fungi maintain asymptomatic colonisation while retaining latent pathogenic potential, only transitioning to disease-causing roles under specific stress conditions (Torres *et al.*, 2020; Mesny *et al.*, 2023). Thus, F80's ability to enhance plant iron nutrition could reflect co-evolutionary adaptation enabling beneficial interactions under certain conditions. This dual potential—for mutualism in one context and pathogenesis in another—highlights the plasticity and context-dependence of endophyte lifestyles (Hacquard *et al.*, 2016). Perhaps Deploying coumarin-interacting endophytes could become a novel agronomic tool to enhance iron nutrition in calcareous soils, reducing reliance on synthetic chelates and soil acidification strategies (Lindsay & Schwab, 1982; Zuo & Zhang, 2011; Vélez-Bermúdez & Schmidt, 2022a; Zuluaga *et al.*, 2023).

5.5 Conclusion

This thesis establishes, for the first time, that a fungal endophyte can directly enhance plant iron nutrition by repurposing a plant-derived coumarin —scopoletin—into potent iron-mobilising catechol compounds like esculetin. It further identifies fraxetin as a keystone molecule enabling both bacterial and fungal partners to liberate iron under more alkaline pH. These discoveries broaden our understanding of plant–microbe co-evolution, situating coumarins at the nexus of nutrient acquisition and microbiome assembly. Harnessing such natural biochemical collaborations offers a sustainable path to improve crop resilience in iron-deficient soils worldwide.

6 Supporting information

Chapter 2:

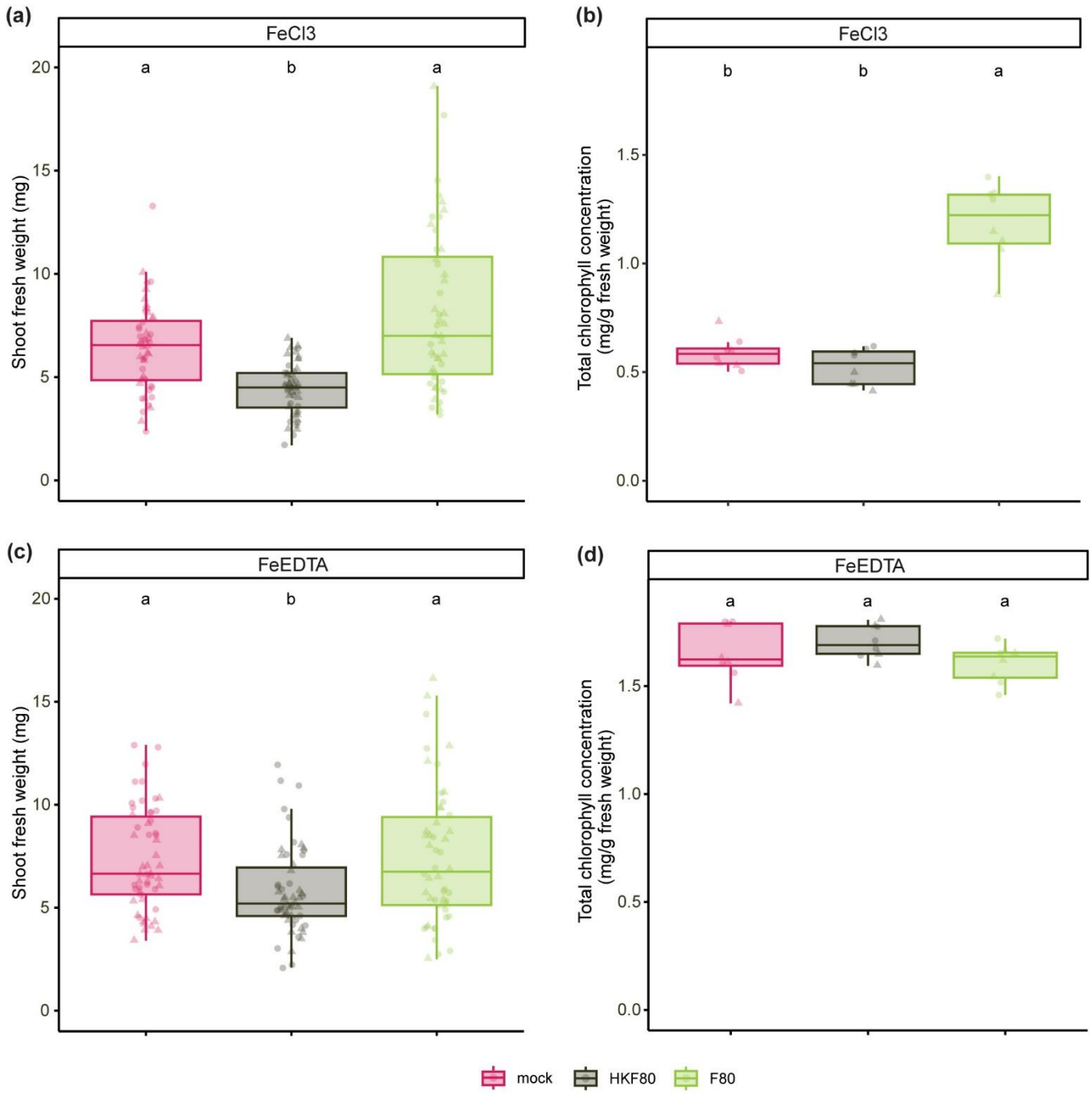

Fig. S1 Heat-killed fungal endophyte F80 does not improve *Arabidopsis* growth under iron-limited conditions.
(a,c) SFW and (b,d) shoot chlorophyll concentration at 2 weeks of growth after transfer. 7-day-old Col-0 seedlings were transferred to half-strength MS medium with unavailable iron (50 µM $FeCl_3$) (a,b) or available iron (50 µM FeEDTA) (c,d) at pH 5.7 mock or inoculated with heat-killed (HK) or live F80. Letters indicate significant pairwise differences between groups (p-adj≤0.05) by a Dunn pairwise comparison test with Benjamini-Hochberg correction. Data are from two full factorial replicates (represented by different shapes).

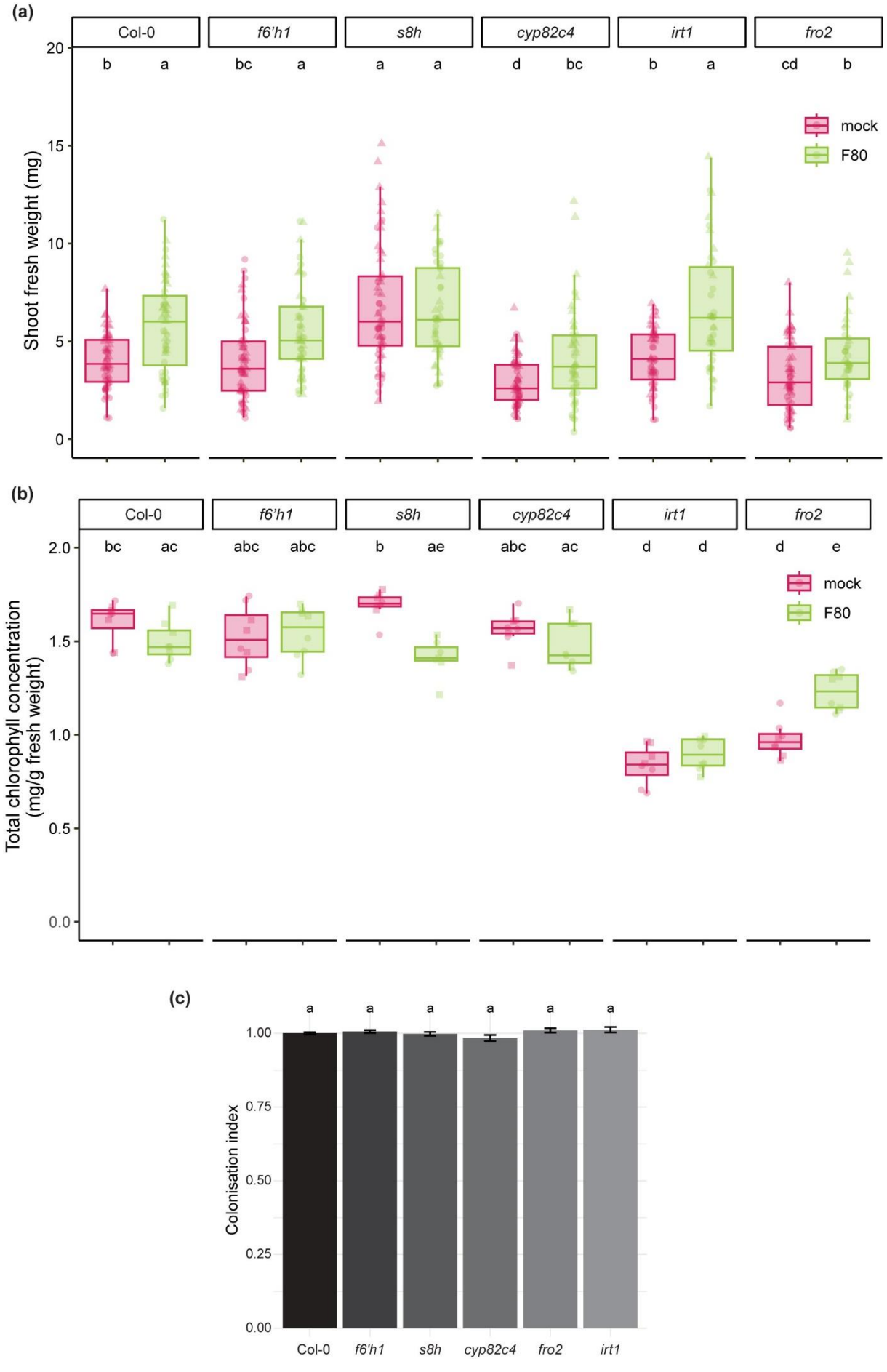
(a)
Col-0
f6'h1
s8h
cyp82c4
irt1
fro2
b a
bc a
a a
d bc
b a
cd b
mock
F80
Shoot fresh weight (mg)
20
15
10
5
0
(b)
Col-0
f6'h1
s8h
cyp82c4
irt1
fro2
bc ac
abc abc
b ae
abc ac
d d
d e
mock
F80
Total chlorophyll concentration (mg/g fresh weight)
2.0
1.5
1.0
0.5
0.0
(c)
a a a a a a
Colonisation index
1.00
0.75
0.50
0.25
0.00
Col-0
f6'h1
s8h
cyp82c4
fro2
irt1

Fig. S2 Phenotypes of mutants disrupted in coumarin biosynthesis or reductive iron uptake under available iron conditions in the presence or not of the fungal endophyte F80.
(a) SFW and (b) shoot chlorophyll content at 2 weeks of growth after transfer of indicated mutants in the coumarin biosynthesis pathway and the iron reductive import mechanism. 7-day-old seedlings were transferred to half-strength MS medium with available iron (50 µM FeEDTA) at pH 5.7 mock or inoculated with F80. Letters indicate significant pairwise differences between groups (p-adj≤0.05) by a Dunn pairwise comparison test with Benjamini-Hochberg correction. Data are from two full factorial replicates (represented by different shapes). (c) F80 colonisation index normalised to Col-0 control, corresponding to experiment shown in Figure 3a,b. Letters indicate significant pairwise differences between groups (p-adj≤0.05) by a Tukey's HSD corrected for multiple comparisons.

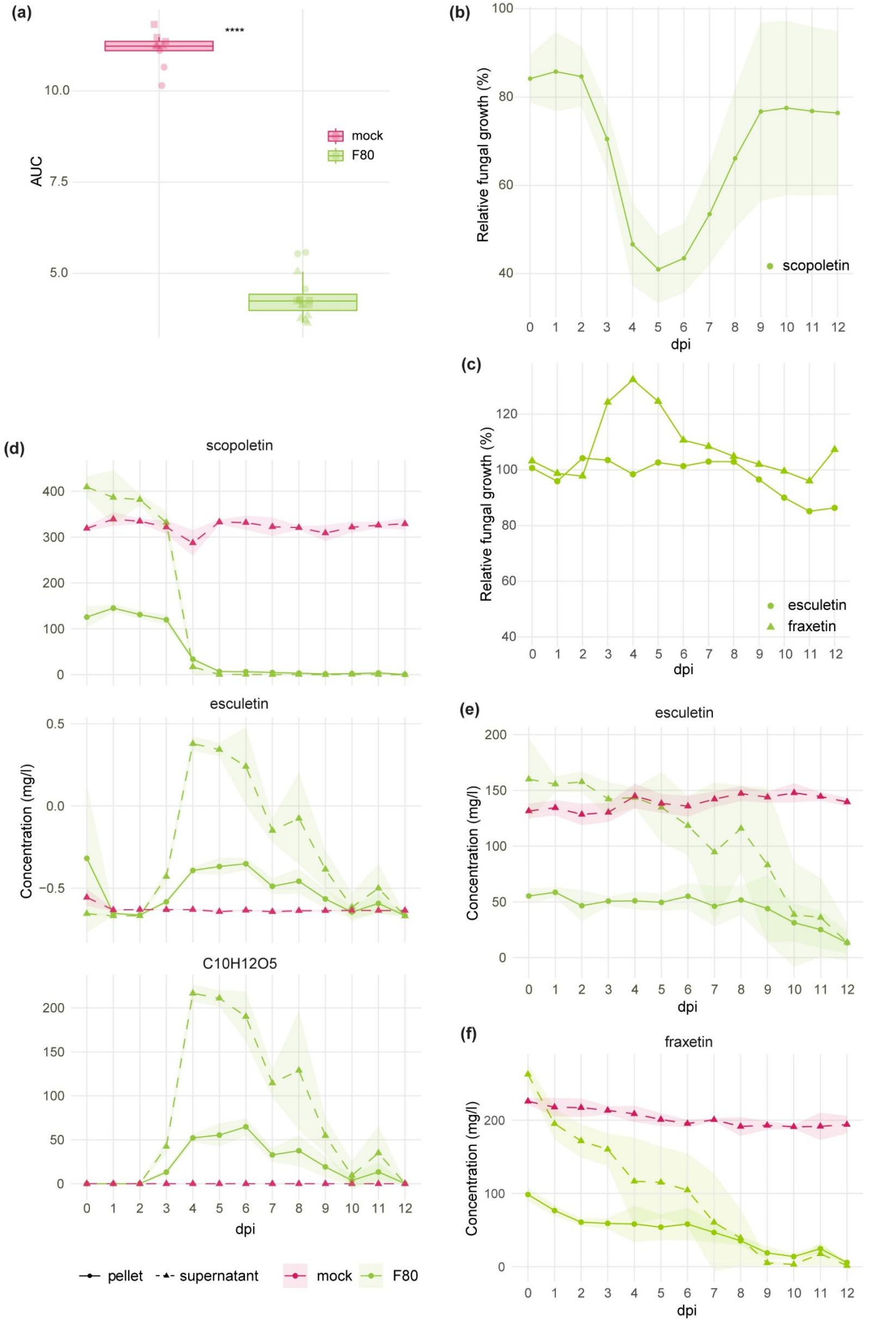
(a)
****
AUC
10.0
7.5
5.0
mock
F80
(b)
Relative fungal growth (%)
100
80
60
40
scopoletin
0 1 2 3 4 5 6 7 8 9 10 11 12
dpi
(c)
Relative fungal growth (%)
120
100
80
60
40
esculetin
fraxetin
0 1 2 3 4 5 6 7 8 9 10 11 12
dpi
(d)
scopoletin
400
300
200
100
0
esculetin
0.5
0.0
−0.5
C10H12O5
200
150
100
50
0
Concentration (mg/l)
0 1 2 3 4 5 6 7 8 9 10 11 12
dpi
pellet
supernatant
mock
F80
(e)
esculetin
200
150
100
50
0
Concentration (mg/l)
0 1 2 3 4 5 6 7 8 9 10 11 12
dpi
(f)
fraxetin
200
100
0
Concentration (mg/l)
0 1 2 3 4 5 6 7 8 9 10 11 12
dpi

Fig. S3 Metabolite profiles of *M. phaseolina* F80 cultures when supplemented with scopoletin. (a) Area Under the Curve (AUC) of the scopoletin detection plot in Figure 4a. Specific scopoletin fluorescence measured in *in vitro* mock and F80 cultures supplemented with 2 mM scopoletin (excitation at 385nm and emission detected at 470nm). (b) The mean OD600 of F80 cultures in 2 mM scopoletin relative to the OD600 of cultures in the absence of scopoletin from 0-12 dpi. Data combined from 3 independent biological experiments. The curve-shade indicates the standard error. (c) The mean OD600 of F80 cultures in 2 mM esculetin (circles) or fraxetin (triangles) relative to the OD600 of cultures in the absence of coumarins from 0-12 dpi. Data combined from 2 independent biological experiments. (d) Absolute quantification of the MS-QTOF-IDA-MS/MS peak area data shown in Figure 4b of the indicated compounds in F80 culture supernatant (dashed line) and the fungal pellet (full line) grown for 0-12 dpi supplemented with 2 mM scopoletin. Curve-shade indicates the standard deviation. (e) Absolute quantification of the MS-QTOF-IDA-MS/MS peak area data shown in Figure 4c of esculetin in F80 culture supernatant (dashed line) and the fungal pellet (full line) grown for 0-12 dpi supplemented with 2 mM esculetin. Curve-shade indicates the standard deviation. (f) Absolute quantification of the MS-QTOF-IDA-MS/MS peak area data shown in Figure 4d of fraxetin in F80 culture supernatant (dashed line) and the fungal pellet (full line) grown for 0-12 dpi supplemented with 2mM fraxetin. Curve-shade indicates the standard deviation.

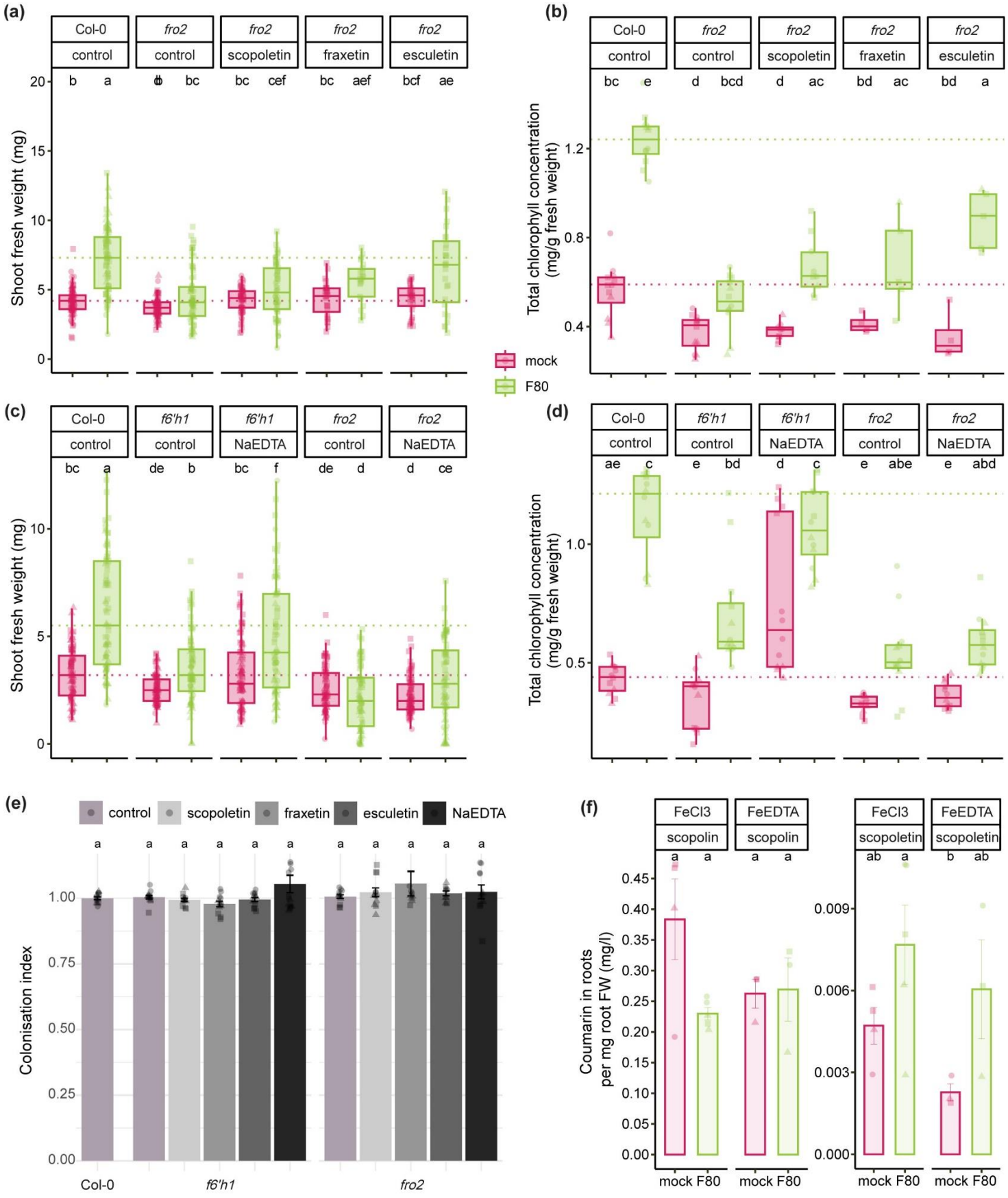

Fig. S4 Coumarin supplementation does not rescue *fro2* while Na_2EDTA supplementation rescues *f6'h1*, but not *fro2*.

(a,c) SFW and (b,d) shoot chlorophyll concentration at 2 weeks of growth after transfer. 7-day-old Col-0, *f6'h1* and *fro2* seedlings were transferred to half-strength MS medium with unavailable iron (50 µM FeCl3) at pH 5.7, supplemented with 10 µM of scopoletin, fraxetin, esculetin or Na_2EDTA (indicated above the graphs) or an equal amount of DMSO (control), mock or inoculated with F80. Dashed line indicates the mean of Col-0. Letters indicate significant pairwise differences between groups (*p*-

adj≤0.05) by a Dunn pairwise comparison test with Benjamini-Hochberg correction. Data are from three full factorial replicates (represented by different shapes). (e) F80 colonisation index normalised to Col-0, corresponding to experiment shown in Figure 5 (a,b) and S4 (a,b,c,d). Letters indicate significant pairwise differences between groups (*p*-adj≤0.05) by a Tukey's HSD corrected for multiple comparisons. (f) The concentration of scopoline and scopoletin in roots 1 week past transfer of 9-day-old seedlings to half-strength MS medium with unavailable iron (50 µM $FeCl_3$) or available (50 µM FeEDTA) at pH 5.7 mock or inoculated with F80. Approximately 150-250 mg of roots pooled from 10 plates were used to extract metabolites and analysed with MS-QTOF-IDA-MS/MS. Bars represent the mean from 3 biological replicates (n=1-2) with standard error bars. Letters indicate significant pairwise differences between groups (*p*-adj≤0.05) by a Tukey's HSD corrected for multiple comparisons.

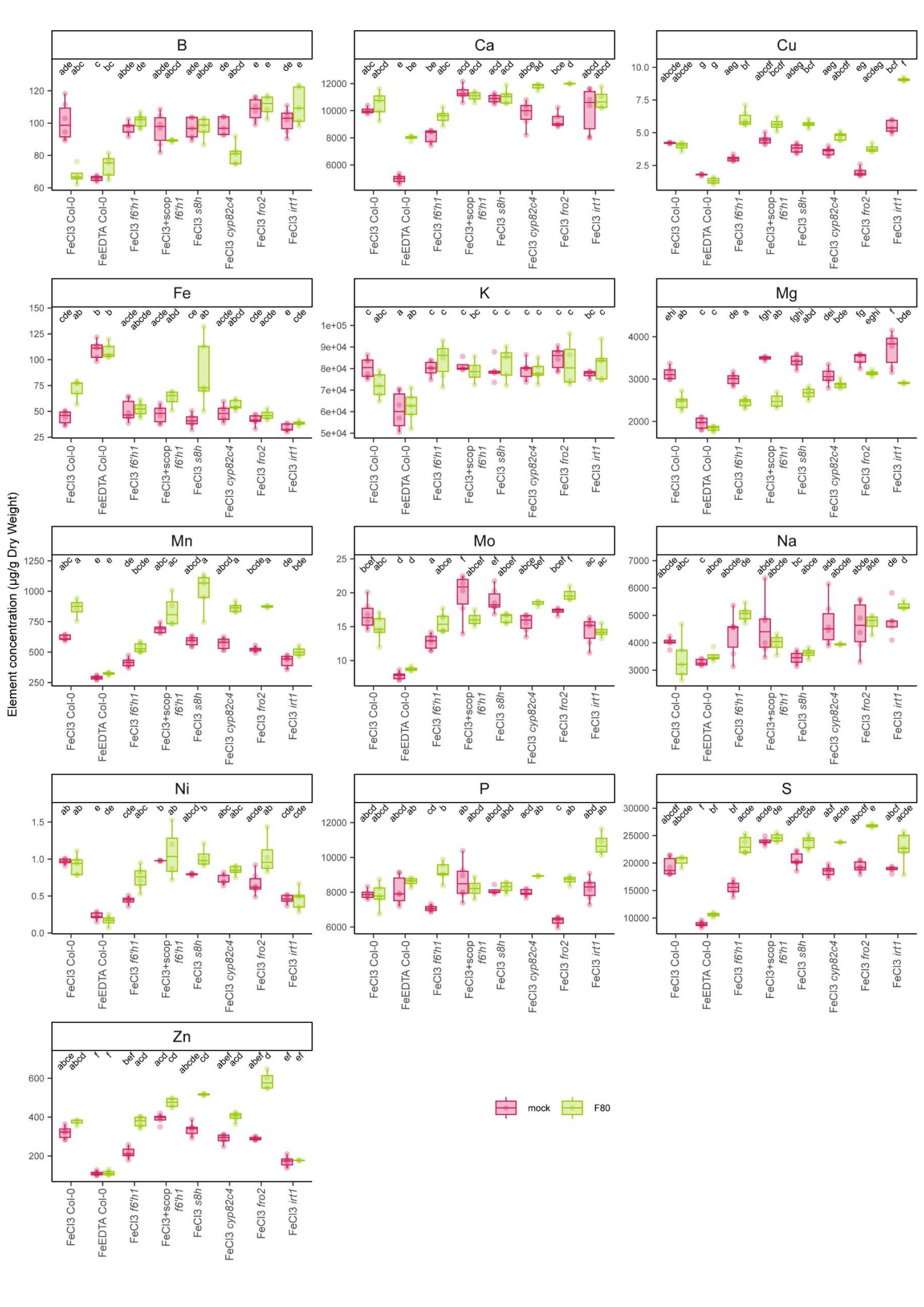
B
Ca
Cu
Fe
K
Mg
Mn
Mo
Na
Ni
P
S
Zn
Element concentration (µg/g Dry Weight)
FeCl3 Col-0
FeEDTA Col-0
FeCl3 f6'h1
FeCl3+scop f6'h1
FeCl3 s8h
FeCl3 cyp82c4
FeCl3 fro2
FeCl3 irt1
mock
F80

Fig. S5 Concentrations of mineral elements in shoots measured by ICP-MS.
Shoot mineral element concentrations at 2 weeks of growth after transfer. 7-day-old seedlings were transferred to half-strength MS medium at pH 5.7. Each plot depicts (from left to right) Col-0 grown on 50 µM $FeCl_3$, Col-0 grown on 50 µM FeEDTA, *f6'h1* grown on 50 µM $FeCl_3$, *f6'h1* grown on 50 µM $FeCl_3$ supplemented with 10 µM scopoletin, *s8h* grown on 50 µM $FeCl_3$, *cyp82c4* grown on 50 µM $FeCl_3$, *fro2* grown on 50 µM $FeCl_3$ and *irt1* grown on 50 µM $FeCl_3$. Letters indicate significant pairwise differences between groups (p-adj≤0.05) by a Tukey's HSD corrected for multiple comparisons when the data were normally distributed or by a Dunn pairwise comparison test with Benjamini-Hochberg correction when not normally distributed. Data are from three full factorial replicates.

Table S1 medium composition of ARE and vitamin solutions used in the 96-Well fungal culture assay.

5X ARE (artificial root exudates)	
compound	**g/l**
Glucose	8.2
Fructose	8.2
Saccharose	4.2
Citric Acid	3.2
Lactic Acid	3.2
Succinic Acid	4.6
Alanine	4
Serine	4.8
Glutamic Acid	4
100X Vitamins	
compound	**mg/l**
thiamine-HCl	10.12
nicotinic acid	12.31
folic acid	1.99
pyridoxine hydrochloride	20.56
4-aminobenzoic acid	4.11
Calcium D pantothenate	4.77
biotin	1.00

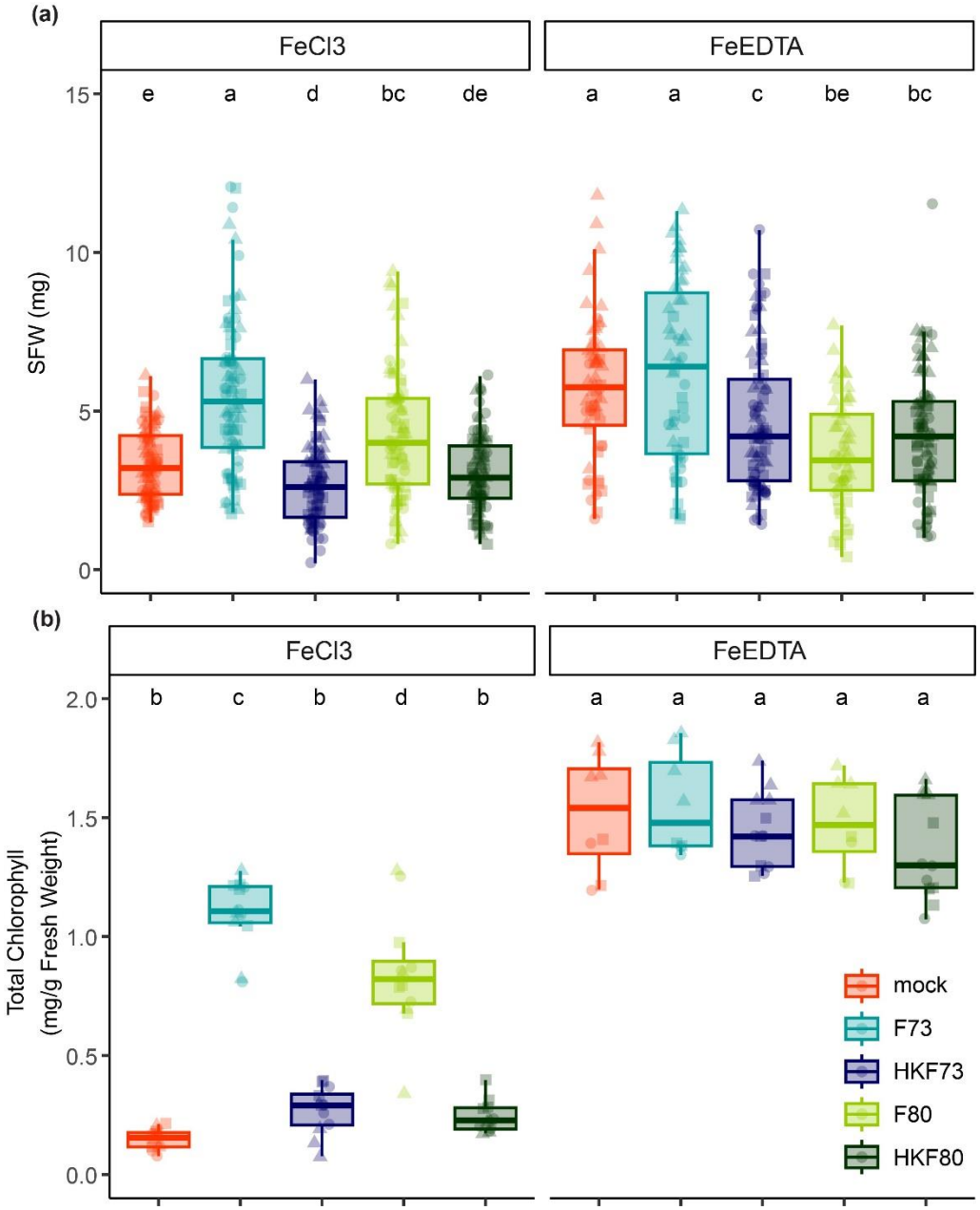

Figure S6. Heat-killed F73 and F80 do not enhance *Arabidopsis* iron status indicators at pH 7.3. (a) SFW and (b) shoot chlorophyll content of Col-0 *Arabidopsis* seedlings, 7-day old seedlings were transferred to 0.5MS medium grown for 2 weeks on mock, heat-killed or live F73 or F80 inoculated plates at pH 7.3 (10mM MOPS) in unavFe (100µM FeCl3) or avFe (100µM FeEDTA). Letters indicate significant pairwise differences between groups (p-adj≤0.05) by Dunn pairwise comparison test with Benjamini-Hochberg correction (a) or a Tukey's HSD corrected for multiple comparisons (b). Data are from three biological replicates (represented by different shapes).

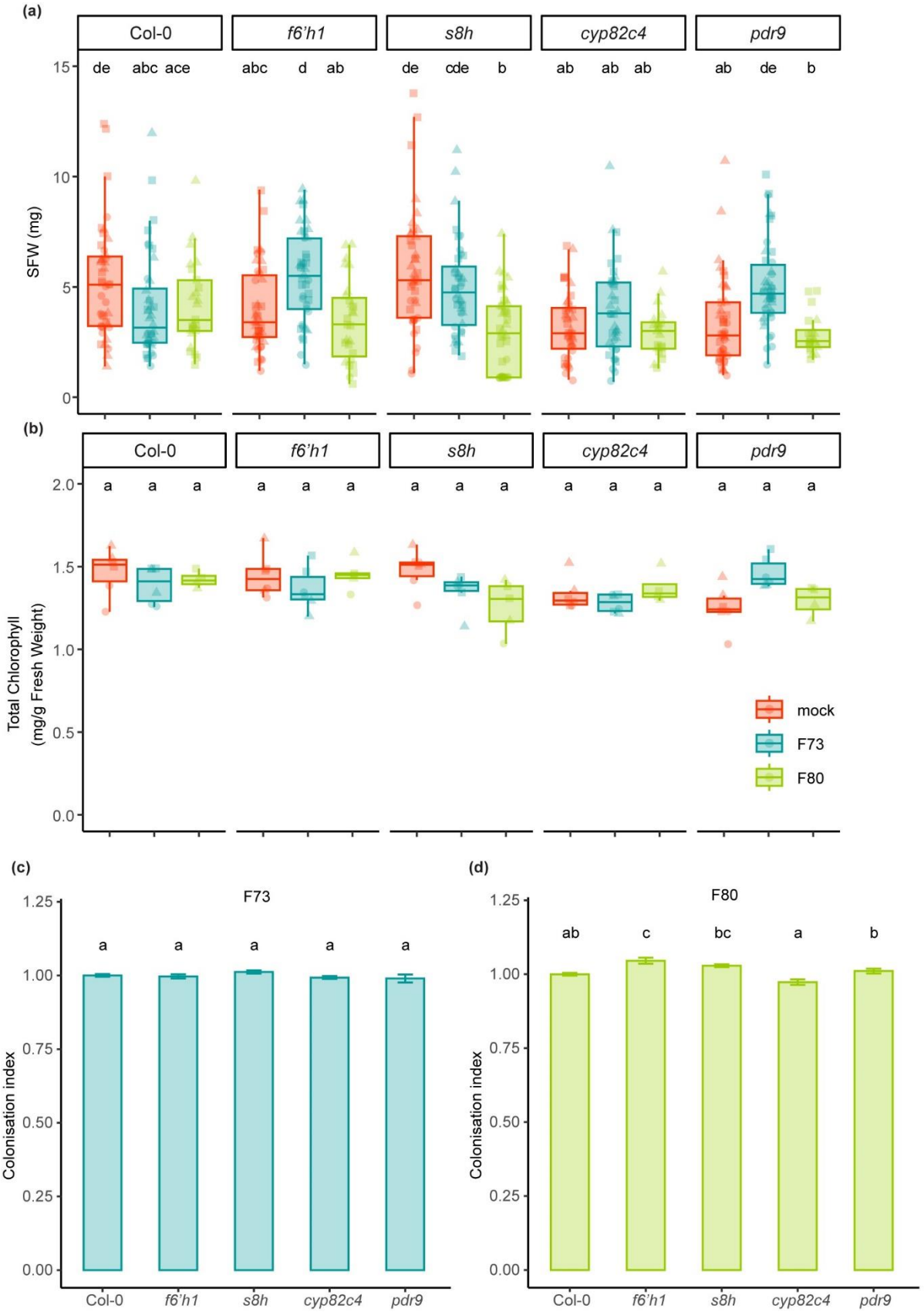

Figure S7. F73 and F80 coumarin mutant *Arabidopsis* phenotypes in avFe conditions and colonisation index.

(a) SFW and (b) shoot chlorophyll content after 2 weeks of growth of indicated mutants in coumarin biosynthesis and exudation. 7-day old seedlings were transferred to 0.5MS medium with avFe (100µM FeEDTA) at pH 7.3 mock or inoculated with F73 or F80. (c) F73 and (d) F80 colonisation index normalised to Col-0 control, corresponding to experiment shown in Figure 2. Letters indicate significant pairwise differences between groups (p-adj≤0.05) by a Dunn pairwise comparison test with Benjamini-Hochberg correction (a,d) or a Tukey's HSD corrected for multiple comparisons (b,c). Data are from three biological replicates (represented by different shapes).

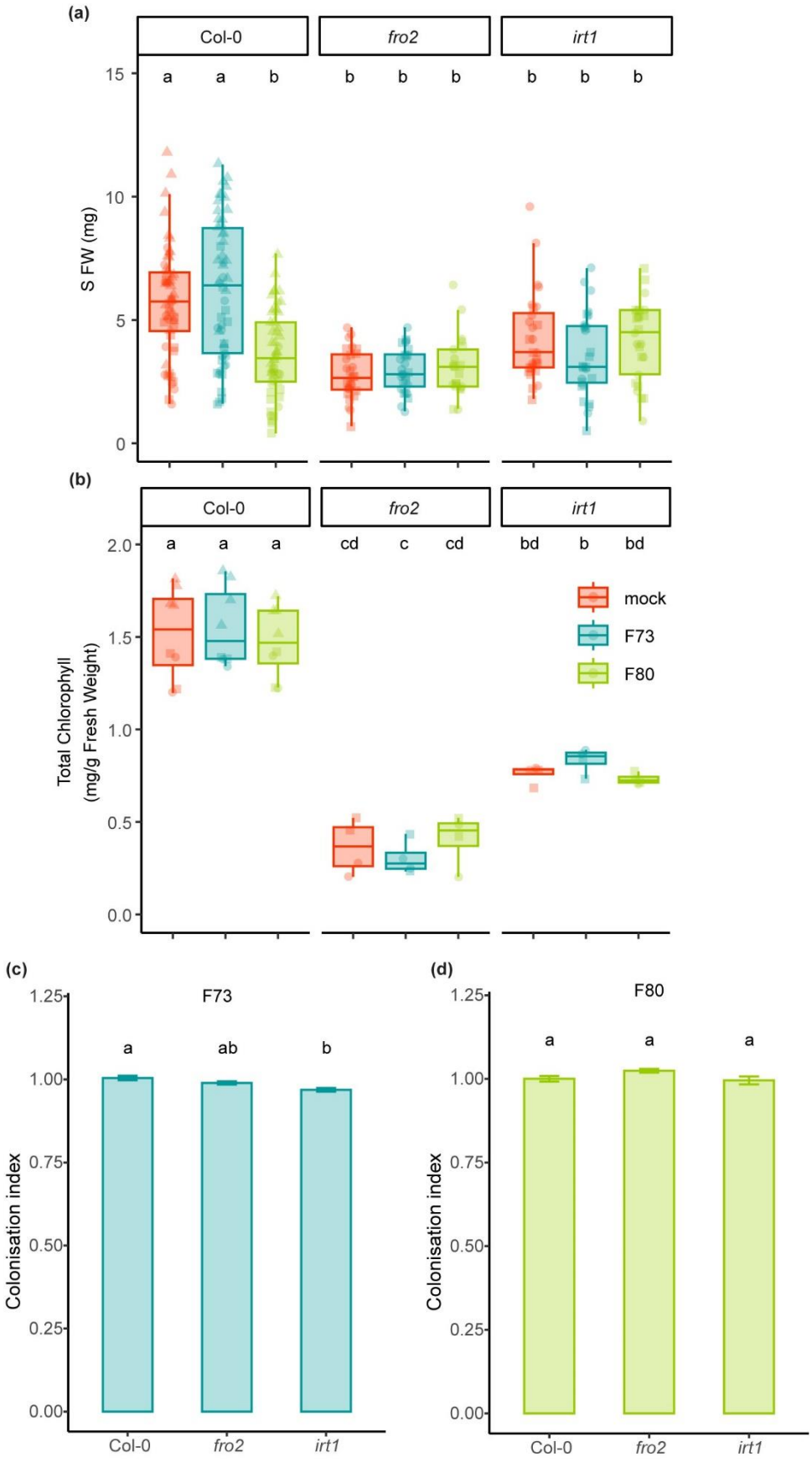

Figure S8. F73 and F80 iron reductive import mutant *Arabidopsis* phenotypes in avFe conditions and colonisation index. (a) SFW and (b) shoot chlorophyll content after 2 weeks of growth of indicated mutants in the iron reductive import pathway. 7-day old seedlings were transferred to 0.5MS medium with avFe (100µM FeEDTA) at pH 7.3 mock or inoculated with F73 or F80. (c) F73 and (d) F80 colonisation index normalised to Col-0 control, corresponding to experiment shown in Figure 9. Letters indicate significant pairwise differences between groups (p-adj≤0.05) by a Tukey's HSD corrected for multiple comparisons. Data are from three biological replicates (represented by different shapes).

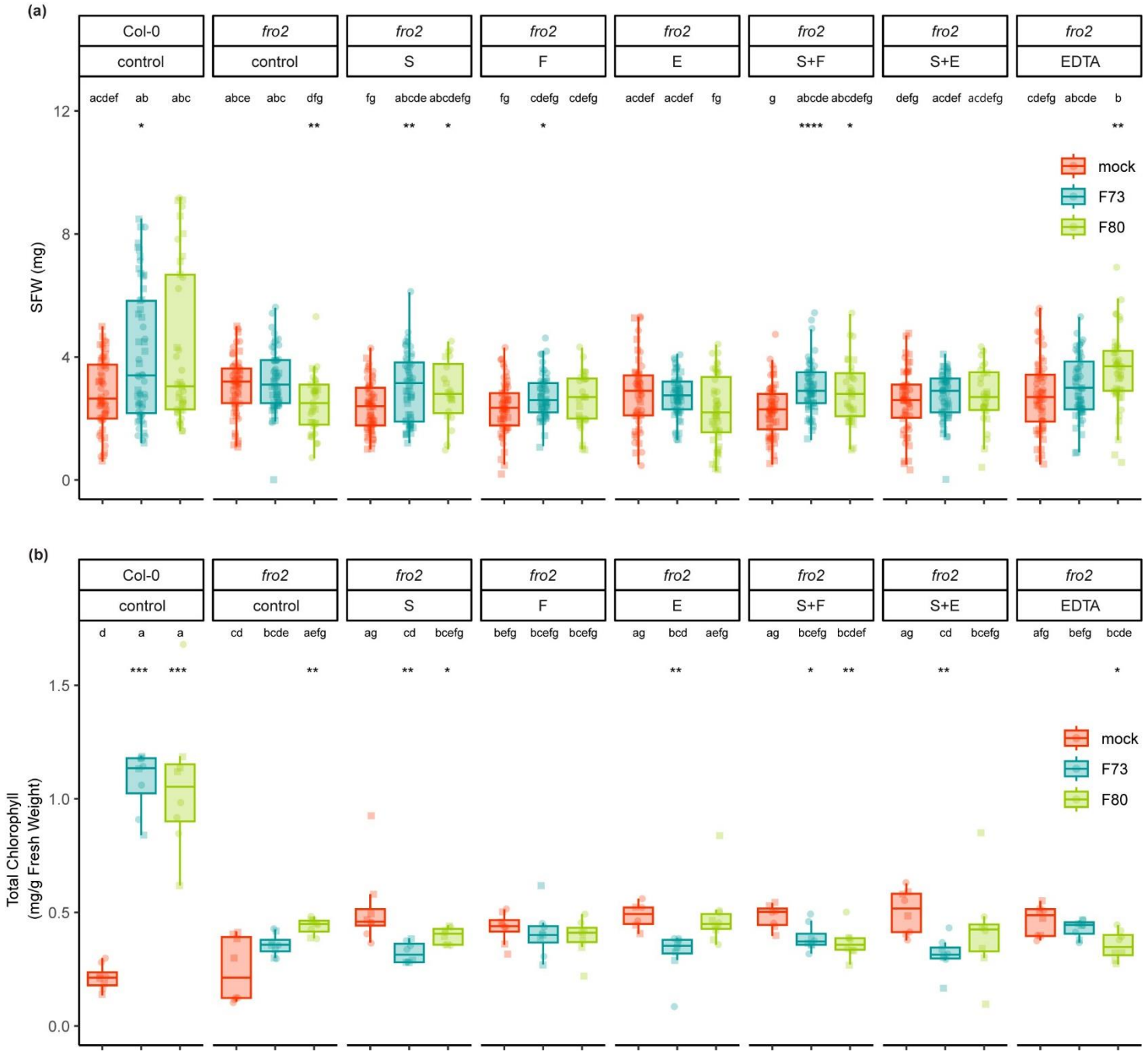

Figure S9. Coumarin supplementation does not rescue nor restores fungal endophyte mediated rescue in *fro2*. (a) SFW and (b) leaf chlorophyll content after 2 weeks of growth, 7-day old Col-0 and *fro2* seedlings were transferred to 0.5MS medium with unavFe (100µM FeCl3) at pH 7.3, mock or inoculated with fungal hyphae (50 µg/ml) supplemented with 100 µM scopoletin (S), fraxetin (F), esculetin (E), Na_2EDTA (EDTA) or scopoletin combined with fraxetin (S+F) and esculetin (S+E) or an equal amount of DMSO (control) (indicated above the graphs). Data are from two biological replicates (represented by different shapes). Letters indicate significant pairwise differences between groups (p-adj≤0.05) by a Dunn pairwise comparison test with Benjamini-Hochberg correction. Pairwise comparisons between fungi-treated and mock-treated samples within each genotype were assessed using the Wilcoxon rank-sum test, with *p < 0.05, **p < 0.01, ***p < 0.001, and ****p < 0.0001 indicating significance.

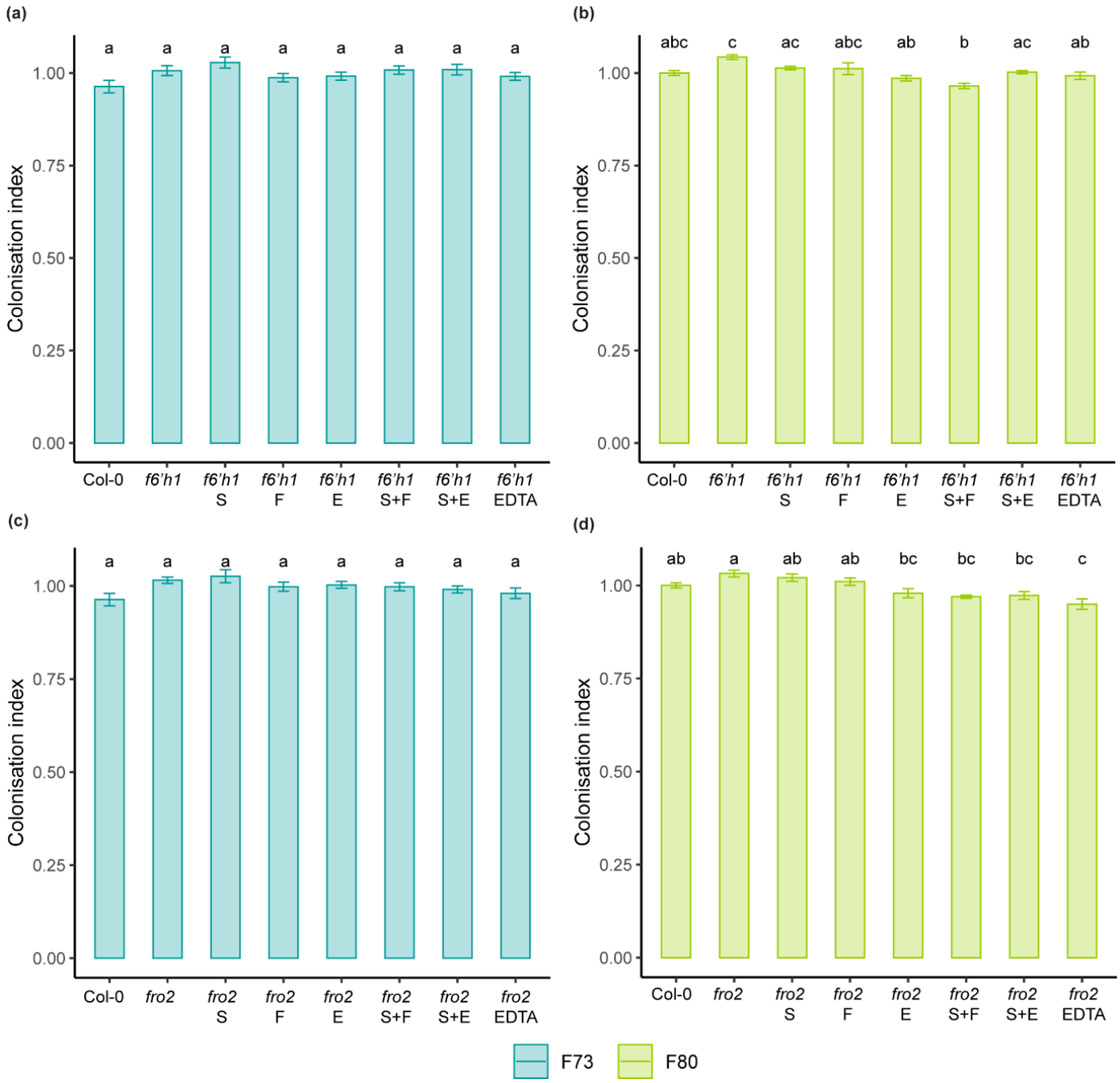

Figure S10. Coumarin supplementation does not cause extensive changes in F73 and F80 colonisation in *f6'h1* and *fro2*. (a) F73 colonisation index in *f6'h1*, (b) F80 colonisation index in *f6'h1*, (c) F73 colonisation index in *fro2*, (b) F80 colonisation index in *fro2* normalised to Col-0, corresponding to experiment shown in Figure 10 and S9. Letters indicate significant pairwise differences between groups (p-adj≤0.05) by a Dunn pairwise comparison test with Benjamini-Hochberg correction (a,b,c) or a Tukey's HSD corrected for multiple comparisons (d).

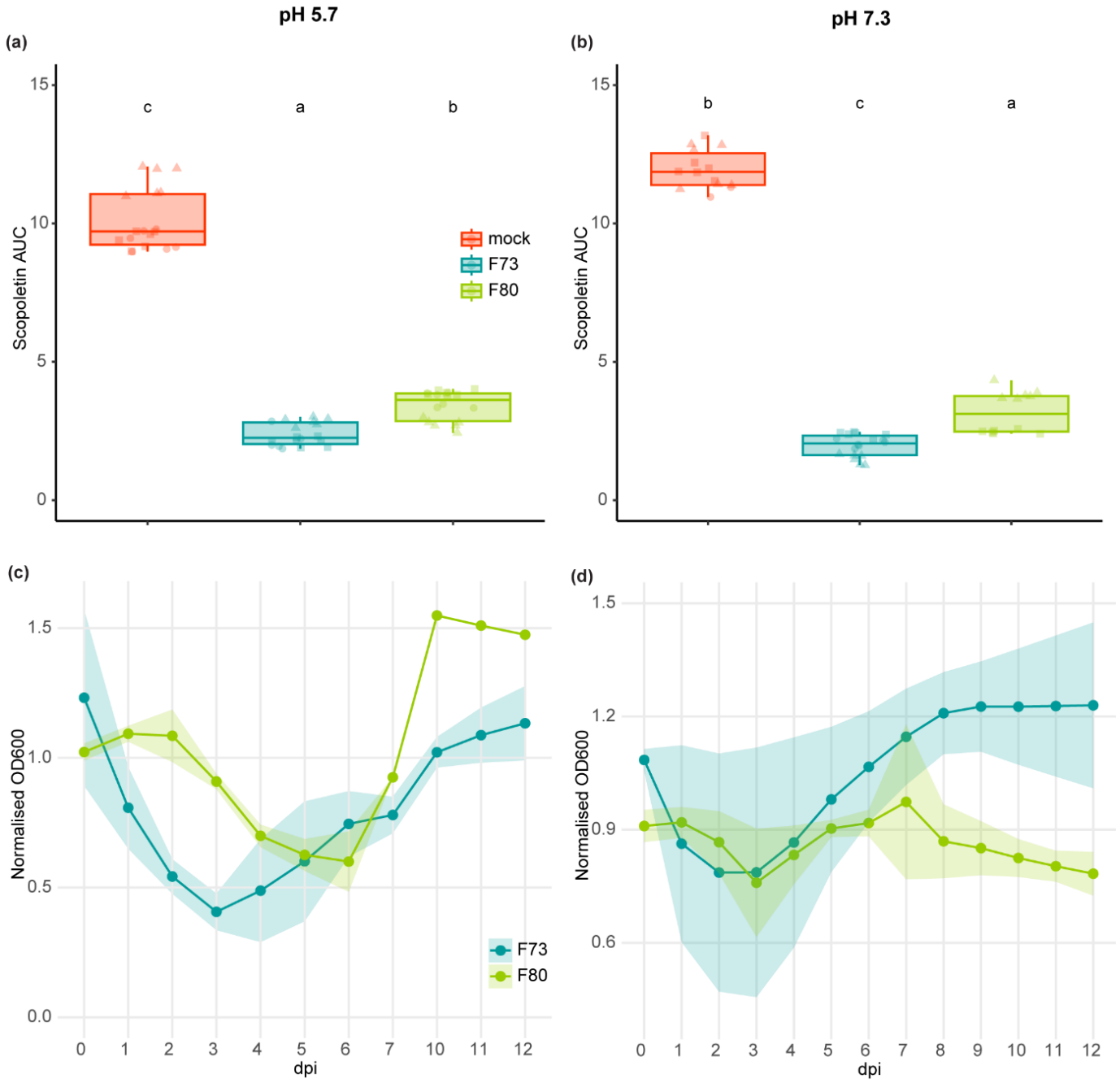

Figure S11. F73 and F80 growth response to scopoletin. (a,b) Area Under the Curve (AUC) of the scopoletin detection plots in Figure 11, specific scopoletin fluorescence measured in mock, F73 and F80 cultures buffered at pH 5.7 (a) and pH 7.3 (b) supplemented with 2mM scopoletin (exciting at 385nm and emission detected at 470nm). (c,d) The OD600 of F73 and F80 cultures buffered at pH 5.7 (c) and pH 7.3 (d) in 2mM scopoletin relative to the OD600 of cultures in the absence of scopoletin from 0-12 dpi. Data combined from 3 independent biological experiments. The curve-shade indicates the standard deviation.

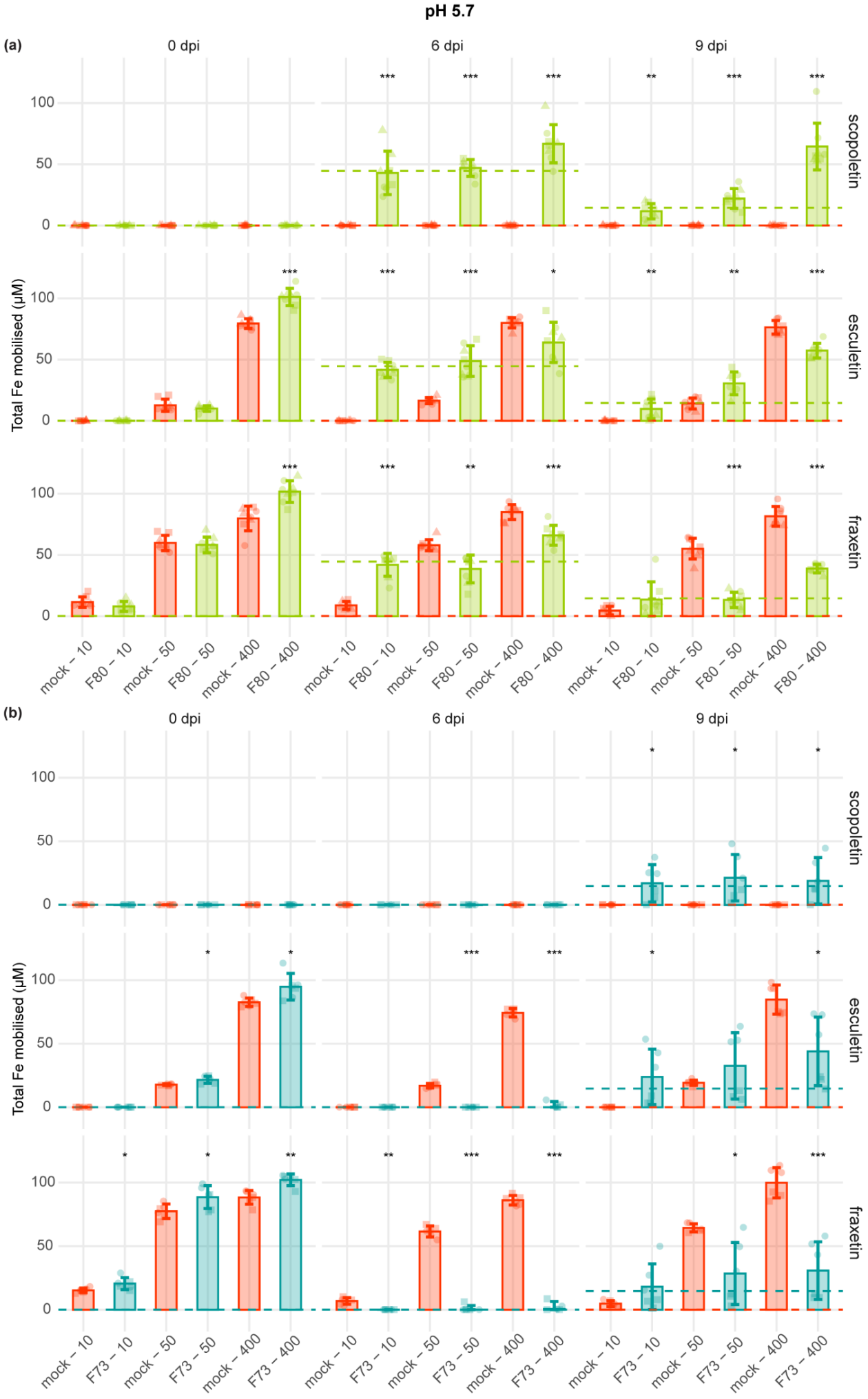
pH 5.7
(a)
0 dpi
6 dpi
9 dpi
scopoletin
esculetin
fraxetin
Total Fe mobilised (μM)
mock – 10
F80 – 10
mock – 50
F80 – 50
mock – 400
F80 – 400
(b)
F73 – 10
F73 – 50
F73 – 400

Figure S12. Total iron mobilisation in F80 and F73 cultures supplemented with scopoletin, fraxetin, and esculetin at pH 5.7. The total iron mobilised in (a) F80, (b) F73 or mock (MgCl2, indicated with the red dashed lines) supernatant of cultures grown with scopoletin, fraxetin, esculetin (final concentration of 10, 50, or 400 µM), or an equal amount of DMSO (control indicated with the green/blue dashed lines) at 0, 6, or 9 dpi at pH 5.7 (10 mM MES). Mobile iron was measured spectrophotometrically based on the formation of Fe^{2+}-ferrozine complexes, mean ± SD of 3 (a) and 2 (b) biological replicates are shown (represented by different shapes), significance levels shown for comparisons when applicable. Statistical differences between treatments were assessed using t-tests for normally distributed residuals or, otherwise, Wilcoxon rank-sum tests, significance levels are indicated by asterisks with *p <0.05, **p < 0.01, and ***p < 0.001.

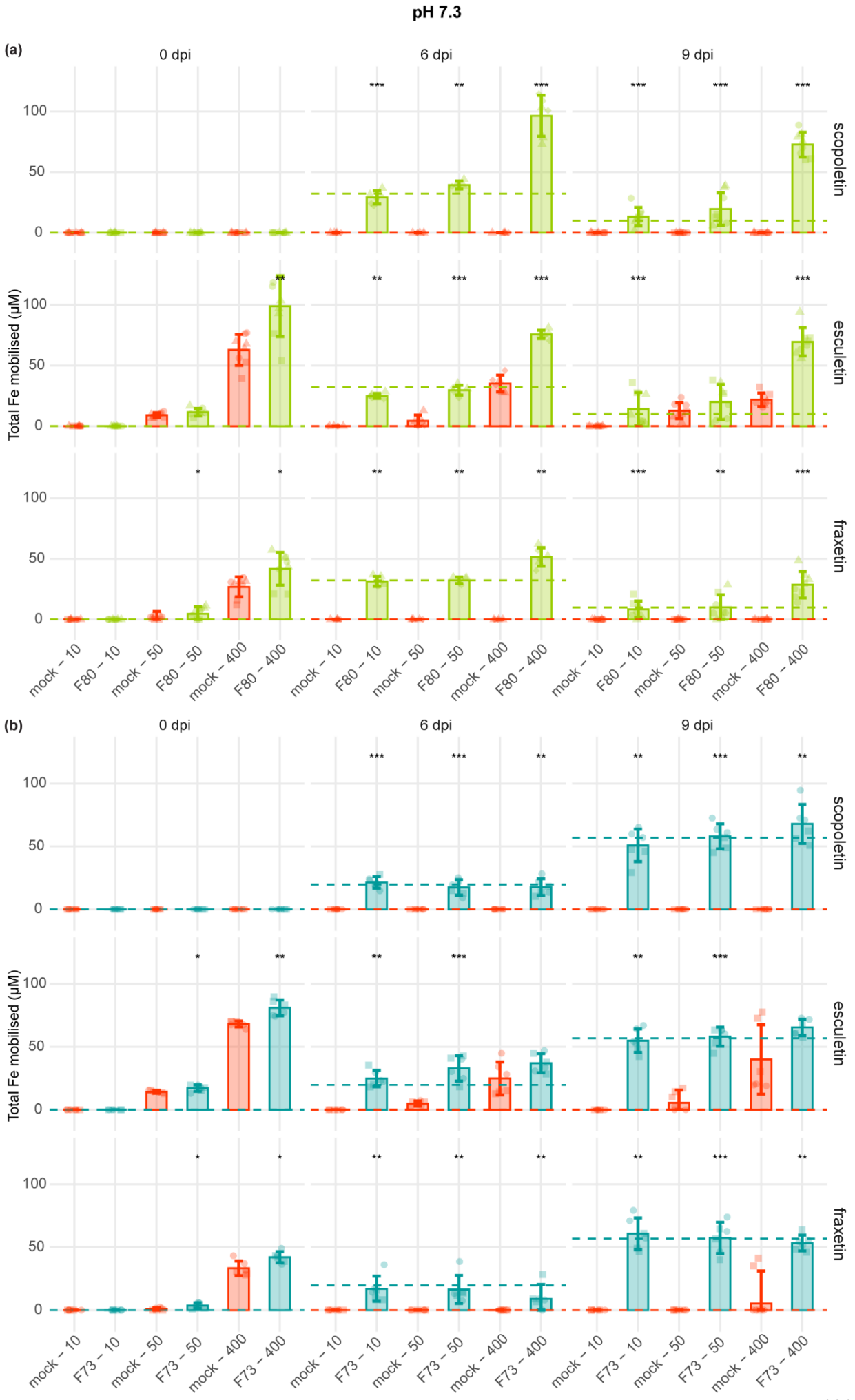
pH 7.3
(a)
0 dpi
6 dpi
9 dpi
scopoletin
esculetin
fraxetin
Total Fe mobilised (μM)
mock – 10
F80 – 10
mock – 50
F80 – 50
mock – 400
F80 – 400
(b)
F73 – 10
F73 – 50
F73 – 400

Figure S13. Total iron mobilisation in F80 and F73 cultures supplemented with scopoletin, fraxetin, and esculetin at pH 7.3. The total iron mobilised in (a) F80, (b) F73 or mock (MgCl2, indicated with the red dashed lines) supernatant of cultures grown with scopoletin, fraxetin, esculetin (final concentration of 10, 50, or 400 µM), or an equal amount of DMSO (control indicated with the green/blue dashed lines) at 0, 6, or 9 dpi at pH 7.3 (10 mM MOPS). Mobile iron was measured spectrophotometrically based on the formation of Fe^{2+}-ferrozine complexes, mean ± SD of 3 (a) and 2 (b) biological replicates are shown (represented by different shapes), significance levels shown for comparisons when applicable. Statistical differences between treatments were assessed using t-tests for normally distributed residuals or, otherwise, Wilcoxon rank-sum tests, significance levels are indicated by asterisks with *p <0.05, **p < 0.01, and ***p < 0.001.

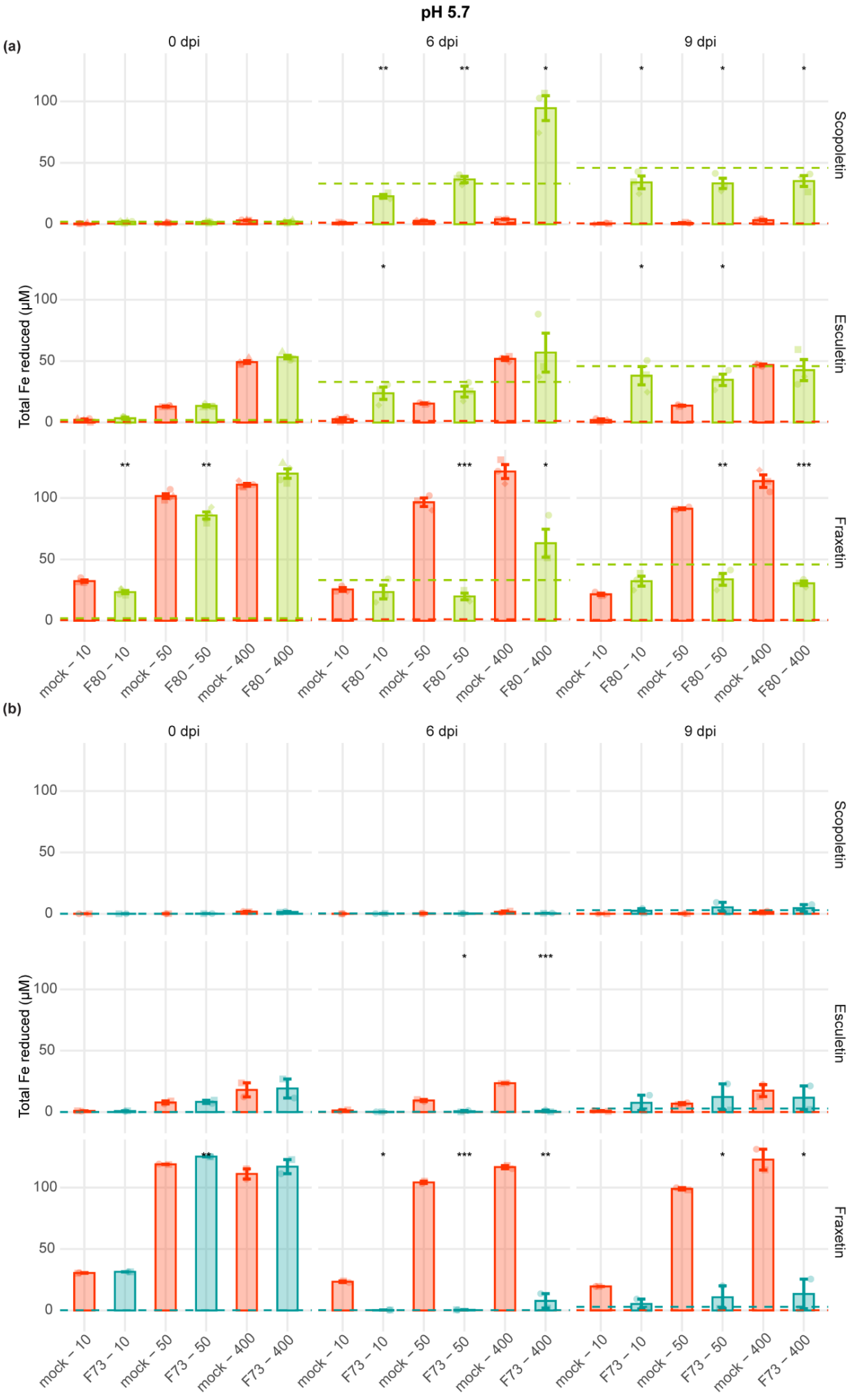
pH 5.7
(a)
0 dpi
6 dpi
9 dpi
Scopoletin
Esculetin
Fraxetin
Total Fe reduced (μM)
mock – 10
F80 – 10
mock – 50
F80 – 50
mock – 400
F80 – 400
(b)
F73 – 10
F73 – 50
F73 – 400

Figure S14. Total iron reduction in F80 and F73 cultures supplemented with scopoletin, fraxetin, and esculetin at pH 5.7. The total iron reduced in (a) F80, (b) F73 or mock (MgCl2, indicated with the red dashed lines) supernatant of cultures grown with scopoletin, fraxetin, esculetin (final concentration of 10, 50, or 400 µM), or an equal amount of DMSO (control indicated with the green/blue dashed lines) at 0, 6, or 9 dpi at pH 5.7 (10 mM MES). Reduced iron was measured spectrophotometrically based on the formation of Fe^{2+}-ferrozine complexes, mean ± SD of 3 (a) and 2 (b) biological replicates are shown (represented by different shapes), significance levels shown for comparisons when applicable. Statistical differences between treatments were assessed using t-tests for normally distributed residuals or, otherwise, Wilcoxon rank-sum tests, significance levels are indicated by asterisks with *p <0.05, **p < 0.01, and ***p < 0.001.

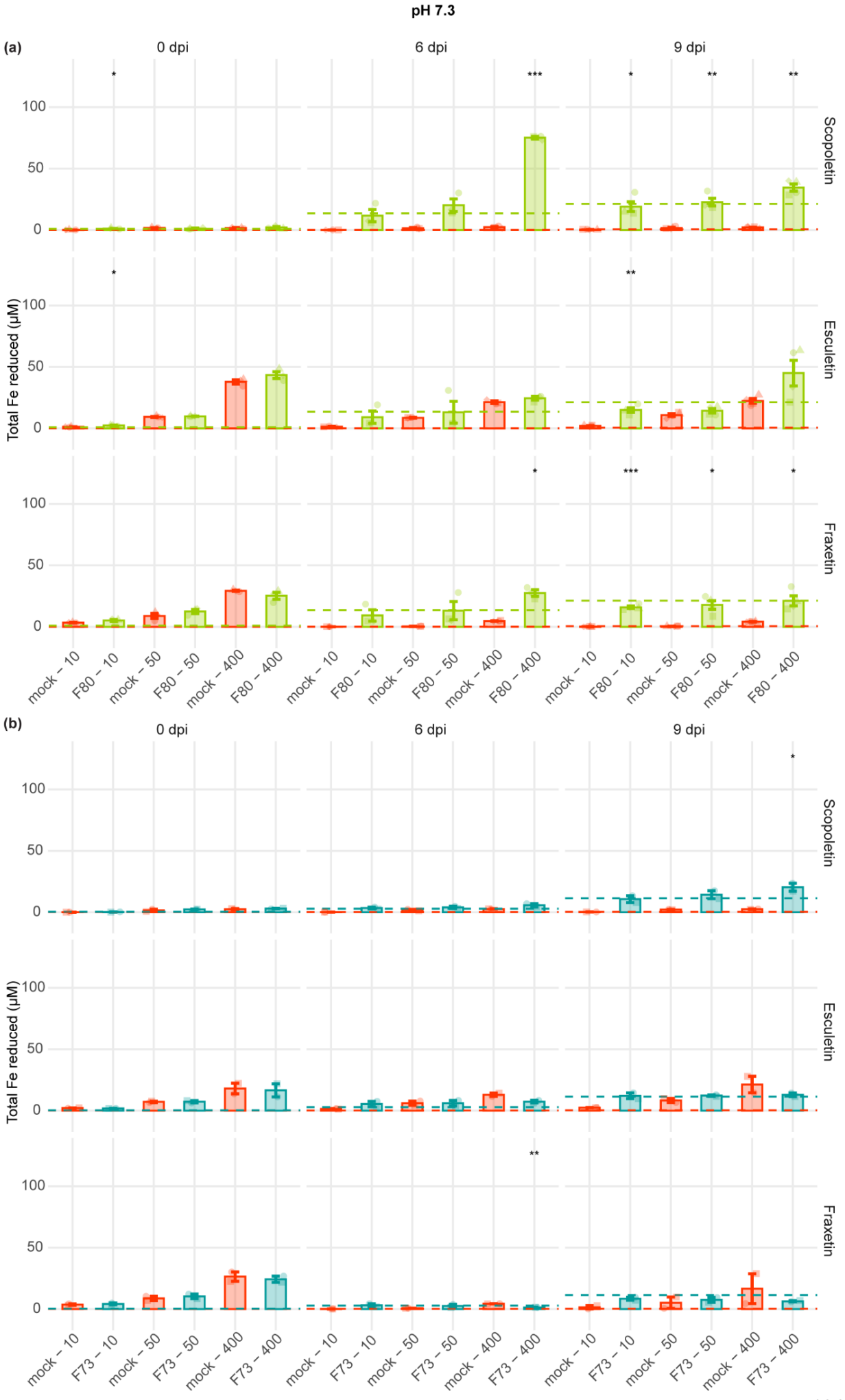
pH 7.3
(a)
0 dpi
6 dpi
9 dpi
Scopoletin
Esculetin
Fraxetin
Total Fe reduced (µM)
100
50
0
mock – 10
F80 – 10
mock – 50
F80 – 50
mock – 400
F80 – 400
(b)
F73 – 10
F73 – 50
F73 – 400

Figure S15. Total iron reduction in F80 and F73 cultures supplemented with scopoletin, fraxetin, and esculetin at pH 7.3. The total iron reduced in (a) F80, (b) F73 or mock (MgCl2, indicated with the red dashed lines) supernatant of cultures grown with scopoletin, fraxetin, esculetin (final concentration of 10, 50, or 400 µM), or an equal amount of DMSO (control indicated with the green/blue dashed lines) at 0, 6, or 9 dpi at pH 7.3 (10 mM MOPS). Reduced iron was measured spectrophotometrically based on the formation of Fe^{2+}-ferrozine complexes, mean ± SD of 3 (a) and 2 (b) biological replicates are shown (represented by different shapes), significance levels shown for comparisons when applicable. Statistical differences between treatments were assessed using t-tests for normally distributed residuals or, otherwise, Wilcoxon rank-sum tests, significance levels are indicated by asterisks with *p <0.05, **p < 0.01, and ***p < 0.001.

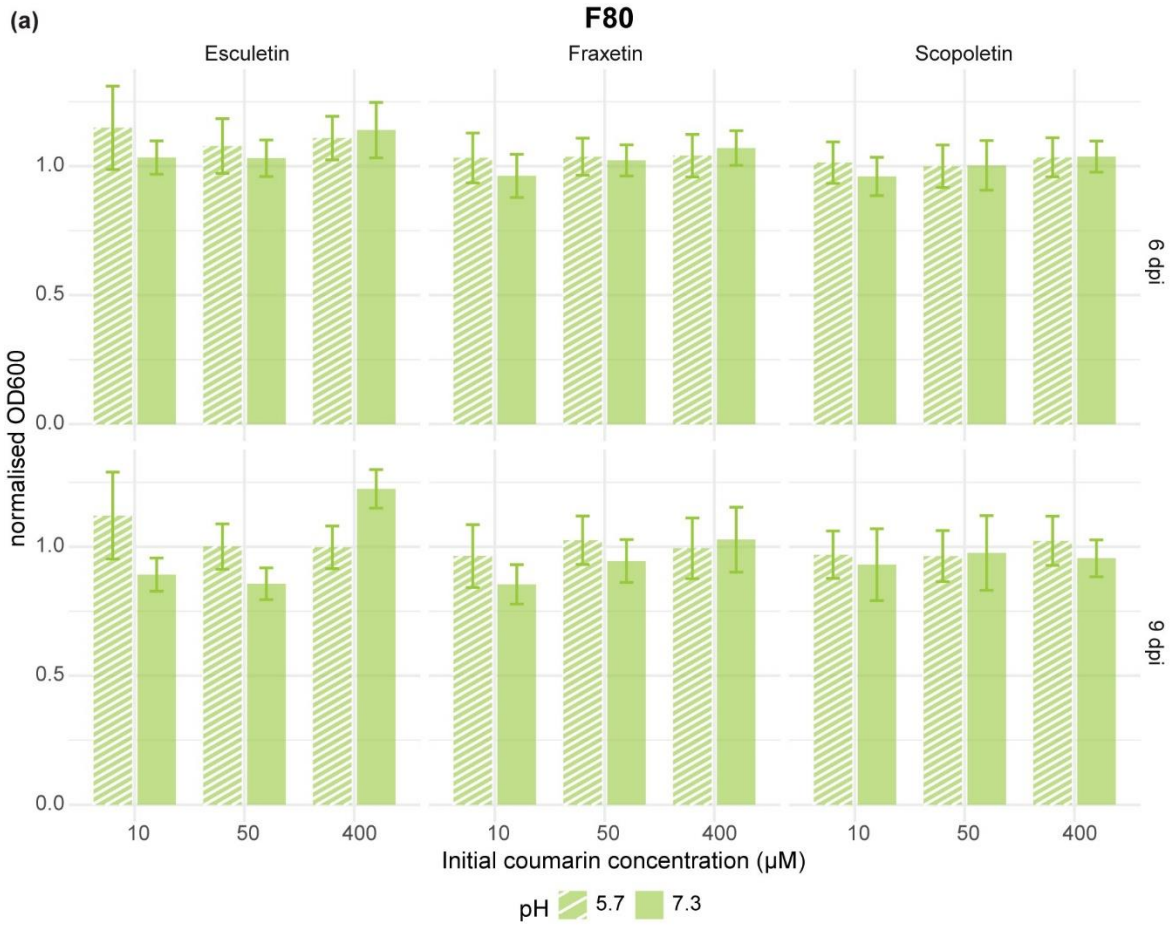
(a)
F80
Esculetin
Fraxetin
Scopoletin
normalised OD600
0.0
0.5
1.0
6 dpi
9 dpi
10
50
400
Initial coumarin concentration (µM)
pH
5.7
7.3

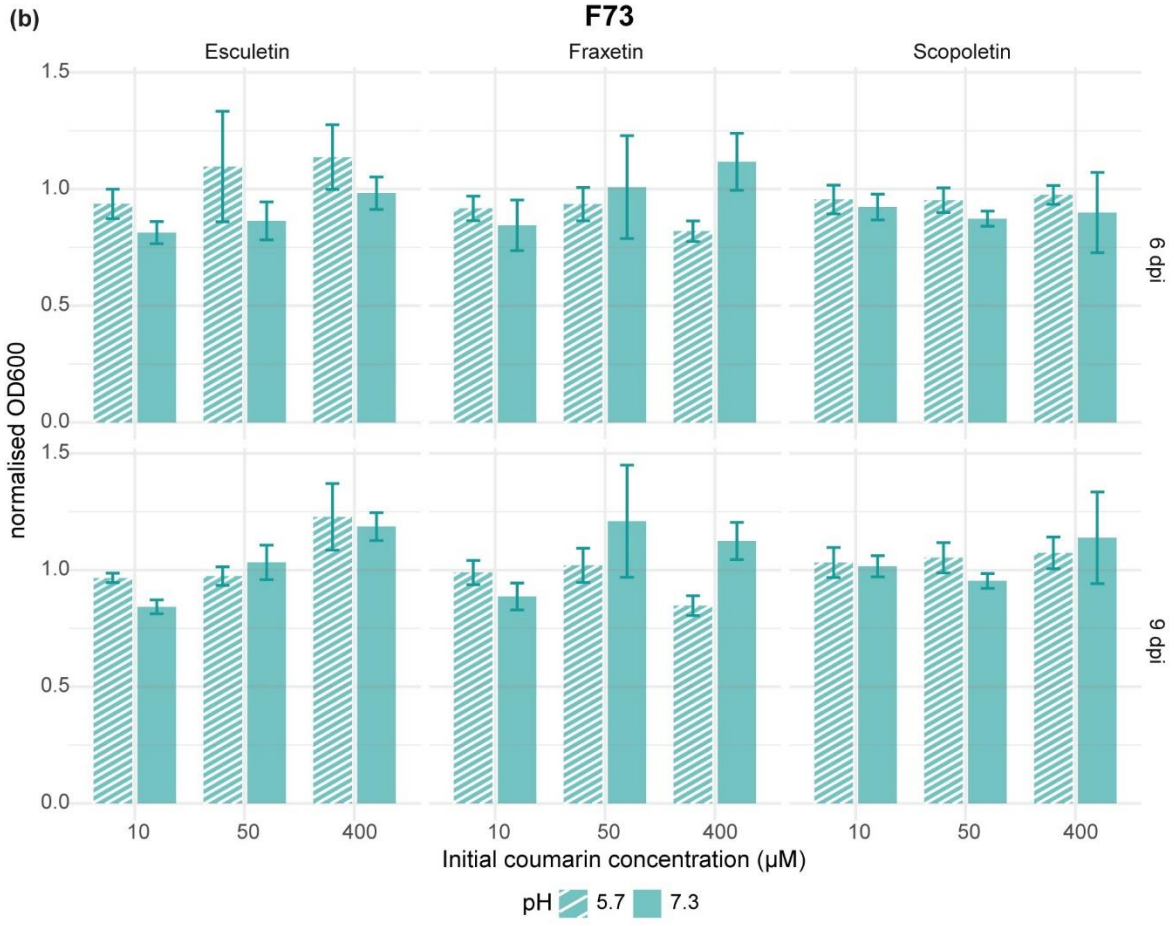
(b)
F73
Esculetin
Fraxetin
Scopoletin
normalised OD600
0.0
0.5
1.0
1.5
6 dpi
9 dpi
10
50
400
Initial coumarin concentration (µM)
pH
5.7
7.3

Figure S16. Normalised F80 and F73 growth in cultures supplemented with scopoletin, fraxetin, and esculetin at pH 5.7 and 7.3. The OD600 in the different cultures indicated on figure normalised to OD600 of control cultures of (a) F80, (b) F73 grown with scopoletin, fraxetin, esculetin (final concentration of 10, 50, or 400 µM) (to control cultures an equal amount of DMSO was added) 6 or 9 dpi at pH 5.7 (dashed bars) 7.3 (full bars). Mean ± SD of 3 (a) and 2 (b) biological replicates are shown. Statistical differences between conditions were assessed using t-tests for normally distributed residuals or, otherwise, Wilcoxon rank-sum tests, but no significant differences were found.

Chapter 4:

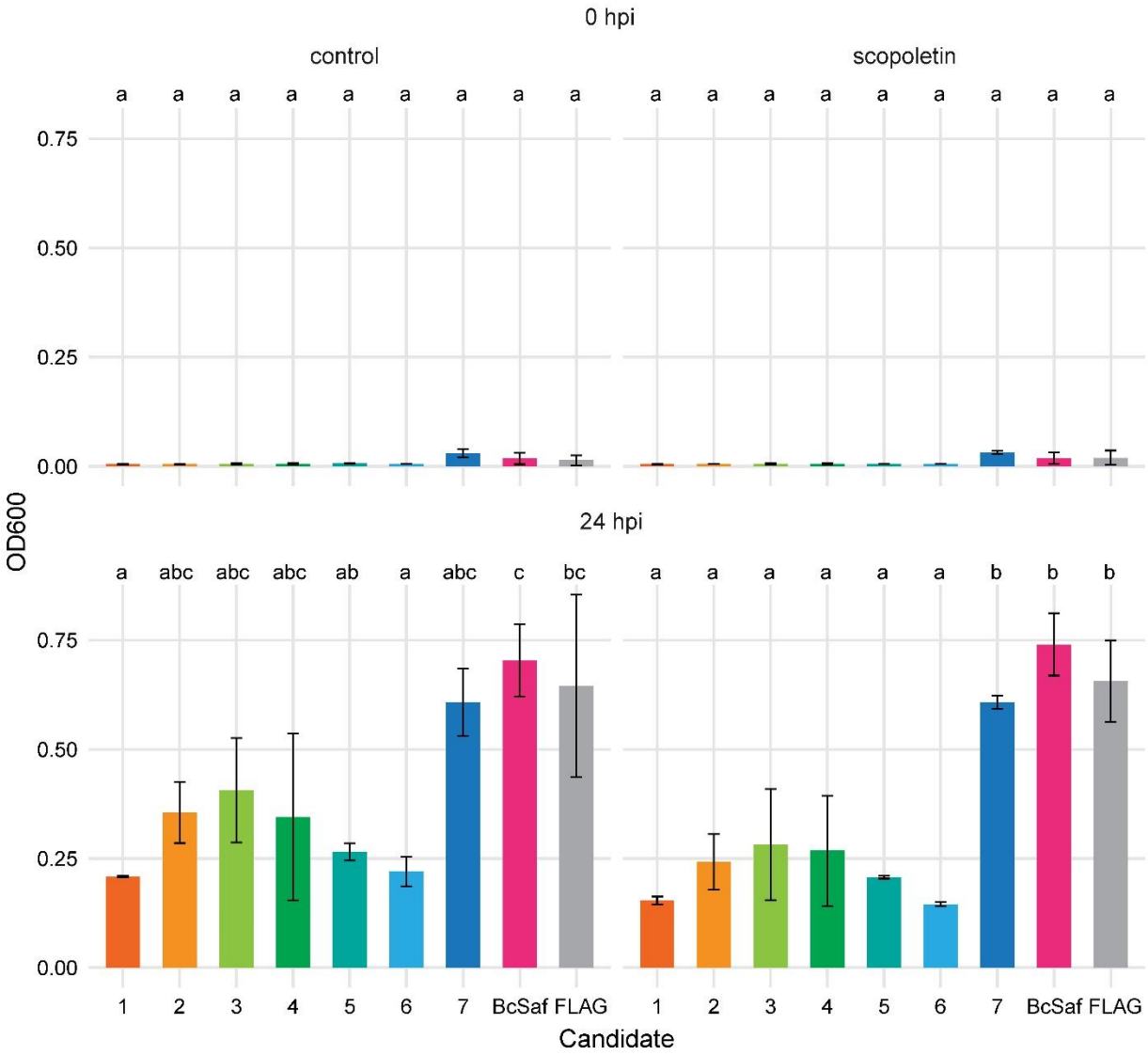

Figure S17. Growth in *S. cerevisiae* cultures expressing F80 candidate genes. The candidate genes 1-7 were cloned and expressed in *S. cerevisiae* as N-terminally FLAG-tagged proteins and grown in culture with 0.5 mM scopoletin or DMSO (control) to assess their scopoletin-degradation capacity. OD600 was measured at the start and 24 hours past inoculation (hpi). BcSaf1 was used as a positive control (BcSaf) and an empty FLAG-vector as negative control (FLAG). Bars represent the mean ± SD, Letters indicate significant pairwise differences between groups (p-adj≤0.05) by a pairwise t-test with Bonferroni correction. Data are from two biological replicates (3 technical replicates each).

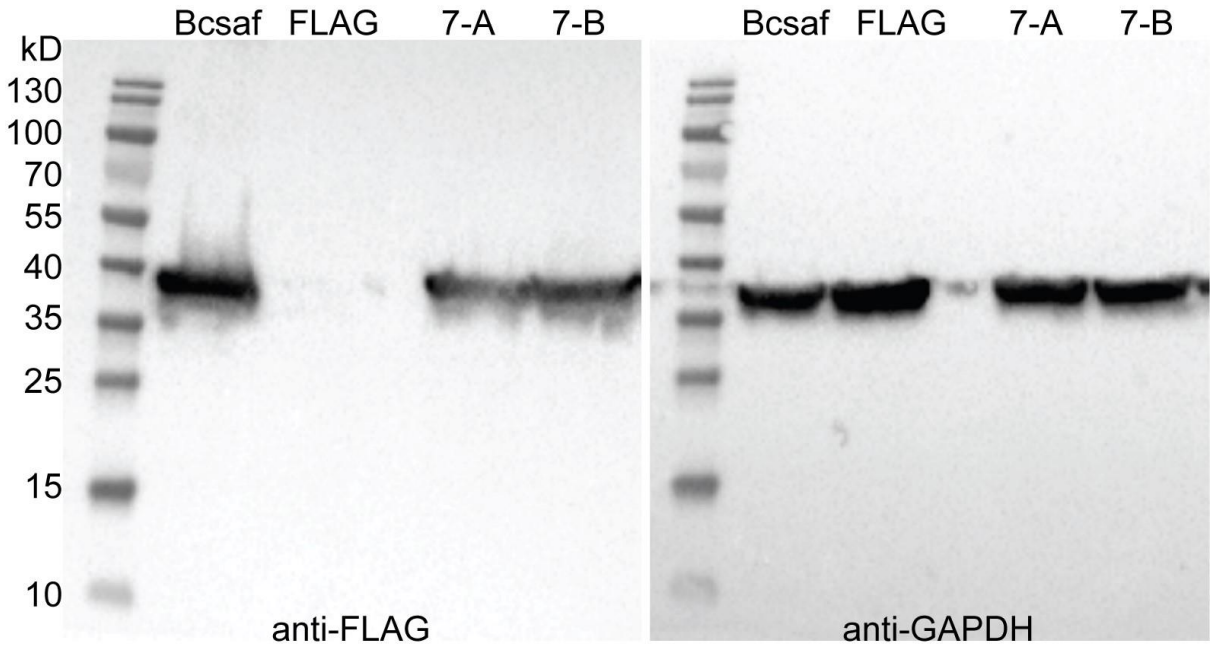

Figure S18. Immunoblots to assess expression of FLAG-tagged F80 candidate 7 in *S. cerevisiae*. Protein extracts were prepared from overnight cultures of transformants grown in SD-W. Immunoblots were probed with anti-FLAG or anti-GAPDH. As GAPDH runs at the same approximate molecular weight as BcSaf and candidate 7, separate blots were performed for each antibody.

Table S2 List of primers used for cloning the F80 candidates and controls in yeast.

Primers used for cloning in yeast		
To amplify	**Name**	**Sequence**
Vector backbone	nAP1069	CTTGTCATCATCGTCCTTATAGTCAGACATTTTTTTACTAGTCTTTCAGGAGGCTTGCTTCAAG
Vector backbone	nAP1070	ACTAGTCATATGGCCATGGAGGCCGAATTC
Candidate 1	nLVD067-F801_Sc_F	GACGATGATGACAAGTCTGCTGGCATGCTGATAG
Candidate 1	nLVD068-F801_Sc_R	CATGGCCATATGACTAGTCTAATTGGATTTCCTTGGATGCACCTTG
Candidate 2	nLVD069-F802_Sc_F	GACGATGATGACAAGCGTGCAGTCCTGTTCCC
Candidate 2	nLVD070-F802_Sc_R	CATGGCCATATGACTAGTTCAATCAATAATATCTCGCTTCCTAATCGAC
Candidate 3	nLVD071-F803_Sc_F	GACGATGATGACAAGGAATCACTTTCGTACCAATCAAAG
Candidate 3	nLVD072-F803_Sc_R	CATGGCCATATGACTAGTTTACTCCGCTCTATTCAGACCCAC
Candidate 4	nLVD073-F804_Sc_F	GACGATGATGACAAGCGCGGAAAGCTGATTATCT
Candidate 4	nLVD074-F804_Sc_R	CATGGCCATATGACTAGTTTAGACGAGCTTAAATCCGCCG
Candidate 5	nLVD081-F808_Sc_F	GACGATGATGACAAGGGCTTCAACATCTTTGAAAAGTTGC
Candidate 5	nLVD082-F808_Sc_R	CATGGCCATATGACTAGTTCAGAGACGAATGCACATCCCT
Candidate 6	nLVD087-F8011_Sc_F	GACGATGATGACAAGGATGCTCAGTCGATTACCCAG
Candidate 6	nLVD088-F8011_Sc_R	CATGGCCATATGACTAGTTCAAAGAGAACAGGGCGACATCT
Candidate 7	nLVD102-F8012_Sc_R	GACGATGATGACAAGTCTACCCAGTCAGCTCTCCT
Candidate 7	nLVD103-F8012_Sc_F	CATGGCCATATGACTAGTTTACTCTGAGATGCGGAAGTGCG
Flag-only vector	nAP1069	CTTGTCATCATCGTCCTTATAGTCAGACATTTTTTTACTAGTCTTTCAGGAGGCTTGCTTCAAG
Flag-only vector	nAP1071	GACGATGATGACAAGTAAACTAGTCATATGGCCATGGAGGCCGAATTC
BcSaf1	nAP1076	GACGATGATGACAAGACCGGTATGAGAGTTGCTC
BcSaf1	nAP1077	CATGGCCATATGACTAGTCTATACCTGTGGTTGCACAATAAC

7 References

Abadia J, Terry N. **1986**. Function of iron in chloroplasts. *Journal of Plant Nutrition* **9**: 609–646.

Almario J, Jeena G, Wunder J, Langen G, Zuccaro A, Coupland G, Bucher M. **2017**. Root-associated fungal microbiota of nonmycorrhizal Arabis alpina and its contribution to plant phosphorus nutrition. *Proceedings of the National Academy of Sciences of the United States of America* **114**: E9403–E9412.

Aznar A, Chen NWG, Rigault M, Riache N, Joseph D, Desmaële D, Mouille G, Boutet S, Soubigou-Taconnat L, Renou JP, *et al.* 2014. Scavenging iron: A novel mechanism of plant immunity activation by microbial siderophores. *Plant Physiology* **164**: 2167–2183.

Aznar A, Chen NWG, Thomine S, Dellagi A. **2015**. Immunity to plant pathogens and iron homeostasis. *Plant Science* **240**: 90–97.

Ba R, Alfa T, Gbaguidi F, Novidzro KM, Dotse K, Koudouvo K, Houngue U, Hounsode MTD, Koumaglo KH, Ameyapoh Y, *et al.* 2017. Maize Fungal Growth Control with Scopoletin of Cassava Roots Produced in Benin. *International Journal of Microbiology* **2017**.

Baakza A, Vala AK, Dave BP, Dube HC. **2004**. A comparative study of siderophore production by fungi from marine and terrestrial habitats. *Journal of Experimental Marine Biology and Ecology* **311**: 1–9.

Bai Y, Müller DB, Srinivas G, Garrido-Oter R, Potthoff E, Rott M, Dombrowski N, Münch PC, Spaepen S, Remus-Emsermann M, *et al.* 2015. Functional overlap of the Arabidopsis leaf and root microbiota. *Nature* **528**: 364–369.

Bandara YMAY, Weerasooriya DK, Liu S, Little CR. **2018**. The necrotrophic fungus macrophomina phaseolina promotes charcoal rot susceptibility in grain sorghum through induced host cell-wall-degrading enzymes. *Phytopathology* **108**: 948–956.

Bargaz A, Lyamlouli K, Chtouki M, Zeroual Y, Dhiba D. **2018**. Soil Microbial Resources for Improving Fertilizers Efficiency in an Integrated Plant Nutrient Management System. *Frontiers in Microbiology* **9**: 1606.

Baune M, Kang K, Schenkeveld WDC, Kraemer SM, Hayen H, Weber G. **2020**. Importance of oxidation products in coumarin-mediated Fe(hydr)oxide mineral dissolution. *BioMetals* **33**: 305–321.

Bchini R, Darnet S, de Butler A, Doan A, Oliveira-Correia L, Navarro D, Record E, Morel-Rouhier M. **2024**. Responses to and detoxification of esculin in white-rot fungi. *Fungal biology* **128**.

Beesley A, Beyer SF, Wanders V, Levecque S, Bredenbruch S, Habash SS, Schleker ASS, Gätgens J, Oldiges M, Schultheiss H, *et al.* 2023. Engineered coumarin accumulation reduces mycotoxin-induced oxidative stress and disease susceptibility. *Plant Biotechnology Journal* **21**: 2490–2506.

Beyer SF, Beesley A, Rohmann PFW, Schultheiss H, Conrath U, Langenbach CJG. **2019**. The Arabidopsis non-host defence-associated coumarin scopoletin protects soybean from Asian soybean rust. *The Plant Journal* **99**: 397.

Boorboori MR, Zhang HY. **2022**. The Role of Serendipita indica (Piriformospora indica) in Improving Plant Resistance to Drought and Salinity Stresses. *Biology* **11**: 952.

Borges F, Roleira F, Milhazes N, Santana L, Uriarte E. **2005**. Simple Coumarins and Analogues in Medicinal Chemistry: Occurrence, Synthesis and Biological Activity. *Current Medicinal Chemistry* **12**: 887–916.

Boukhalfa H, Crumbliss AL. **2002**. Chemical aspects of siderophore mediated iron transport. *BioMetals* **15**: 325–339.

Burkhardt AK, Childs KL, Wang J, Ramon ML, Martin FN. **2019**. Assembly, annotation, and comparison of Macrophomina phaseolina isolates from strawberry and other hosts. *BMC Genomics* **20**: 1–18.

Cantalapiedra CP, Herņandez-Plaza A, Letunic I, Bork P, Huerta-Cepas J. **2021**. eggNOG-mapper v2: Functional Annotation, Orthology Assignments, and Domain Prediction at the Metagenomic Scale. *Molecular Biology and Evolution* **38**: 5825–5829.

Cao M, Platre MP, Tsai H-H, Zhang L, Nobori T, Armengot L, Chen Y, He W, Brent L, Coll NS, *et al.* 2024. Spatial IMA1 regulation restricts root iron acquisition on MAMP perception. *Nature 2024*: 1–10.

Carpinella MC, Ferrayoli CG, Palacios SM. **2005**. Antifungal synergistic effect of scopoletin, a hydroxycoumarin isolated from Melia azedarach L. fruits. *Journal of Agricultural and Food Chemistry* **53**: 2922–2927.

Chaverri P, Branco-Rocha F, Jaklitsch W, Gazis R, Degenkolb T, Samuels GJ. **2015**. Systematics of the Trichoderma harzianum species complex and the re-identification of commercial biocontrol strains. *Mycologia* **107**: 558–590.

Connolly EL, Campbell NH, Grotz N, Prichard CL, Guerinot M Lou. **2003**. Overexpression of the FRO2 Ferric Chelate Reductase Confers Tolerance to Growth on Low Iron and Uncovers Posttranscriptional Control. *Plant Physiology* **133**: 1102.

Cornell RM, Schwertmann U. **2003**. The Iron Oxides. *The Iron Oxides*.

Crowley DE, Wang YC, Reid CPP, Szaniszlo PJ. **1991**. Mechanisms of iron acquisition from siderophores by microorganisms and plants. *Plant and Soil* **130**: 179–198.

Curie C, Panaviene Z, Loulergue C, Dellaporta SL, Briat J-F, Walker EL, Curie C, Panaviene Z, Loulergue C, Dellaporta SL, *et al.* 2001. Maize yellow stripe1 encodes a membrane protein directly involved in Fe(III) uptake. *Natur* **409**: 346–349.

Van Dijck L, Esposto D, Hülsmann C, Malisic M, Piro A, Giehl RFH, Balcke GU, Tissier A, Parker JE. **2025**. Cooperation between a root fungal endophyte and host-derived coumarin scopoletin mediates Arabidopsis iron nutrition. *bioRxiv*: 2025.06.04.657782.

Durairaj P, Hur JS, Yun H. **2016**. Versatile biocatalysis of fungal cytochrome P450 monooxygenases. *Microbial Cell Factories 2016 15:1* **15**: 1–16.

Durán P, Thiergart T, Garrido-Oter R, Agler M, Kemen E, Schulze-Lefert P, Hacquard S. **2018**. Microbial Interkingdom Interactions in Roots Promote Arabidopsis Survival. *Cell* **175**: 973-983.e14.

Eide D, Broderius M, Fett J, Guerinot M Lou. **1996**. A novel iron-regulated metal transporter from plants identified by functional expression in yeast. *Proceedings of the National Academy of Sciences* **93**: 5624–5628.

Fasusi OA, Babalola OO, Adejumo TO. **2023**. Harnessing of plant growth-promoting rhizobacteria and arbuscular mycorrhizal fungi in agroecosystem sustainability. *CABI Agriculture and Bioscience* **4**: 1–15.

Fodor F. **2024**. Iron Nutrition and Its Biochemical Interactions in Plants: Iron Uptake, Biofortification, Bacteria, and Fungi in Focus. *Plants 2024, Vol. 13, Page 561* **13**: 561.

Fourcroy P, Sisó-Terraza P, Sudre D, Savirón M, Reyt G, Gaymard F, Abadía A, Abadia J, Álvarez-Fernández A, Briat JF. **2014**. Involvement of the ABCG37 transporter in secretion of scopoletin and derivatives by Arabidopsis roots in response to iron deficiency. *New Phytologist* **201**: 155–167.

Francis K, Nishino SF, Spain JC, Gadda G. **2012**. A novel activity for fungal nitronate monooxygenase: Detoxification of the metabolic inhibitor propionate-3-nitronate. *Archives of Biochemistry and Biophysics* **521**: 84–89.

Galán-Pérez JA, Gámiz B, Celis R. **2021**. Determining the effect of soil properties on the stability of scopoletin and its toxicity to target plants. *Biology and Fertility of Soils* **57**: 643–655.

Gao L, Wang P, Yan X, Li J, Ma L, Hu M, Ge X, Li F, Hou Y. **2024**. Feruloyl-CoA 6′-hydroxylase-mediated scopoletin accumulation enhances cotton resistance to Verticillium dahliae. *Plant Physiology* **196**: 3007–3022.

Gautam CK, Tsai HH, Schmidt W. **2021**. IRONMAN tunes responses to iron deficiency in concert with environmental pH. *Plant Physiology* **187**: 1728–1745.

Gnonlonfin GJB, Sanni A, Brimer L. **2012**. Review Scopoletin – A Coumarin Phytoalexin with Medicinal Properties. *https://doi.org/10.1080/07352689.2011.616039* **31**: 47–56.

Goodwin RH, Kavanagh F. **1949**. The Isolation of Scopoletin, a Blue-Fluorescing Compound from Oat Roots. *Bulletin of the Torrey Botanical Club* **76**: 255.

Govindarajulu M, Pfeffer PE, Jin H, Abubaker J, Douds DD, Allen JW, Bücking H, Lammers PJ, Shachar-Hill Y. **2005**. Nitrogen transfer in the arbuscular mycorrhizal symbiosis. *Nature* **435**: 819–823.

Graña E, Costas-Gil A, Longueira S, Celeiro M, Teijeira M, Reigosa MJ, Sánchez-Moreiras AM. **2017**. Auxin-like effects of the natural coumarin scopoletin on Arabidopsis cell structure and morphology. *Journal of Plant Physiology* **218**: 45–55.

Guillierme E, Gevaert K, Goormachtig S, Struk S. **2025**. About How Nitrate Controls Nodulation: Will Soybean Spill the Bean? *Plant, Cell and Environment*.

Hacquard S, Garrido-Oter R, González A, Spaepen S, Ackermann G, Lebeis S, McHardy AC, Dangl JL, Knight R, Ley R, *et al.* 2015. Microbiota and Host Nutrition across Plant and Animal Kingdoms. *Cell Host & Microbe* **17**: 603–616.

Hacquard S, Kracher B, Hiruma K, Münch PC, Garrido-Oter R, Thon MR, Weimann A, Damm U, Dallery JF, Hainaut M, *et al.* 2016. Survival trade-offs in plant roots during colonization by closely related beneficial and pathogenic fungi. *Nature Communications* **7**: 11362.

Hagel JM, Facchini PJ. **2010**. Biochemistry and occurrence of O-demethylation in plant metabolism. *Frontiers in Physiology* **1 JUL**: 1863.

Harborne JB. **1982**. THE NATURAL COUMARINS: OCCURRENCE, CHEMISTRY AND BIOCHEMISTRY (Book). *Plant, Cell & Environment* **5**: 435–436.

Harbort CJ, Hashimoto M, Inoue H, Niu Y, Guan R, Rombolà AD, Kopriva S, Voges MJEEE, Sattely ES, Garrido-Oter R, *et al.* 2020. Root-Secreted Coumarins and the

Microbiota Interact to Improve Iron Nutrition in Arabidopsis. *Cell Host and Microbe* **28**: 825-837.e6.

Harley JL, Smith SE. **1983**. *Mycorrhizal Symbiosis.* London and New York: Academic Press.

Hider RC, Liu ZD, Khodr HH. **2001**. Metal chelation of polyphenols. *Methods in Enzymology* **335**: 190–203.

Hindt MN, Guerinot M Lou. **2022**. Getting a sense for signals: Regulation of the plant iron deficiency response. *Biochimica et Biophysica Acta (BBA) - Molecular Cell Research* **1823**: 1521–1530.

Hiscox JD, Israelstam GF. **2011**. A method for the extraction of chlorophyll from leaf tissue without maceration. *https://doi.org/10.1139/b79-163* **57**: 1332–1334.

Hördt W, Römheld V, Winkelmann G. **2000**. Fusarinines and dimerum acid, mono- and dihydroxamate siderophores from Penicillium chrysogenum, improve iron utilization by strategy I and strategy II plants. *BioMetals* **13**: 37–46.

Ishimaru Y, Suzuki M, Tsukamoto T, Suzuki K, Nakazono M, Kobayashi T, Wada Y, Watanabe S, Matsuhashi S, Takahashi M, *et al.* 2006. Rice plants take up iron as an Fe3+-phytosiderophore and as Fe2+. *The Plant Journal* **45**: 335–346.

Islam MS, Haque MS, Islam MM, Emdad EM, Halim A, Hossen QMM, Hossain MZ, Ahmed B, Rahim S, Rahman MS, *et al.* 2012. Tools to kill: Genome of one of the most destructive plant pathogenic fungi Macrophomina phaseolina. *BMC Genomics* **13**: 1–16.

Ito M, Tajima Y, Ogawa-Ohnishi M, Nishida H, Nosaki S, Noda M, Sotta N, Kawade K, Kamiya T, Fujiwara T, *et al.* 2024. IMA peptides regulate root nodulation and nitrogen homeostasis by providing iron according to internal nitrogen status. *Nature Communications* **15**: 1–13.

Jakoby M, Wang HY, Reidt W, Weisshaar B, Bauer P. **2004**. FRU (BHLH029) is required for induction of iron mobilization genes in Arabidopsis thaliana. *FEBS Letters* **577**: 528–534.

Jalkanen A, Lassheikki V, Torsti T, Gharib E, Lehtonen M, Juvonen RO. **2020**. Tissue and interspecies comparison of catechol-O-methyltransferase mediated catalysis of 6-O-methylation of esculetin to scopoletin and its inhibition by entacapone and tolcapone. *https://doi.org/10.1080/00498254.2020.1853850* **51**: 268–278.

Jin CW, He YF, Tang CX, Wu P, Zheng SJ. **2006**. Mechanisms of microbially enhanced Fe acquisition in red clover (Trifolium pratense L.). *Plant, Cell & Environment* **29**: 888–897.

Kai K, Mizutani M, Kawamura N, Yamamoto R, Tamai M, Yamaguchi H, Sakata K, Shimizu BI. **2008**. Scopoletin is biosynthesized via ortho-hydroxylation of feruloyl CoA by a 2-oxoglutarate-dependent dioxygenase in Arabidopsis thaliana. *Plant Journal* **55**: 989–999.

Kai K, Shimizu BI, Mizutani M, Watanabe K, Sakata K. **2006**. Accumulation of coumarins in Arabidopsis thaliana. *Phytochemistry* **67**: 379–386.

Kang K, Schenkeveld WDC, Weber G, Kraemer SM. **2023**. Stability of Coumarins and Determination of the Net Iron Oxidation State of Iron-Coumarin Complexes: Implications for Examining Plant Iron Acquisition Mechanisms. *ACS Earth and Space Chemistry* **7**: 2339–2352.

Kobayashi T, Nakanishi Itai R, Nishizawa NK. **2014**. Iron deficiency responses in rice roots. *Rice* **7**: 1–11.

Kraemer SM. **2004**. Iron oxide dissolution and solubility in the presence of siderophores. *Aquatic Sciences* **66**: 3–18.

Kramer J, Özkaya Ö, Kümmerli R. **2019**. Bacterial siderophores in community and host interactions. *Nature Reviews Microbiology 2019 18:3* **18**: 152–163.

Lee S, Crous PW, Wingfield MJ. **2006**. Pestalotioid fungi from Restionaceae in the Cape Floral Kingdom. *Studies in Mycology* **55**: 175–187.

Lehmann A, Rillig MC. **2015**. Arbuscular mycorrhizal contribution to copper, manganese and iron nutrient concentrations in crops – A meta-analysis. *Soil Biology and Biochemistry* **81**: 147–158.

Lemos ASO, Florêncio JR, Pinto NCC, Campos LM, Silva TP, Grazul RM, Pinto PF, Tavares GD, Scio E, Apolônio ACM, *et al.* 2020. Antifungal Activity of the Natural Coumarin Scopoletin Against Planktonic Cells and Biofilms From a Multidrug-Resistant Candida tropicalis Strain. *Frontiers in Microbiology* **11**.

Li M, Watanabe S, Gao F, Dubos C. **2023**. Iron Nutrition in Plants: Towards a New Paradigm? *Plants 2023, Vol. 12, Page 384* **12**: 384.

Lindsay WL, Schwab AP. **1982**. The chemistry of iron in soils and its availability to plants. *Journal of Plant Nutrition* **5**: 821–840.

Louvet O, Doignon F, Crouzet M. **1997**. Stable DNA-binding yeast vector allowing high-bait expression for use in the two-hybrid system. *BioTechniques* **23**: 816–820.

Ma LJ, Van Der Does HC, Borkovich KA, Coleman JJ, Daboussi MJ, Di Pietro A, Dufresne M, Freitag M, Grabherr M, Henrissat B, *et al.* 2010. Comparative genomics reveals mobile pathogenicity chromosomes in Fusarium. *Nature 2010 464:7287* **464**: 367–373.

Marquez N, Giachero ML, Declerck S, Ducasse DA. **2021**. Macrophomina phaseolina: General Characteristics of Pathogenicity and Methods of Control. *Frontiers in Plant Science* **12**: 666.

Martínez-Medina A, Van Wees SCM, Pieterse CMJ. **2017**. Airborne signals from Trichoderma fungi stimulate iron uptake responses in roots resulting in priming of jasmonic acid-dependent defences in shoots of Arabidopsis thaliana and Solanum lycopersicum. *Plant, Cell & Environment* **40**: 2691–2705.

McLean E, Cogswell M, Egli I, Wojdyla D, De Benoist B. **2009**. Worldwide prevalence of anaemia, WHO Vitamin and Mineral Nutrition Information System, 1993–2005. *Public Health Nutrition* **12**: 444–454.

Merry R, Dobbels AA, Sadok W, Naeve S, Stupar RM, Lorenz AJ. **2022**. Iron deficiency in soybean. *Crop Science* **62**: 36–52.

Mesny F, Hacquard S, Thomma BP. **2023**. Co-evolution within the plant holobiont drives host performance. *EMBO reports* **24**.

Mesny F, Miyauchi S, Thiergart T, Pickel B, Atanasova L, Karlsson M, Hüttel B, Barry KW, Haridas S, Chen C, *et al.* 2021. Genetic determinants of endophytism in the Arabidopsis root mycobiome. *Nature Communications 2021 12:1* **12**: 1–15.

Mino Y, Ishida T, Ota N, Inoue M, Nomoto K, Takemoto T, Tanaka H, Sugiura Y. **1983**. Mugineic Acid-Iron(III) Complex and Its Structurally Analogous Coball(III) Complex:

Characterization and Implication for Absorption and Transport of Iron in Gramineous Plants. *Journal of the American Chemical Society* **105**: 4671–4676.

Mladěnka P, Macáková K, Zatloukalová L, Řeháková Z, Singh BK, Prasad AK, Parmar VS, Jahodář L, Hrdina R, Saso L. **2010**. In vitro interactions of coumarins with iron. *Biochimie* **92**: 1108–1114.

Morrissey J, Guerinot M Lou. **2009**. Iron uptake and transport in plants: The good, the bad, and the ionome. *Chemical Reviews* **109**: 4553–4567.

Murata Y, Ma JF, Yamaji N, Ueno D, Nomoto K, Iwashita T. **2006**. A specific transporter for iron(III)-phytosiderophore in barley roots. *The Plant journal : for cell and molecular biology* **46**: 563–572.

Nozoye T, Nagasaka S, Kobayashi T, Takahashi M, Sato Y, Sato Y, Uozumi N, Nakanishi H, Nishizawa NK. **2011**. Phytosiderophore efflux transporters are crucial for iron acquisition in graminaceous plants. *Journal of Biological Chemistry* **286**: 5446–5454.

Paffrath V, Tandron Moya YA, Weber G, von Wirén N, Giehl RFH. **2023**. A major role of coumarin-dependent ferric iron reduction in strategy I-type iron acquisition in Arabidopsis. *The Plant Cell*.

Palmer CM, Hindt MN, Schmidt H, Clemens S, Guerinot M Lou. **2013**. MYB10 and MYB72 Are Required for Growth under Iron-Limiting Conditions. *PLOS Genetics* **9**: e1003953.

Pan L, Li X, Jin H, Yang X, Qin B. **2017**. Antifungal activity of umbelliferone derivatives: Synthesis and structure-activity relationships. *Microbial Pathogenesis* **104**: 110–115.

Pecoraro L, Wang X, Shah D, Song X, Kumar V, Shakoor A, Tripathi K, Ramteke PW, Rani R. **2021**. Biosynthesis Pathways, Transport Mechanisms and Biotechnological Applications of Fungal Siderophores. *Journal of Fungi* **8**: 21.

Rajniak J, Giehl RFH, Chang E, Murgia I, Von Wirén N, Sattely ES. **2018**. Biosynthesis of redox-active metabolites in response to iron deficiency in plants. *Nature Chemical Biology* **14**: 442–450.

Rehman A ur, Masood S, Khan NU, Abbasi ME, Hussain Z, Ali I. **2021**. Molecular basis of Iron Biofortification in crop plants; A step towards sustainability. *Plant Breeding* **140**: 12–22.

Reinhardt D, Roux C, Corradi N, Di Pietro A. **2021**. Lineage-Specific Genes and Cryptic Sex: Parallels and Differences between Arbuscular Mycorrhizal Fungi and Fungal Pathogens. *Trends in Plant Science* **26**: 111–123.

Reuveni M, Cohen Y. **1978**. Growth retardation and changes in phenolic compounds, with special reference to scopoletin, in mildewed and ethylene-treated tobacco plants. *Physiological Plant Pathology* **12**: 179–189.

Robe K, Conejero G, Gao F, Lefebvre-Legendre L, Sylvestre-Gonon E, Rofidal V, Hem S, Rouhier N, Barberon M, Hecker A, *et al.* 2021a. Coumarin accumulation and trafficking in Arabidopsis thaliana: a complex and dynamic process. *The New phytologist* **229**: 2062–2079.

Robe K, Conjero G, Dubos C. **2023**. The Use of Spectral Imaging to Follow the Iron and pH-Dependent Accumulation of Fluorescent Coumarins. *Methods in Molecular Biology* **2665**: 23–30.

Robe K, Izquierdo E, Vignols F, Rouached H, Dubos C. **2021b**. The Coumarins: Secondary Metabolites Playing a Primary Role in Plant Nutrition and Health. *Trends in Plant Science* **26**: 248–259.

Robe K, Stassen M, Chamieh J, Gonzalez P, Hem S, Santoni V, Dubos C, Izquierdo E. **2021c**. Uptake of Fe-fraxetin complexes, an IRT1 independent strategy for iron acquisition in Arabidopsis thaliana. *bioRxiv*: 2021.08.03.454955.

Robey MT, Caesar LK, Drott MT, Keller NP, Kelleher NL. **2021**. An interpreted atlas of biosynthetic gene clusters from 1,000 fungal genomes. *Proceedings of the National Academy of Sciences of the United States of America* **118**: e2020230118.

Robinson NJ, Procter CM, Connolly EL, Guerinot M Lou. **1999**. A ferric-chelate reductase for iron uptake from soils. *Nature 1999 397:6721* **397**: 694–697.

De Rocchis V, Jammer A, Camehl I, Franken P, Roitsch T. **2022**. Tomato growth promotion by the fungal endophytes Serendipita indica and Serendipita herbamans is associated with sucrose de-novo synthesis in roots and differential local and systemic effects on carbohydrate metabolisms and gene expression. *Journal of Plant Physiology* **276**: 153755.

Rodríguez-Celma J, Chun Pan I, Li W, Lan P, Buckhout TJ, Schmidt W. **2013a**. The transcriptional response of Arabidopsis leaves to Fe deficiency. *Frontiers in Plant Science* **4**: 276.

Rodríguez-Celma J, Lin WD, Fu GM, Abadía J, López-Millán AF, Schmidt W. **2013b**. Mutually Exclusive Alterations in Secondary Metabolism Are Critical for the Uptake of Insoluble Iron Compounds by Arabidopsis and Medicago truncatula. *Plant Physiology* **162**: 1473.

Römheld V. **1987**. Different strategies for iron acquisition in higher plants. *Physiologia Plantarum* **70**: 231–234.

Römheld V, Marschner H. **1986**. Evidence for a Specific Uptake System for Iron Phytosiderophores in Roots of Grasses. *Plant Physiology* **80**: 175–180.

Rosenkranz T, Oburger E, Baune M, Weber G, Puschenreiter M. **2021**. Root exudation of coumarins from soil-grown Arabidopsis thaliana in response to iron deficiency. *Rhizosphere* **17**: 100296.

Saleem S, Sekara A, Pokluda R. **2022**. Serendipita indica—A Review from Agricultural Point of View. *Plants* **11**.

Santi S, Schmidt W. **2009**. Dissecting iron deficiency-induced proton extrusion in Arabidopsis roots. *New Phytologist* **183**: 1072–1084.

Schmid NB, Giehl RFH, Döll S, Mock HP, Strehmel N, Scheel D, Kong X, Hider RC, von Wirén N. **2014**. Feruloyl-CoA 6′-Hydroxylase1-Dependent Coumarins Mediate Iron Acquisition from Alkaline Substrates in Arabidopsis. *Plant Physiology* **164**: 160–172.

Schmidt H, Gü Nther C, Weber M, Spö Rlein C, Loscher S. **2014**. Metabolome Analysis of Arabidopsis thaliana Roots Identifies a Key Metabolic Pathway for Iron Acquisition. *PLoS ONE* **9**: 102444.

Schroeder MM, Lai Y, Shirai M, Alsalek N, Tsuchiya T, Roberts P, Eulgem T. **2019**. A novel Arabidopsis pathosystem reveals cooperation of multiple hormonal response-pathways

in host resistance against the global crop destroyer Macrophomina phaseolina. *Scientific Reports 2019 9:1* **9**: 1–14.

Schwertmann U. **1991**. Solubility and dissolution of iron oxides. *Plant and Soil* **130**: 1–25.

Sequeira L, Kelman A. 1962. The accumulation of growth substances in plants infected by Pseudomonas solanacearum. *Phytopathology* **52**: 439–448.

Shirai M, Eulgem T. **2023**. Molecular interactions between the soilborne pathogenic fungus Macrophomina phaseolina and its host plants. *Frontiers in Plant Science* **14**: 1264569.

Sinha N, Patra SK, Ghosh S. **2022**. Secretome Analysis of Macrophomina phaseolina Identifies an Array of Putative Virulence Factors Responsible for Charcoal Rot Disease in Plants. *Frontiers in Microbiology* **13**: 847832.

Sisó-Terraza P, Luis-Villarroya A, Fourcroy P, Briat JF, Abadía A, Gaymard F, Abadía J, Álvarez-Fernández A. **2016**. Accumulation and secretion of coumarinolignans and other coumarins in Arabidopsis thaliana roots in response to iron deficiency at high pH. *Frontiers in Plant Science* **7**: 1711.

Siwinska J, Siatkowska K, Olry A, Grosjean J, Hehn A, Bourgaud F, Meharg AA, Carey M, Lojkowska E, Ihnatowicz A. **2018**. Scopoletin 8-hydroxylase: a novel enzyme involved in coumarin biosynthesis and iron-deficiency responses in Arabidopsis. *Journal of Experimental Botany* **69**: 1735–1748.

Smith SE, Read DJ. **2008**. *Mycorrhizal Symbiosis*. Oxford: Academic Press.

Sokolova O, Sivicka I, Krivmane B, Kārkliņa K. **2022**. First report of Truncatella angustata causing leaf spot on oregano (Origanum vulgare) in Latvia. *Journal of Phytopathology* **170**: 167–175.

Spooren J, van Bentum S, Thomashow LS, Pieterse CMJ, Weller DM, Berendsen RL. **2024**. Plant-Driven Assembly of Disease-Suppressive Soil Microbiomes. *Annual review of phytopathology*.

Stassen MJJ, Hsu SH, Pieterse CMJ, Stringlis IA. **2021**. Coumarin Communication Along the Microbiome–Root–Shoot Axis. *Trends in Plant Science* **26**: 169–183.

Stringlis IA, De Jonge R, Pieterse CMJ. **2019**. The Age of Coumarins in Plant-Microbe Interactions. *Plant and Cell Physiology* **60**: 1405–1419.

Stringlis IA, Proietti S, Hickman R, Van Verk MC, Zamioudis C, Pieterse CMJ. **2018a**. Root transcriptional dynamics induced by beneficial rhizobacteria and microbial immune elicitors reveal signatures of adaptation to mutualists. *The Plant Journal* **93**: 166–180.

Stringlis IA, Yu K, Feussner K, De Jonge R, Van Bentum S, Van Verk MC, Berendsen RL, Bakker PAHM, Feussner I, Pieterse CMJ. **2018b**. MYB72-dependent coumarin exudation shapes root microbiome assembly to promote plant health. *Proceedings of the National Academy of Sciences of the United States of America* **115**: E5213–E5222.

Su G, Suh S-O, Schneider RW, Russin JS. **2001**. Host Specialization in the Charcoal Rot Fungus, Macrophomina phaseolina. *Phytopathology*: 120–126.

Sun H, Wang L, Zhang B, Ma J, Hettenhausen C, Cao G, Sun G, Wu J, Wu J. **2014a**. Scopoletin is a phytoalexin against Alternaria alternata in wild tobacco dependent on jasmonate signalling. *Journal of Experimental Botany* **65**: 4305–4315.

Sun H, Wang L, Zhang B, Ma J, Hettenhausen C, Cao G, Sun G, Wu J, Wu J. **2014b**. Scopoletin is a phytoalexin against Alternaria alternata in wild tobacco dependent on jasmonate signalling. *Journal of Experimental Botany* **65**: 4305–4315.

Suter D, Banwart S, Stumm W. **1991**. Dissolution of Hydrous Iron(III) Oxides by Reductive Mechanisms. *Langmuir* **7**: 809–813.

Syed K, Doddapaneni H, Subramanian V, Lam YW, Yadav JS. **2010**. Genome-to-function characterization of novel fungal P450 monooxygenases oxidizing polycyclic aromatic hydrocarbons (PAHs). *Biochemical and biophysical research communications* **399**: 492.

Taguchi G, Fujikawa S, Yazawa T, Kodaira R, Hayashida N, Shimosaka M, Okazaki M. **2000**. Scopoletin uptake from culture medium and accumulation in the vacuoles after conversion to scopolin in 2,4-D-treated tobacco cells. *Plant Science* **151**: 153–161.

Takagi SI, Nomoto K, Takemoto T. **1984**. Physiological aspect of mugineic acid, a possible phytosiderophore of graminaceous plants. *Journal of Plant Nutrition* **7**: 469–477.

Tang J, Matsuda Y. **2024**. Discovery of fungal onoceroid triterpenoids through domainless enzyme-targeted global genome mining. *Nature Communications* **15**: 4312.

Thiergart T, Durán P, Ellis T, Vannier N, Garrido-Oter R, Kemen E, Roux F, Alonso-Blanco C, Ågren J, Schulze-Lefert P, *et al.* 2020. Root microbiota assembly and adaptive differentiation among European Arabidopsis populations. *Nature Ecology and Evolution* **4**: 122–131.

Torres DE, Oggenfuss U, Croll D, Seidl MF. **2020**. Genome evolution in fungal plant pathogens: looking beyond the two-speed genome model. *Fungal Biology Reviews* **34**: 136–143.

Trapet PL, Verbon EH, Bosma RR, Voordendag K, Van Pelt JA, Pieterse CMJ. **2021**. Mechanisms underlying iron deficiency-induced resistance against pathogens with different lifestyles. *Journal of Experimental Botany* **72**: 2231–2241.

Tsai HH, Rodríguez-Celma J, Lan P, Wu YC, Vélez-Bermúdez IC, Schmidt W. **2018**. Scopoletin 8-Hydroxylase-Mediated Fraxetin Production Is Crucial for Iron Mobilization. *Plant Physiology* **177**: 194–207.

Tsai HH, Schmidt W. **2017**. One way. Or another? Iron uptake in plants. *New Phytologist* **214**: 500–505.

Tsai HH, Schmidt W. **2020**. PH-dependent transcriptional profile changes in iron-deficient Arabidopsis roots. *BMC Genomics* **21**: 1–11.

Tsugawa H, Cajka T, Kind T, Ma Y, Higgins B, Ikeda K, Kanazawa M, Vandergheynst J, Fiehn O, Arita M. **2015**. MS-DIAL: Data-independent MS/MS deconvolution for comprehensive metabolome analysis. *Nature Methods* **12**: 523–526.

Vanholme R, Sundin L, Seetso KC, Kim H, Liu X, Li J, De Meester B, Hoengenaert L, Goeminne G, Morreel K, *et al.* 2019. COSY catalyses trans–cis isomerization and lactonization in the biosynthesis of coumarins. *Nature Plants 2019 5:10* **5**: 1066–1075.

Varotto C, Maiwald D, Pesaresi P, Jahns P, Salamini F, Leister D. **2002**. The metal ion transporter IRT1 is necessary for iron homeostasis and efficient photosynthesis in Arabidopsis thaliana. *The Plant Journal* **31**: 589–599.

Vélez-Bermúdez IC, Schmidt W. **2022a**. Plant strategies to mine iron from alkaline substrates. *Plant and Soil 2022 483:1* **483**: 1–25.

Vélez-Bermúdez IC, Schmidt W. **2022b**. Plant strategies to mine iron from alkaline substrates. *Plant and Soil 2022 483:1* **483**: 1–25.

Venkatesagowda B, Dekker RFH. **2021**. Microbial demethylation of lignin: Evidence of enzymes participating in the removal of methyl/methoxyl groups. *Enzyme and Microbial Technology* **147**.

Verma A, Shameem N, Jatav HS, Sathyanarayana E, Parray JA, Poczai P, Sayyed RZ. **2022**. Fungal Endophytes to Combat Biotic and Abiotic Stresses for Climate-Smart and Sustainable Agriculture. *Frontiers in Plant Science* **13**: 953836.

Vert G, Grotz N, Dédaldéchamp F, Gaymard F, Guerinot M Lou, Briat JF, Curie C. **2002**. IRT1, an Arabidopsis transporter essential for iron uptake from the soil and for plant growth. *The Plant cell* **14**: 1223–1233.

Vismans G, van Bentum S, Spooren J, Song Y, Goossens P, Valls J, Snoek BL, Thiombiano B, Schilder M, Dong L, *et al.* 2022. Coumarin biosynthesis genes are required after foliar pathogen infection for the creation of a microbial soil-borne legacy that primes plants for SA-dependent defenses. *Scientific Reports* **12**: 22473.

Voges MJEEE, Bai Y, Schulze-Lefert P, Sattely ES. **2019**. Plant-derived coumarins shape the composition of an Arabidopsis synthetic root microbiome. *Proceedings of the National Academy of Sciences of the United States of America* **116**: 12558–12565.

Vyas TK, Bardhan K, Singh S. **2024**. The Role of Arbuscular Mycorrhiza Fungi in Zinc and Iron Nutrition of Crops. *Arbuscular Mycorrhizal Fungi in Sustainable Agriculture: Nutrient and Crop Management*: 167–192.

Wenneker M, Pham KTK, Boekhoudt LC, De Boer FA, Van Leeuwen PJ, Hollinger TC, Thomma BPHJ. **2017**. First report of truncatella angustata causing postharvest rot on 'topaz' apples in the Netherlands. *Plant Disease* **101**: 508.

Winkelmann G. **1992**. Structures and functions of fungal siderophores containing hydroxamate and complexone type iron binding ligands. *Mycological Research* **96**: 529–534.

Yi Y, Guerinot M Lou. **1996**. Genetic evidence that induction of root Fe(III) chelate reductase activity is necessary for iron uptake under iron deficiency†. *The Plant Journal* **10**: 835–844.

You Y, Suraj HM, Matz L, Herrera Valderrama AL, Ruigrok P, Shi-Kunne X, Pieterse FPJ, Oostlander A, Beenen HG, Chavarro-Carrero EA, *et al.* 2024. Botrytis cinerea combines four molecular strategies to tolerate membrane-permeating plant compounds and to increase virulence. *Nature Communications* **15**: 6448.

Yu K, Stringlis IA, van Bentum S, de Jonge R, Snoek BL, Pieterse CMJ, Bakker PAHM, Berendsen RL. **2021**. Transcriptome Signatures in Pseudomonas simiae WCS417 Shed Light on Role of Root-Secreted Coumarins in Arabidopsis-Mutualist Communication. *Microorganisms 2021, Vol. 9, Page 575* **9**: 575.

Yuan Y, Wu H, Wang N, Li J, Zhao W, Du J, Wang D, Ling HQ. **2008**. FIT interacts with AtbHLH38 and AtbHLH39 in regulating iron uptake gene expression for iron homeostasis in Arabidopsis. *Cell Research 2008 18:3* **18**: 385–397.

Yuan X, Yang F, Wang Y, Li S, Zhang D, Liang W, Yang Q. **2024**. Scopoletin negatively regulates the HOG pathway and exerts antifungal activity against Botrytis cinerea by interfering with infection structures, cell wall, and cell membrane formation. *Phytopathology Research* **6**: 1–14.

Zamioudis C, Hanson J, Pieterse CMJ. **2014**. β-Glucosidase BGLU42 is a MYB72-dependent key regulator of rhizobacteria-induced systemic resistance and modulates iron deficiency responses in Arabidopsis roots. *New Phytologist* **204**: 368–379.

Zamioudis C, Korteland J, Van Pelt JA, Van Hamersveld M, Dombrowski N, Bai Y, Hanson J, Van Verk MC, Ling HQ, Schulze-Lefert P, *et al.* 2015. Rhizobacterial volatiles and photosynthesis-related signals coordinate MYB72 expression in Arabidopsis roots during onset of induced systemic resistance and iron-deficiency responses. *Plant Journal* **84**: 309–322.

Zaynab M, Khan J, Al-Yahyai R, Sadder M, Li S. **2024**. Toxicity of coumarins in plant defense against pathogens. *Toxicon* **250**: 108118.

Zhao M, Ma L, Song N, Cheng J, Zhao Z, Wu J. **2022**. The regulation of Alternaria alternata resistance by LRR-RK4 through ERF109, defensin19 and phytoalexin scopoletin in Nicotiana attenuata. *Plant Science* **323**: 111414.

Zhao L, Wang Y, Kong S. **2020**. Effects of Trichoderma asperellum and its siderophores on endogenous auxin in Arabidopsis thaliana under iron-deficiency stress. *International Microbiology* **23**: 501–509.

Ziegler J, Schmidt S, Strehmel N, Scheel D, Abel S. **2017**. Arabidopsis Transporter ABCG37/PDR9 contributes primarily highly oxygenated Coumarins to Root Exudation. *Scientific Reports 2017 7:1* **7**: 1–11.

Zinder B, Furrer G, Stumm W. **1986**. The coordination chemistry of weathering: II. Dissolution of Fe(III) oxides. *Geochimica et Cosmochimica Acta* **50**: 1861–1869.

Zulfiqar U, Ayub A, Hussain S, Ahmad M, Rehman A, Ishfaq M, Ali MF, Shabaan M, Yong JWH. **2024**. Iron biofortification in cereal crops: Recent progress and prospects. *Food and Energy Security* **13**: e547.

Zuluaga MYA, Cardarelli M, Rouphael Y, Cesco S, Pii Y, Colla G. **2023**. Iron nutrition in agriculture: From synthetic chelates to biochelates. *Scientia Horticulturae* **312**: 111833.

Zuo Y, Zhang F. **2011**. Soil and crop management strategies to prevent iron deficiency in crops. *Plant and Soil* **339**: 83–95.